THE MINISTRY OF NATIONAL
INFRASTRUCTURES
GEOLOGICAL SURVEY OF ISRAEL

Seismic hazard evaluation of the Haifa and Eilat Bay areas, Israel

**Heimann, A., Frydman, S.,
Wachs, D., Talwani, P.**

**Submitted as a final report to the
US - Israel Binational Science Foundation**

Report GSI / 40 / 2001 **Jerusalem, December 2001**

THE MINISTRY OF NATIONAL
INFRASTRUCTURES
GEOLOGICAL SURVEY OF ISRAEL

Seismic hazard evaluation of the Haifa and Eilat Bay areas, Israel

**Heimann, A., Frydman, S.,
Wachs, D., Talwani, P.**

**Submitted as a final report to the
US - Israel Binational Science Foundation**

Report GSI / 40 / 2001 **Jerusalem, December 2001**

1 Contents

List of Figures

2 Abstract

The cities of Haifa and Eilat and their neighboring cities are sited on the active Dead Sea Transform Fault and its major branch the Carmel Fault. Earthquakes of magnitude 7 and above in the Eilat area, and 6 and above in the Haifa Bay area are possible. Thus, and as both cities forms areas with a large population, the seismic hazard is high.

In the present study we tried to evaluate some components of the hazard of the area. We surveyed both areas for paleoliquefaction features, we made a geotechnical study and in the Haifa area studied the neotectonic and paleoseismology of the Carmel Fault.

No paleoliqefaction features were observed in sites in the Haifa and Eilat Bay areas although these sites had the potential to have such features. The Carmel Fault is seismically active and it displaced Pleistocene features such as alluvial fans and stream channels.

No evidence for surface rupture was detected in the trenches opened along the Carmel Fault although faults were located in a seismic line. A zone of deformation was located in the trench underneath the fault scarp directly above one of the faults identified in the seismic line. This could be interpreted as a blind fault.

It is possible therefore to conclude that although the Carmel Fault is seismically active and it displaced Pleistocene features such as alluvial fans and stream channels, there was no surface rupture along it during the last few tens of thousands of years. This may be because during this time the Carmel Fault did not initiate earthquakes with magnitude M>5.5. It may be that the recurrence time of earthquakes that cause surface rupture on the Carmel Fault is longer than tens of thousands of years. Still, as suggested above, although no fault rupture occurred, thrusting and deformation of the surface might have occurred during that period.

The geotechnical studies described in the above sections have indicated a significant difference between the liquefaction potential of the Eilat and Kishon sites. The Eilat site appears to have a potential for liquefaction under the action of an earthquake of magnitude 6.0 or greater, producing a peak ground acceleration of 0.3g or more. On the other hand, at the Kishon site, a peak ground acceleration

of 0.3g would only be expected to cause liquefaction if it resulted from an earthquake of magnitude about 7.5. It is not surprising, therefore, that no signs of paleoliquefaction are evident at the Kishon site. On the other hand, such signs may have been expected at the Eilat site, since magnitude 6 events, developing peak ground accelerations of 0.3g, may conceivably have occurred in the past.

It seems therefore that earthquakes with magnitude of 6 and above (that rupture the surface) did not occur along the Carmel Fault in the last few tens of thousand of years. The geotechnical information suggest that liquefaction in the Haifa Bay would occur as a result of earthquakes greater than 7.5. Such events did not occur on the Carmel Fault for a very long time and thus the non-finding of paleoliquefaction features is not surprising. It is therefore suggested that the seismic hazard resulting from surface rupture or liquefaction in the Haifa Bay area is not high.

In Eilat, an area producing earthquakes with magnitudes higher than 7, the geotechnical studies show that liquefaction could occur as a result of an earthquake of magnitude 6 or higher. Therefore, the non-finding of paleoliquefaction features is surprising. We suggest that the seismic hazard of Eilat, as a result of liquefaction must be regarded as high.

3 Introduction

The city of Haifa, a metropolis inhabited by 700,000 people and a major industrial area of Israel, is situated along the active Carmel Fault (Figures 3.1). In August 1984 a magnitude 5.2 earthquake, located only 10 km east of Haifa, occurred (Figure 3.2). Prior to this event, there is no record of earthquakes with magnitudes greater than 5 along the Carmel Fault; therefore the frequency-magnitude relations for this fault are not known. It has been suggested (Wachs and Siman-Tov, 1991) that this fault is capable of producing earthquakes with magnitudes of 6.0 or larger. Such an earthquake could cause heavy loss of life as a result of direct damage to structures and of environmental disaster. The potential environmental damage from a strong earthquake is enormous due to the large number of chemical plants in the vicinity, e.g. underground pipelines containing flammable gas or potentially pollutant liquids.

The city of Eilat and the neighboring city of Aqaba are similarly sited on the active Dead Sea Transform Fault (Figs. 3.1). Eilat is a major tourist town and together with Aqaba forms an area with a large population. Earthquakes of magnitude 7 and above are possible in the area (Vered, 1978).

Many structures (industrial and residential) in Haifa and Eilat were not designed for such earthquakes. The problem is compounded by the presence of unfavorable ground conditions (e.g. materials that amplify seismic waves), meaning that a large earthquake could result in a disaster.

In order to evaluate the seismic risk of an area, in addition to recognizing its seismic hazards, knowledge of the area's seismic history is necessary. The seismic histories of both areas are poorly known.

Common methods of studying the seismic history of an area involve trenching of active faults, geomorphological studies and other techniques loosely grouped under the term paleoseismology. These methods can provide information about the magnitudes of past earthquakes. Still, this method does not yield data about past ground accelerations, which is of a primary importance in evaluating seismic hazard. Under certain conditions, when high ground acceleration occurs, particular materials such as sand experience transient high pore water pressures, lose their shear strength and liquefy. Paleoliquefaction features are found in

seismically active areas and are indicative of development of high ground acceleration during past earthquakes. The Haifa and Eilat bay areas both have ground conditions which may facilitate the occurrence of liquefaction (Wachs and Siman-Tov, 1991; Wachs and Zilberman, 1994).

In this study we tried to learn about the existence, or the significance of the non-existence of paleoliquefaction features in these two areas, and in this way contribute to the documentation of their seismic histories. We carried out a geotechnical study in order to understand the nature of the ground and its engineering properties. We also made a paleoseismic study along the Carmel Fault in order to better understand the past earthquakes and their timing.

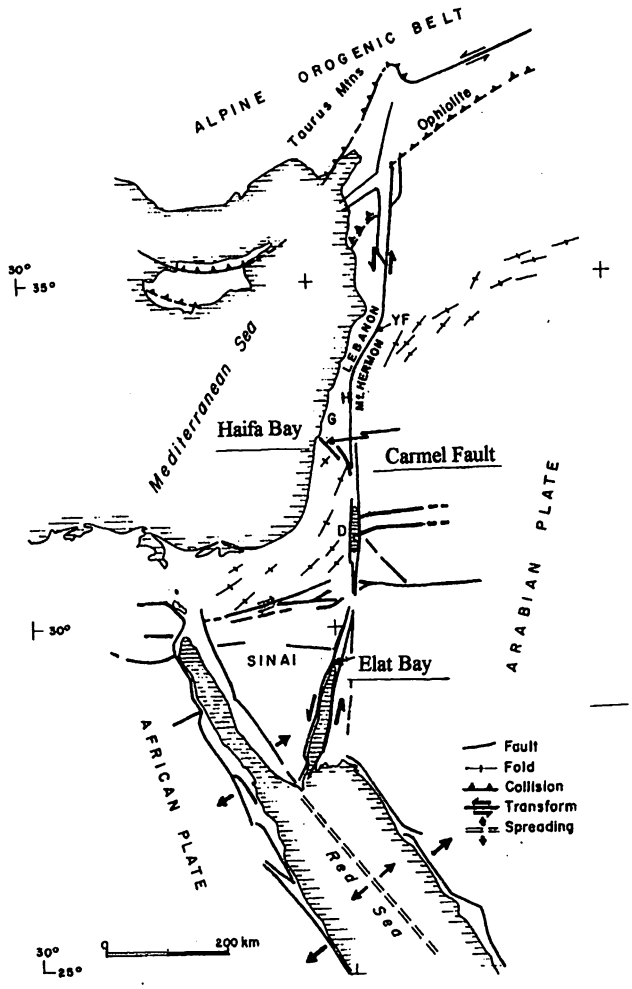

Figure 3.1. General tectonic setting of the Dead Sea Transform (From Heimann, 1990). The investigated areas are marked.

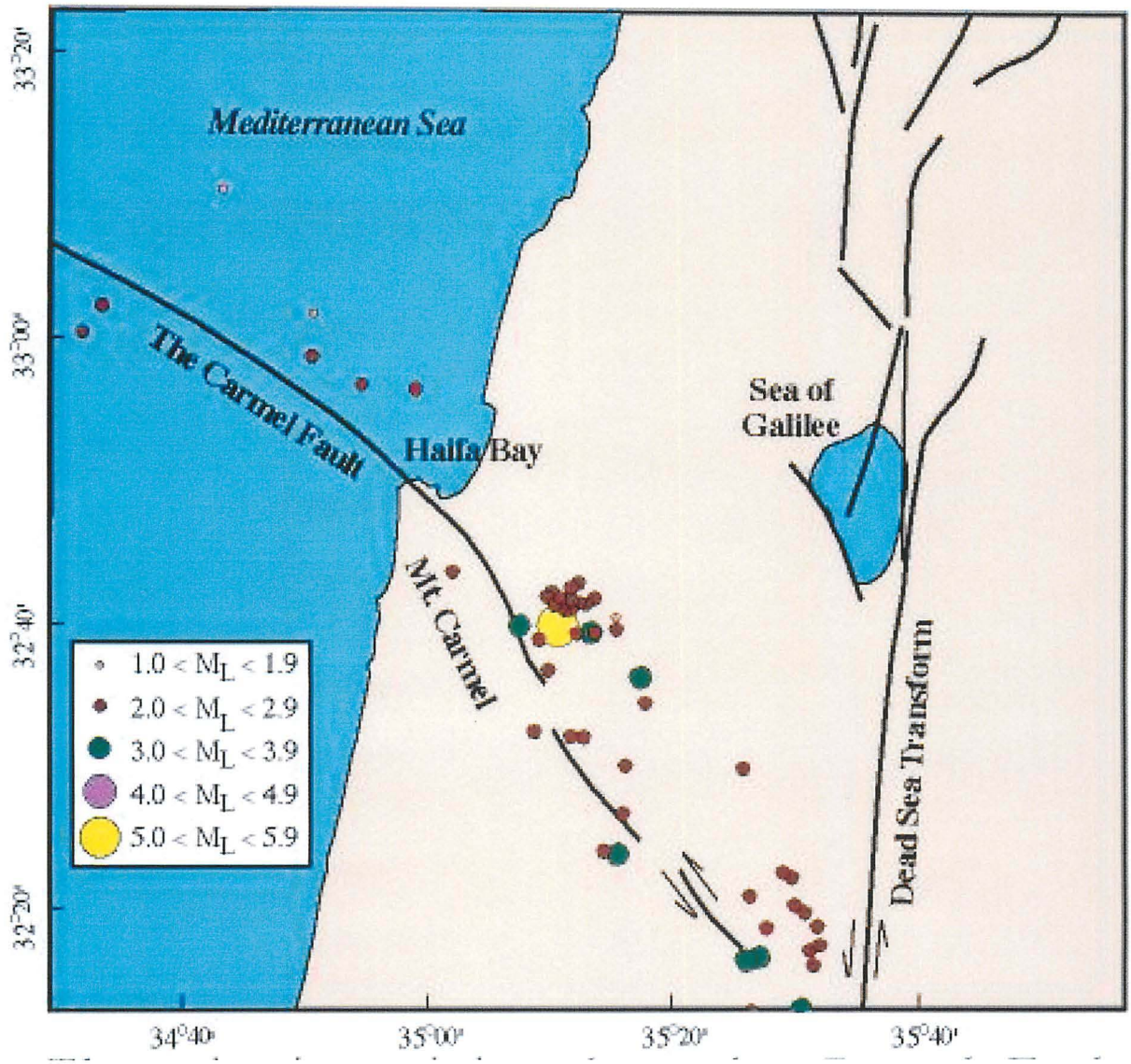

Figure 3.2 Seismicity along the Mt. Carmel Fault observed during the period January 1984 to September 1988 (From Ron et al., 1990).

4 Geological Background

The Dead Sea Rift is the plate boundary between the Sinai-Israel subplate and the Arabian plate (Figure 3.1). This plate boundary is dominantly a left-lateral transform with a small extensional component, which opens the rift depression (Quennell, 1959; Freund et al., 1970; Garfunkel et al., 1981; Heimann, 1990). The transform, more than 1000 km long, links the Red Sea, where crustal spreading takes place, with the Taurus zone of plate collision. The slip postdates Middle Miocene time (Bartov et al., 1980) and is still active (e.g. Rotstein and Arie, 1986; Marco and Agnon, 1995).

The southern part of the Dead Sea Transform is composed of the Arava Fault System, connecting the Dead Sea with the Gulf of Eilat. The city of Eilat is crossed by the Evrona Fault, one of the main faults of the Arava Fault System (Figure 3.1). The fault forms a shear belt 80-90 km long and several hundred meters wide, extending from the Yotveta Basin in the north to the Gulf of Eilat in the south (Garfunkel et al., 1981). Geomorphological studies indicate that this part of the fault is active (Gerson et al., 1993). Six hundred meters of horizontal displacement, detected on displaced alluvial fans, which occurred during the Late Pleistocene and the Holocene, were detected along the Evrona Fault (Zak and Freund, 1966). Evidence of repeated Late Pleistocene to Early Holocene vertical displacement has been observed along the western marginal fault system of the southern Arava Valley, suggesting the occurrence of local earthquakes with magnitudes of 6.0 and higher, once every 2000-3000 years (Gerson et al., 1993; Enzel et al., 1994). Based on these data, it was postulated that the southern Arava Fault System (the Evrona Fault) is capable of producing earthquakes of magnitude 6.0-7 (Wachs and Zilberman, 1994).

The Carmel - Farah Fault zone in northern Israel (Figures 3.1, 3.2) is one of the more important active elements in the geology of Israel and is considered to be the largest splay of the Dead Sea Rift south of Lebanon (Freund, 1965)(Figure 3.1). The fault, striking NW-SE and continuing into the Mediterranean Sea (Figure 3.2), was suggested as taking up some of the transform motion (Ben-Menachem et al., 1976). The fault separates the Yisrael Valley from Mt. Carmel with 400 m of post Miocene uplift and tilt (Picard and Kashai, 1958; Karcz, 1959). The two sides

of the line are characterized by distributed crustal deformation and are underlain by major positive magnetic and gravity anomalies (Ben-Avraham and Hall, 1977; Ben-Avraham and Ginzburg 1990). Although a dip-slip component on the Carmel Fault is apparent, it is commonly assumed that a significant left lateral strike-slip component is also present. The offset was estimated to be 3-10 km (e.g. Arad, 1965; Freund, 1965). A more recent detailed study (Achmon, 1986) showed that the Carmel Fault is a wide fault zone rather than a single fault, and documented a young strike-slip motion of 500-1500 m on some of the fault traces. A series of high-resolution seismic lines which cross the Carmel Fault showed a wide (0.8-3 km) zone of intense deformation (Rotstein et al., 1993). They suggested that where the fault trends N-S (compare to the NW-SE overall trend of the Carmel-Farah Fault) a large component of compression across the fault is evident, and this appears to be a major cause for the recent uplift of Mt. Carmel. More recent geophysical work (Achmon et al., 1994) details and supports the above conclusions. Using high resolution seismic reflection, Feigin (1994) showed that very young (Late Pleistocene - Holocene (?)) faulting affects the flood plain sediments of the Kishon Valley along the Carmel Fault.

To summarize: faults in Elat and Haifa areas are very young; activity along them continued to the Late Pleistocene and Holocene.

Israel and its vicinity is known as an area with relatively high seismicity (Figure 4.1). This is observed in recent history (e.g. destructive earthquakes occurring in 746, 1033, 1546, 1837, 1927 with magnitudes between 6-7.3; Ben Menachem, 1979) and is monitored by the Seismology Division of the Israel Institute of Geophysics (previously the Institute for Petroleum Research and Geophysics) - (IPRG reports and maps since 1980).

The Carmel-Farah Fault zone is characterized by micro-seismic activity, which is as high as that of the Dead Sea Rift itself (Rotstein and Arie, 1986)(Figure 3.2). The city of Haifa, situated on this active fault, is not only affected by nearby earthquakes, but is also vulnerable to the earthquakes generated on the Dead Sea Transform in northern Israel, just 50 km to the east (Shapira and Feldman, 1987)(Figure 4.1). The Eilat area was recognized also as a seismically active area with increasing seismicity in the last years (Shamir and Shapira, 1994)(Figure 4.1).

Earthquakes of magnitude 6 and above and epicenters located in the vicinity of Haifa and the Eilat bay areas are possible in the future. In the case of Eilat the magnitude could exceed 7 (Vered, 1978). Both sites may be in the near field of an earthquake due to their proximity to the potential epicenters.

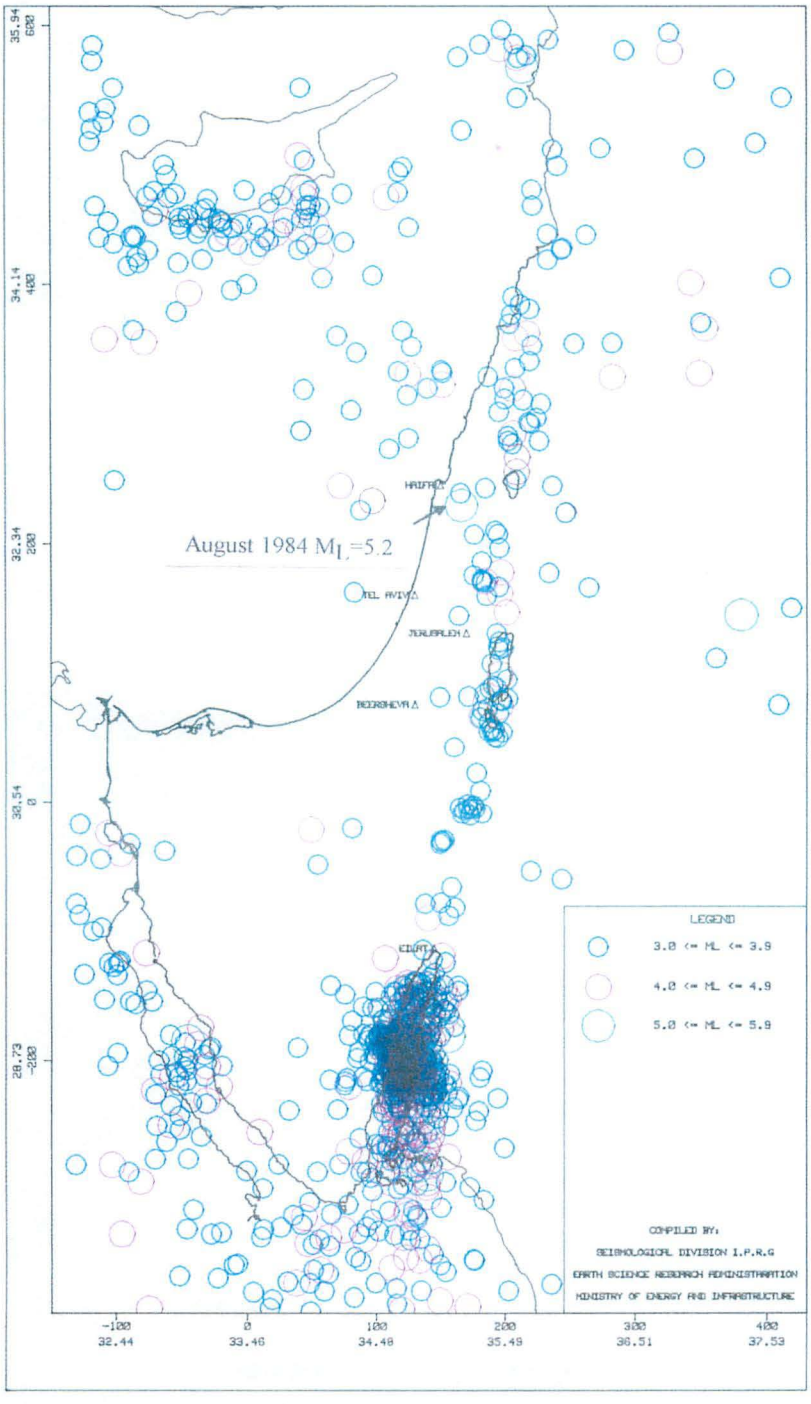

Figure 4.1 Seismicity map of Israel and adjacent areas for the period 1980-1994 (M_L>3.0) (Data from IPRG).

Trenching of active faults, a common method in evaluating seismic history, can only detect relatively large events, which rupture the surface. Moreover, local earthquakes with magnitudes as high as 7 can take place on a fault without rupture of the surface, and faraway earthquakes can cause high levels of ground acceleration in the areas discussed. Therefore, significant seismic events can affect the area and may not be recognized by methods that rely on surface rupture. Thus, a complimentary method for evaluating the seismic hazard and/or the seismic history is essential.

In areas where the sediments are composed of unlithified sand saturated with water, seismic vibration of sufficient strength and duration may lead to a phenomenon known as ground liquefaction (e.g. Niagata, Japan, see Seed and Idris, 1982). When saturated sand is overlaid by an impermeable layer (such as clay), and is being liquefied, the sand penetrates the impermeable layer above it. The result is the formation of paleoliquefaction features such as "sand dikes" and mounds which can be recognized in the buried sediment section (e.g. Obermeier et al., 1990). Similar phenomena were recognized recently near the Dead Sea in the Upper Pleistocene Lisan Formation (Kadan et al., 1995).

Most of Eilat and large portions of Haifa Bay areas are sited on unconsolidated sediments. Preliminary field investigations in the Haifa Bay area show that uniformly sized, unlithified sand deposits (based on standard penetration test (SPT) data) are common and widespread in the area (Wachs and Siman-Tov, 1991)(Figure 7). The water table is less than 3 meters deep and is within the sand. Wachs and Siman-Tov (1991), and Frydman (1993) found that at sites where unconsolidated sediments are 40 meters or less in thickness, amplification of ground surface acceleration may reach up to 4 to 6 times the acceleration of the bedrock below. Wachs and Zilberman (1994) suggested that in Eilat amplification of the ground vibration might also occur; this was substantiated in results of propagation analyses carried out by Frydman (1994). Therefore, earthquake-induced liquefaction of the ground may be feasible for both areas during earthquakes of magnitude 6.0 or above in the vicinity (Wachs and Siman-Tov, 1991; Wachs and Zilberman, 1994, Figure 8), or during larger earthquakes along the Dead Sea Rift.

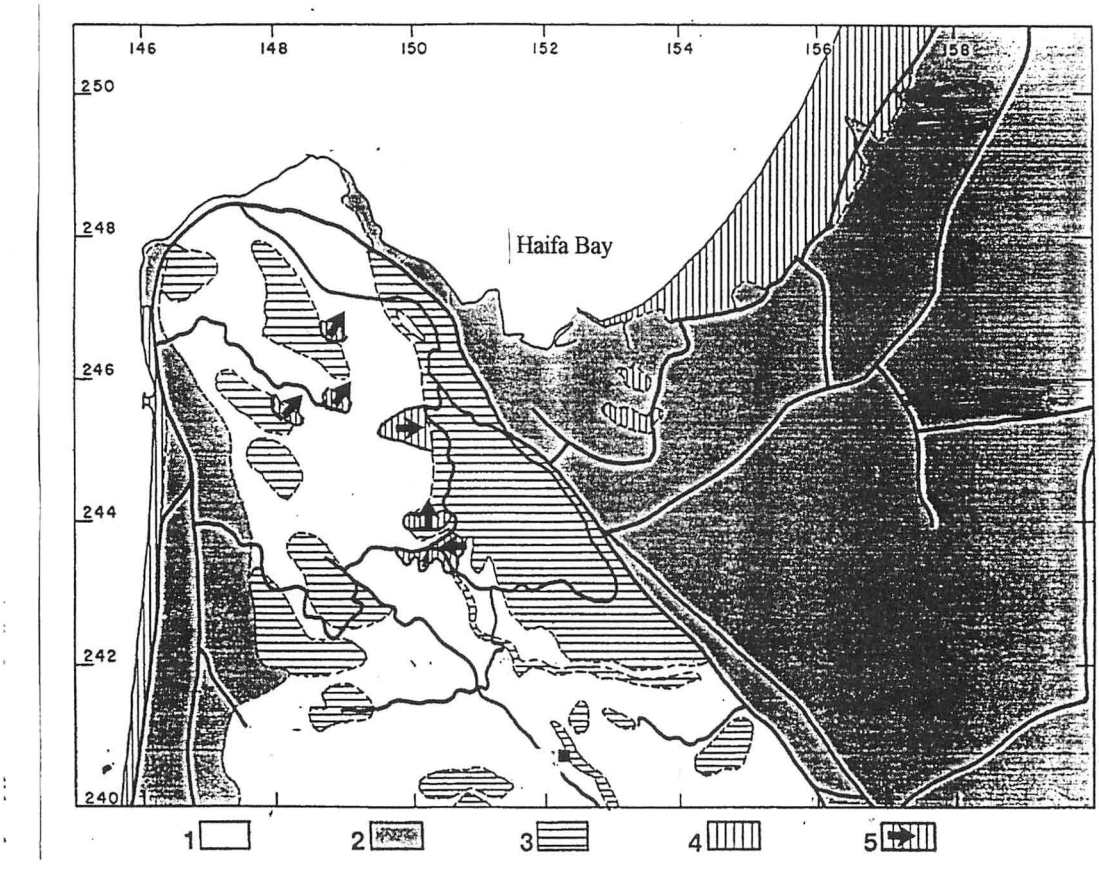

Figure 4.2 Ground condition map of the Haifa Bay area. 1 - chalk; 2 - unconsolidated sediment; 3 - limestone & dolomite; 4 - sands and dunes; 5 - unstable slopes (From Wachs and Siman-Tov, 1991).

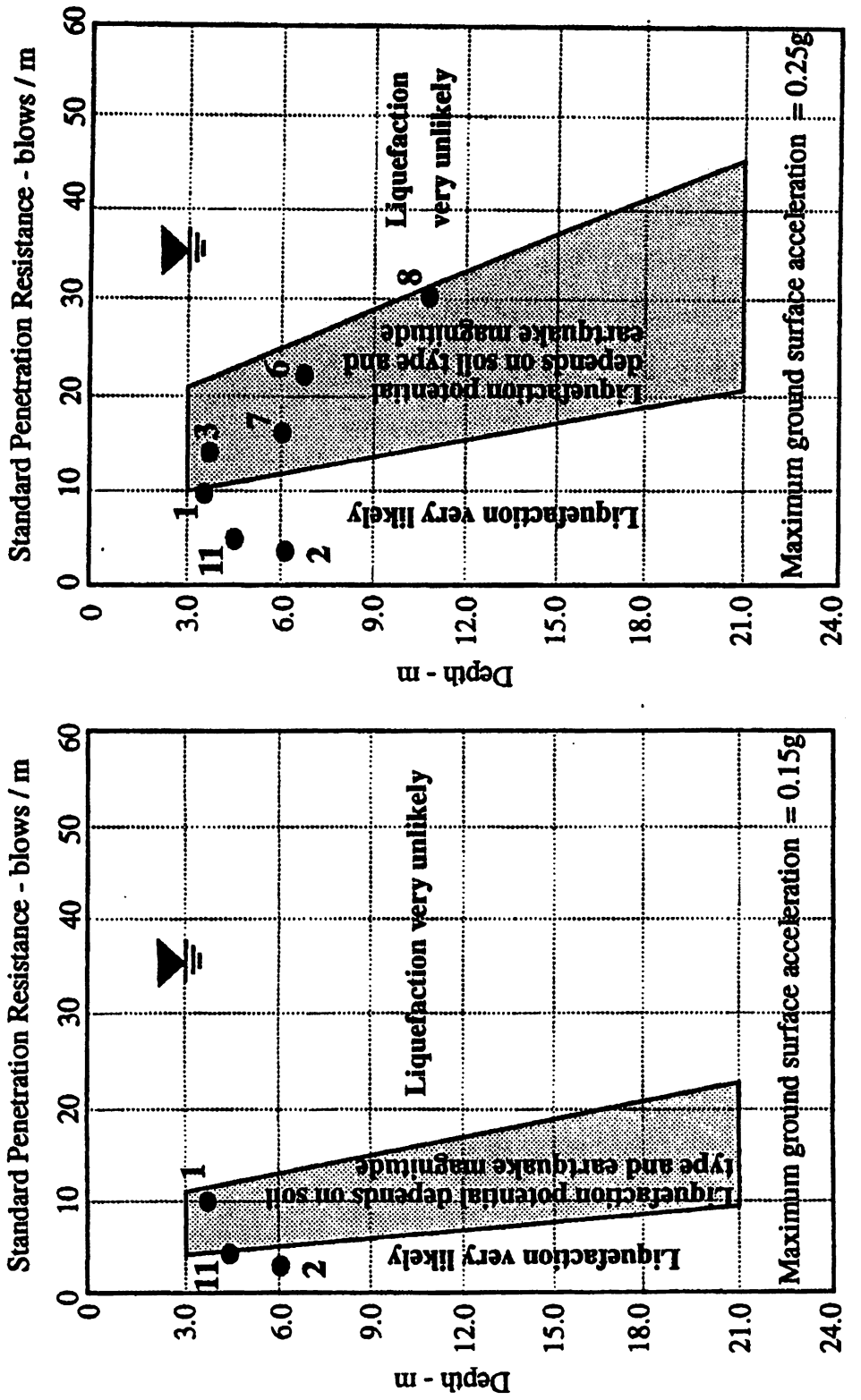

Figure 4.3 Liquefaction potential of sand deposit in Eilat. Numbers are locations of drilling sites (From Wachs and Zilberman, 1994).

Sims (1975) concluded that the correlation of deformational structures (paleoliquefaction features) with seismic events (rather than sedimentary processes) is based on the proximity to presently active seismic zones and the presence of potentially liquefiable sediments. This criterion applies in the proposed study areas (Haifa and Eilat).

Paleoliquefaction features, which exist in shallowly buried unconsolidated sediments, indicate that the areas were exposed to strong ground acceleration from nearby earthquakes, or more distant but stronger earthquakes, that occurred in the past. An absence of paleoliquefaction features in the subsurface is as significant as their existence. This indicates that ground acceleration levels or the duration of the shaking were not sufficient to liquefy the sediments (e.g. Munson et al., 1995). Therefore, in the time span represented by the sediments, the active faults in the vicinity did not produce great enough ground vibrations at the sites to cause liquefaction.

Dating the sediments, which were penetrated by the liquefiable sand, will indicate the maximum age of the seismic event(s) causing the liquefaction. If liquefaction does not exist, dating the base of the sediments will give a minimum time for a period in which liquefaction did not occur. This information provides a major contribution to our knowledge of the seismic history of the two areas.

5 Methodology

The objectives of the research (as discussed above) were achieved through combined study of: morphotectonic and paleoseismology study; engineering properties of the sediments; and detecting and analyzing paleoliquefaction features. We here describe, briefly, the different approaches (more details are given below in each specific chapter).

5.1 Geomorphology and tectonic studies

In order to evaluate the seismic hazard of the areas, the geomorphologic and tectonic settings of the regions were studied. This was achieved through the interpretation of old air-photos (predating vegetation cover and mad-made structures), field mapping, study of well logs and core drilling, and final integration of stratigraphic constraints on tectonic events.

5.2 Paleoseismology

Paleoseismological study was carried out along the Carmel Fault. In order to evaluate the paleoseismic activity of this fault during the Upper Pleistocene and Holocene the following approaches and studies were carried out:

1. Using the geomorphological information, we searched at the base of the mountain front that the Carmel Fault formed and inside it, in order to locate possible young faults, especially sites where thick soils and colluvial profiles are found.
2. We located several sites south of Galami and one near Kibutz Yagur. Previous Ground Penetration Radar study of Feigin (1994) at the site of Yagur showed several potential faults. At the site south of Galami a high resolution seismic line was conducted by the Geophysical Institute of Israel. The results were interpreted by Dr. Ilan Brunner.

3. As a result of the previous studies, several trenches were excavated across some of the lineaments. These trenches were usually 30-70 m long, up to 6 m deep and about 7-10 m wide.
4. The trenches' walls were described in details at a scale of about 1:20.

5.3 Paleoliquefaction

Liquefaction can affect relatively large areas and paleoliquefaction features, exposed on the surface, can be best seen in air photographs. According to Obermeier et al. (1990) and our personal observations (thanks to Dr. Buddy Schweig, USGS) more than 25 percent of the ground surface of an area of 16 square kilometers, located near New Madrid (US), which underwent liquefaction, is covered by vented sand. Therefore, it should be expected that where the sediments are homogeneous and spread on a relatively large area the liquefaction features will be widespread and spatially homogeneous. The geological setting of the two areas that were studied is similar in nature to the situation described above (Figures 4.2, 4.3). Unidentified spots resembling paleoliquefaction features were recognized by us, on old air photographs of Haifa area in the first stages of the study. This site and others in the Kishon area, Ein HaMifratz and Kefar Bialik were thoroughly investigated, as well as the Hotel area in Eilat (as previously also discussed by Wachs and Zilberman, 1994).

5.3.1 Drilling

Boreholes were drilled for establishing preliminary seismic and engineering characteristics of the soil profiles for use in the further research. The drilling was conducted using an Auger driller to a depth of up to 3 m. The drilling was carried on to ensure that the sediment cross-section has the potential make-up for our purpose.

5.3.2 Siting the trenches

There are no natural exposures of sand near the contact with the ground water table. The sand is exposed on the surface, but does not form vertical exposures. Trenching of the sand is the only method by which liquefaction features, if they exist, can be exposed in the subsurface. Locating and choosing sites for more detailed field investigations and trenching requires specific knowledge of the ground conditions and recognizing earthquake-induced liquefaction features on the surface.

In order to select potential sites for trenching, a detailed study of air photographs (identifying vented sand spots) and field reconnaissance was carried out. In addition, information from the subsurface (sand composition and density obtained from SPT, depth to ground water) was gathered in order to locate sites with conditions most favorable for seismically-induced liquefaction. This information was found in the literature and also in archives of the Technion soil engineering laboratory, and of foundation engineering companies.

We used the archive of the Technion, looking into some hundreds of shallow boreholes in order to locate the best sites for trenching. As a result of this study a long strip from Akko to the Kishon was found to be most suitable for further research. Sites for trenching were then chosen, mostly on the basis of site availability and trenching feasibility. Most of the area is populated, built or under construction. Finding undisturbed sites and getting permission to trench is not simple. We ended with three sites: (1) margins of Kibbutz Ein Hamifratz (2) Kefar Bialik – at Sivan Family back yard (thanks to Dr. Dorit Sivan, Haifa University) (3) on the Kishon River margins, inside territory of the Kishon Port.

5.3.3 Trenching

Trenching was done by backhoe to a depth of the ground water (up to 3 m) and to a length determined by the allowable conditions of the sites (man made structures, pipelines etc.). We trenched in Ein Hamifratz about 250 m total length, in Kefar Bialik – 150 m, and in the Kishon Port more than 1200 m (total length of trenches).

5.3.4 Trench investigations

Trench investigations (description, dating and engineering data acquisition) were carried out in each of the trenches. Our first goal, which was to find paleoliquefaction features, was not successful. Nevertheless, a number of trenches were mapped and described at each site.

1) Description of trenches:

The description of the section in each trench (at different scales) include stratigraphy and field relationships.

2) Dating the sediments:

In order to date the sediments we used the OSL method. See description below.

5.4 Engineering investigations in the trenches

In-situ geotechnical tests were performed in the trenches (on the base during excavation, and on the sides following excavation) in order to obtain an indication of the density of the sand layers, and the strength and compressibility of the confining clay layers, and to take undisturbed samples for laboratory testing. In situ testing relied mainly on static and dynamic pentration tests.

In order to carry out engineering tests in the laboratory for analysis of the liquefaction potential, we have developed (in collaboration with Dr. Mark Talesnik, the Technion) a technique to take undisturbed samples of the insitu sand, and from these, to prepare undisturbed test specimens in the laboratory for liquefaction testing. This technique involves taking block samples from the field, freezing them in the laboratory, and then coring cylindrical specimens from the frozen blocks for laboratory triaxial testing. This is in contrast to previous work (and commonly applied practice) whereby reconstituted samples are commonly tested, so ignoring the importance of in-situ soil structure. The present investigation represents improvements relative to standard procedure, since the tests were performed on undisturbed, rather than reconstituted specimens, providing a more reliable evaluation of the actual insitu behaviour. Furthermore,

strain measurements were performed locally, on the soil specimens, leading to greater accuracy in stress-strain-pore pressure relations.

5.5 Luminescence Dating

The luminescence techniques date the last exposure of mineral grains in the sediment to sunlight, which resets the luminescence signal (Aitken, 1988). After burial, the signal increases again with time as a result of the natural ionizing radiation emitted by radioactive isotopes (U, Th, and K) and by cosmic rays that penetrate the sediment. The equivalent dose (De) was determined by the single-aliquot method using the infrared emission at 880 nm for stimulation. External and internal dose rate were obtained. Dr. N. Porat conducted the measurements in the luminescence laboratory at the Geological Survey of Israel. For more details, see Porat et al. (1996, 1997).

6 Liquefaction potential

6.1 General

In order to evaluate the liquefaction potential of the Haifa and Eilat bay areas we used the following approaches:

1. Looking for paleoliquefaction features in these areas in order to learn about the future from the past evidence.
2. Geotechnical study of the sand (to be discussed in other chapter).

Looking for paleoliquefaction features was conducted in several steps:

1. Study of the area from air photos in order to locate potential investigation sites.
2. Locating potential sites for trenching:
    2.1 Geologically potential.
    2.2 Undisturbed sites.
    2.3 Sites that are not planned to be disturbed by man made structure.
3. Augering the site at several points in order to learn about the sub-surface sequence.
4. Obtaining permission to trench.
5. Trenching.
6. Detailed description of the trenches (scale of about 1:20).
7. Field engineering tests (shelby sampling, South African cone, standard penetration and cone penetrometer. Sampling for granulometric analyses
8. Dating the sequence using the OSL method.

In the Haifa Bay we surveyed the archive of the Technion and some private companies in order to learn about the subsurface of the Haifa Bay. This was done in order to identify the area of highest potential vulnerability to liquefaction.

6.2 Eilat Bay Area

The area of Eilat appeared promising in advance for finding paleoliquefaction features, as liquefaction was observed on man-made sand-fill following the 22 November, 1995 earthquake (Mw = 7.1). We noted that the liquefaction occurred only in man made fill, but were not surprised as this earthquake occurred about 150 km south of the city and thus the acceleration at the site was not high.

Augering was performed at 13 sites (Figure 6.1). Sand and clay were found in all of them (Figure 6.2). Based on the augering results, possible sites for trenching were located. Ground penetrating radar (GPR) profiles were applied in order to better determine the exact location and length for digging of trenches. This research was conducted by U. Bason. The GPR profiles indicated sites in which the continuation of subsurface layers was possibly interrupted, perhaps by paleoliquefaction phenomena (see few examples in Figures 6.3-6.5).

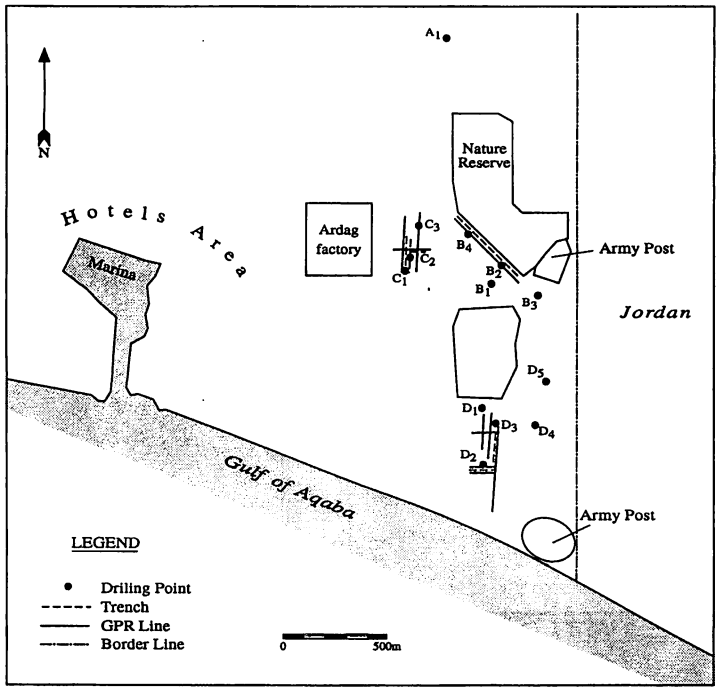

Figure 6.1. Location map of drilling points, Trenches and GPR lines in the northern shore of the Eilat Bay.

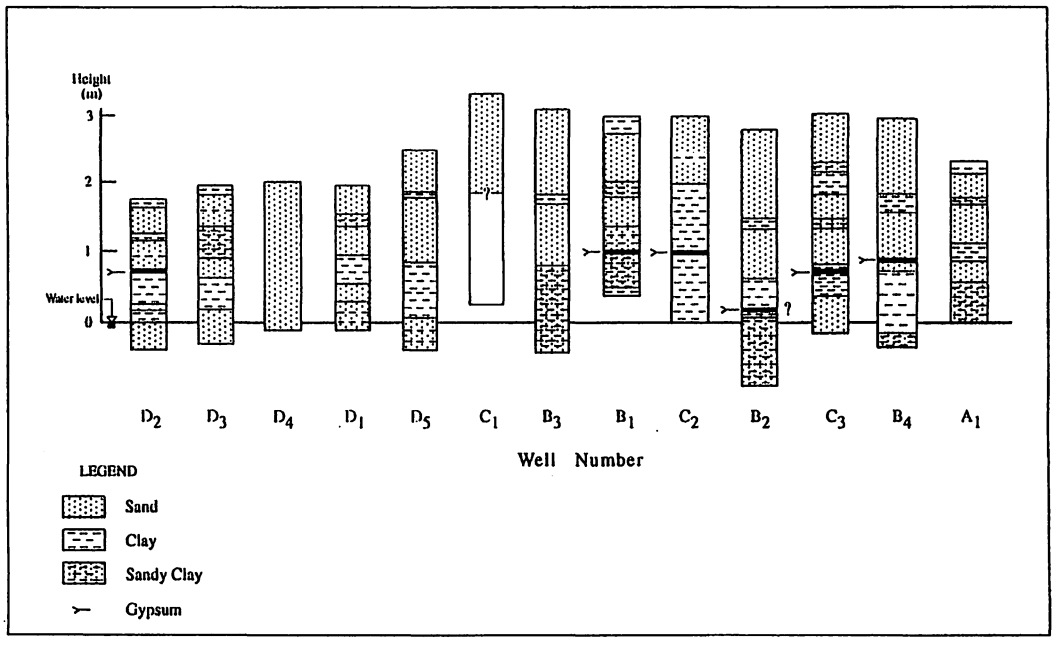

Figure 6.2. Columnar sections of the auger drillings in the northern shore of the Eilat Bay. For location see Figure 6.1.

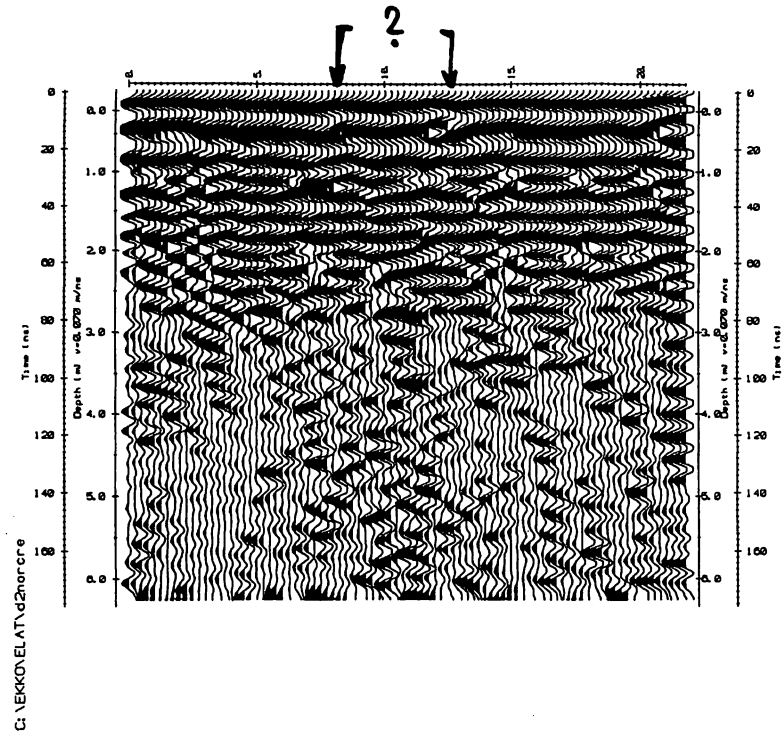

Figure 6.3. GPR image of line d2. The question mark marks the area where disturbances of the sequence were observed.

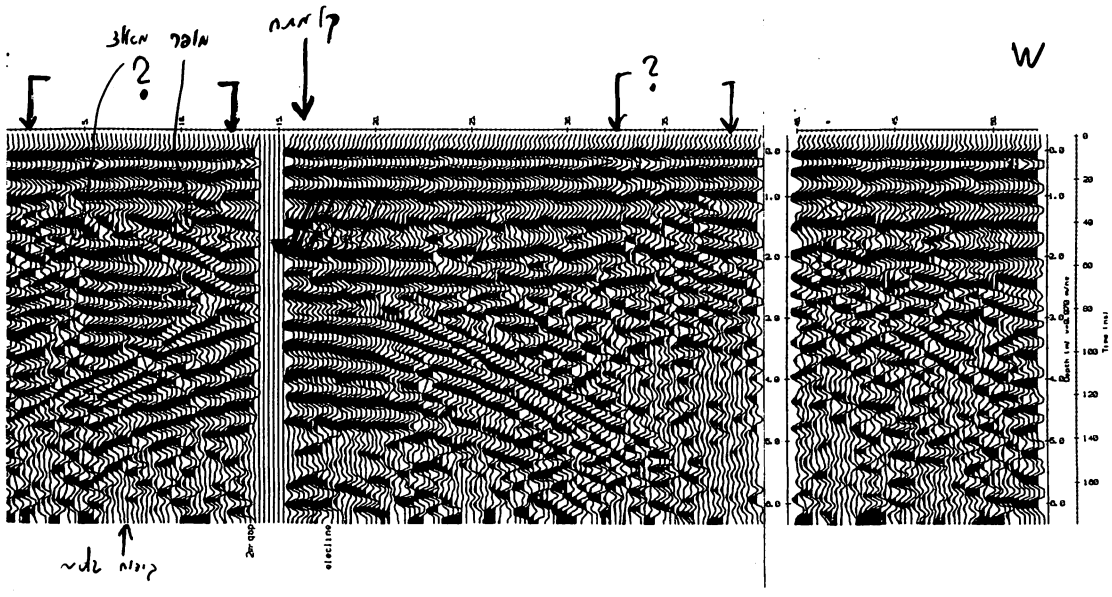

Figure 6.4. GPR image of line c2. The question mark marks the area where disturbances of the sequence were observed.

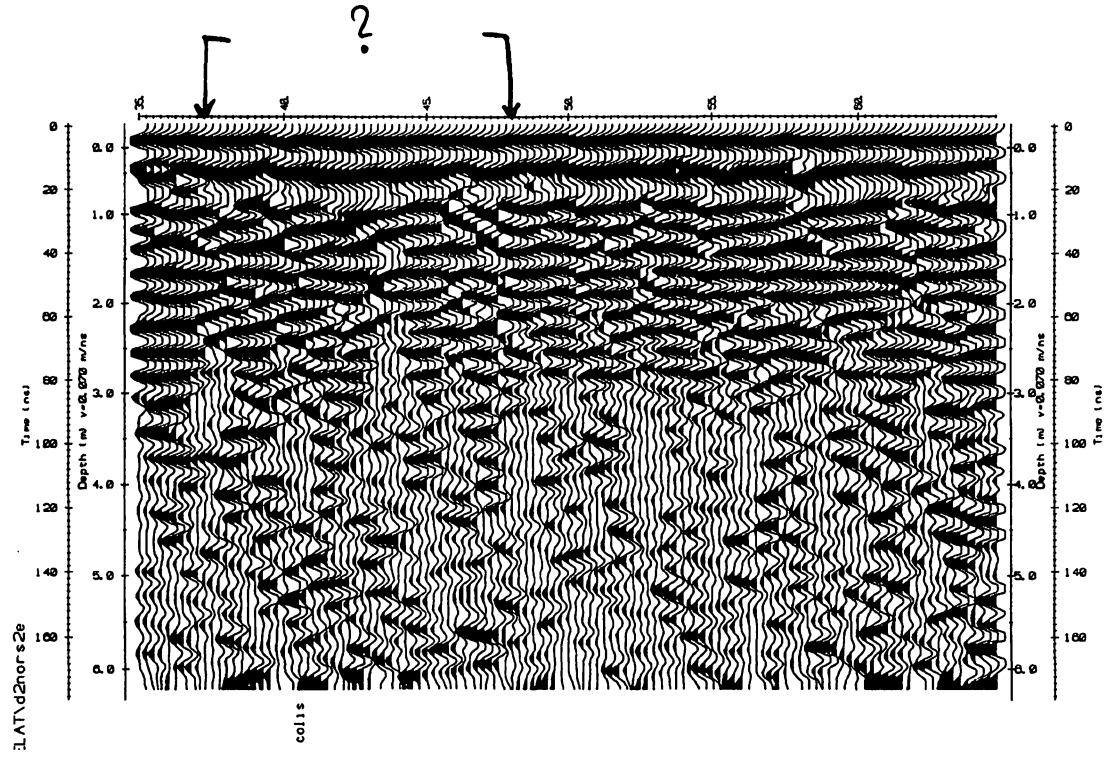

Figure 6.5. GPR image of line B. The question mark marks the area where disturbances of the sequence were observed.

Six trenches were excavated to groundwater depth (1.5-3 m), over a total length of about 200 m (Figure 6.1)(Figures 6.6, 6.7).

Figure 6.6. Trenching site C with a backhoe.

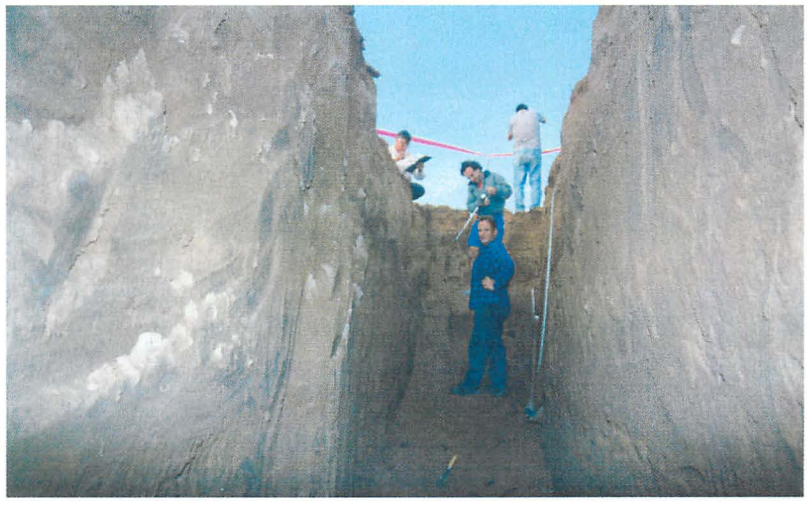

Figure 6.7. Trench at site C.

A detailed study of the trenches (Figure 6.8) revealed no evidence for paleoliquefaction features. In all six trenches, just above the groundwater level, a continuous undisturbed sandy clay layer exists. This layer was interpreted as unliquefiable, and the fact that it was not disturbed supports the assumption that the sand that does exist below, was probably never liquefied.

Figure 6.9. Engineering tests using the South African cone, within the trenches at site C, Eilat.

Figure 6.10. Engineering tests using a Penetrometer, within the trenches at site C, Eilat.

Figure 6.8. Careful study of the trench walls in order to identify paleoliquefaction features.

Undisturbed samples of sandy layers were collected from the trenches walls, to be analyzed and tested in the laboratory in order to determine the likelihood of, and the conditions for possible liquefaction of the sand.

In, and adjacent to the trenches, we also performed engineering tests, using South African cone (Figure 6.9) and penetrometer (Figure 6.10). This was done both above ground water table and below the water table. (See the Geotechnical Aspects chapter).

Samples collected from the auger were analyzed for the granulometric properties of the sand (Figure 6.11).

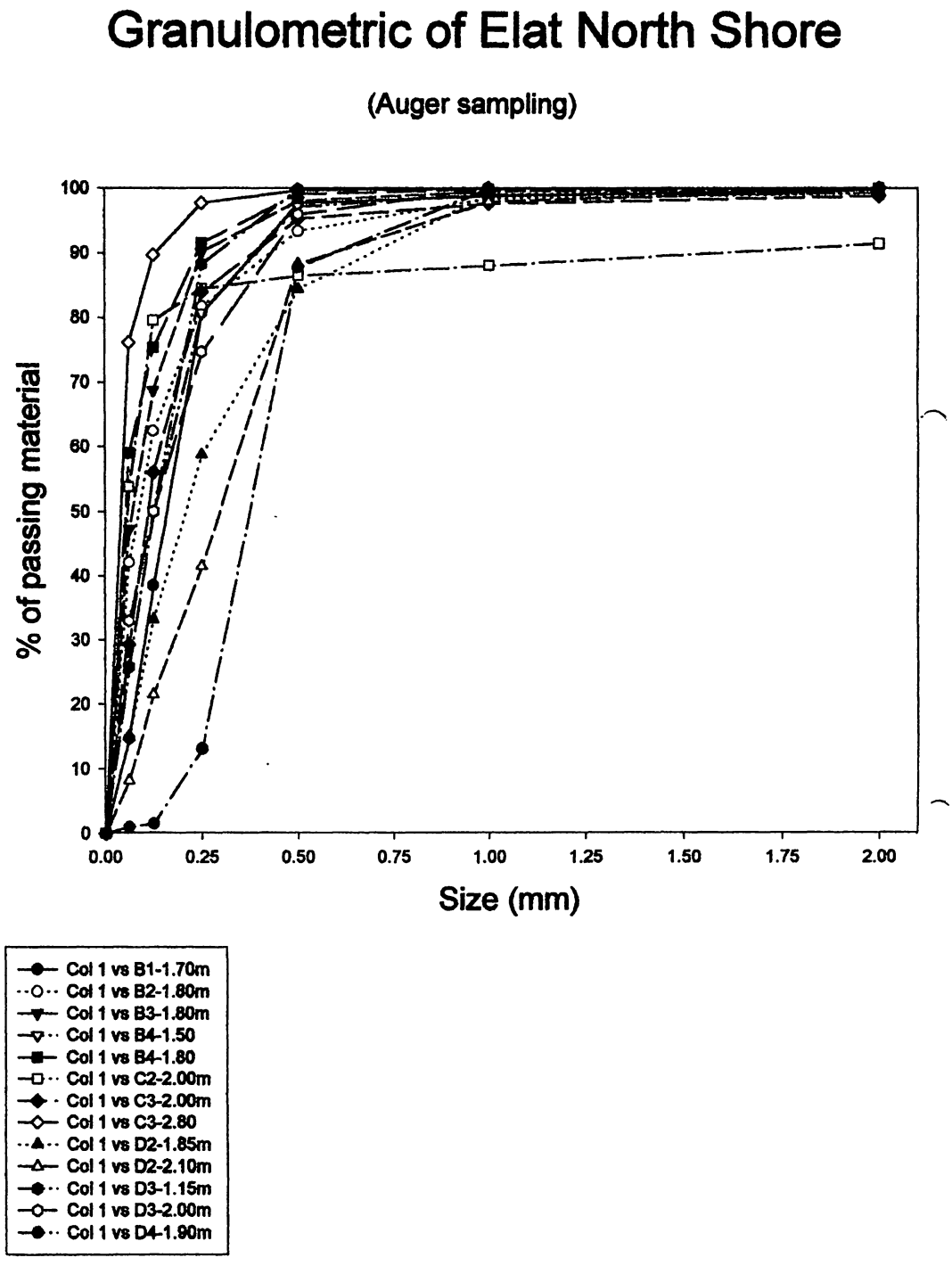

Figure 6.11. Granulometric tests of sand from the Auger drilling of Eilat Bay, Hotels area, northern shore. For location of the auger drillings see Figure 6.1.

It should be noted that basic conditions for liquefaction (sand and high level of the water-table) exist along the northern shore of the Gulf of Aqaba. Most of the "north shore" area (the hotels area) of Eilat is completely covered by man-made structures (hotels etc.). The only area that was vacant at the time that we carried out our tests was the one close to the Israel-Jordanian international border. At the present this area is also under construction and no further work can be carried on there.

It should be noted that although standard penetration tests (SPT) measurements and other evidence indicate a high potential for liquefaction, we did not find evidence of liquefaction occurrence. On the other hand we were able to perform our research only in a limited area, close to the international border.

It might be that this area is representative, and that, in fact, no paleoliquefaction features exist in Eilat. On the other hand, it is possible that paleoliquefaction feature do exist, but in other areas, where a study could not be done.

The geotechnical study aimed at investigating if the sand in the trenches is liquefiable at all, and if so, under what conditions (see below).

Thus, in order to evaluate the liquefaction seismic hazard of Eilat, we have to combine the lack of observation of paleoliquefaction features in the northern shore of Eilat with the results of the geotechnical study (see discussion).

6.3 Haifa Bay Area

Logs of a few hundreds of shallow drills where checked in the archives of several institutes (Technion and private companies).

Based of the evaluation of the logs, the boreholes were divided into three groups:

(1) Boreholes showing the presence of interfingering layers of sand and clay in the upper five meters. These sites were interpreted to have the highest potential for the observation of paleoliquefaction features.

(2) Boreholes showing predominantly sand layers were classified as having the next higher potential for observing paleoliquefaction features.

(3) Boreholes that encountered only clay in the top five meters were interpreted to have the lowest potential for the formation and observation of paleoliquefaction features.

Compilation of the data led us to produce a map, which describes the likelihood for liquefaction in the Haifa Bay area (Figure 6.12). The map shows that a strip running from north to south, several km east of the Mediterranean Sea shore, and the areas near the estuary of Kishon and Na'aman rivers have the highest potential for finding paleoliquefaction features.

This classification was confirmed by visiting construction sites, ditches, and the banks of the Kishon and Na'aman rivers. The field observations also served to indicate which sites could not be further investigated because of the presence of buildings and other structures. The remaining sites were thus identified for further investigation.

We visited each of the potential sites in order to see if trenching is technically possible. The studied area is located in the very dense populated area of the "Kerayot". Many of the potential sites are at present under roads, buildings, industrial areas etc. Therefore, not many potentially interesting sites were feasible for our purposes.

The sites which were still potential for trenching were augered by motorized auger and we looked for sites with interfingering of sandy and clay layers.

To summarize: in order to select a site for trenching it should fulfill the following criteria:

1. The site should be located in the "potential area" of Figure 6.12.
2. The site is not covered by man-made constructions and has not been previously disturbed.
3. Augering findings should show sand below a shallow clay cover.

According to the findings we selected three sites for trenching: Kibbutz En Hamifraz, Kefar Bialik and the Kishon Port (Figure 6.12)

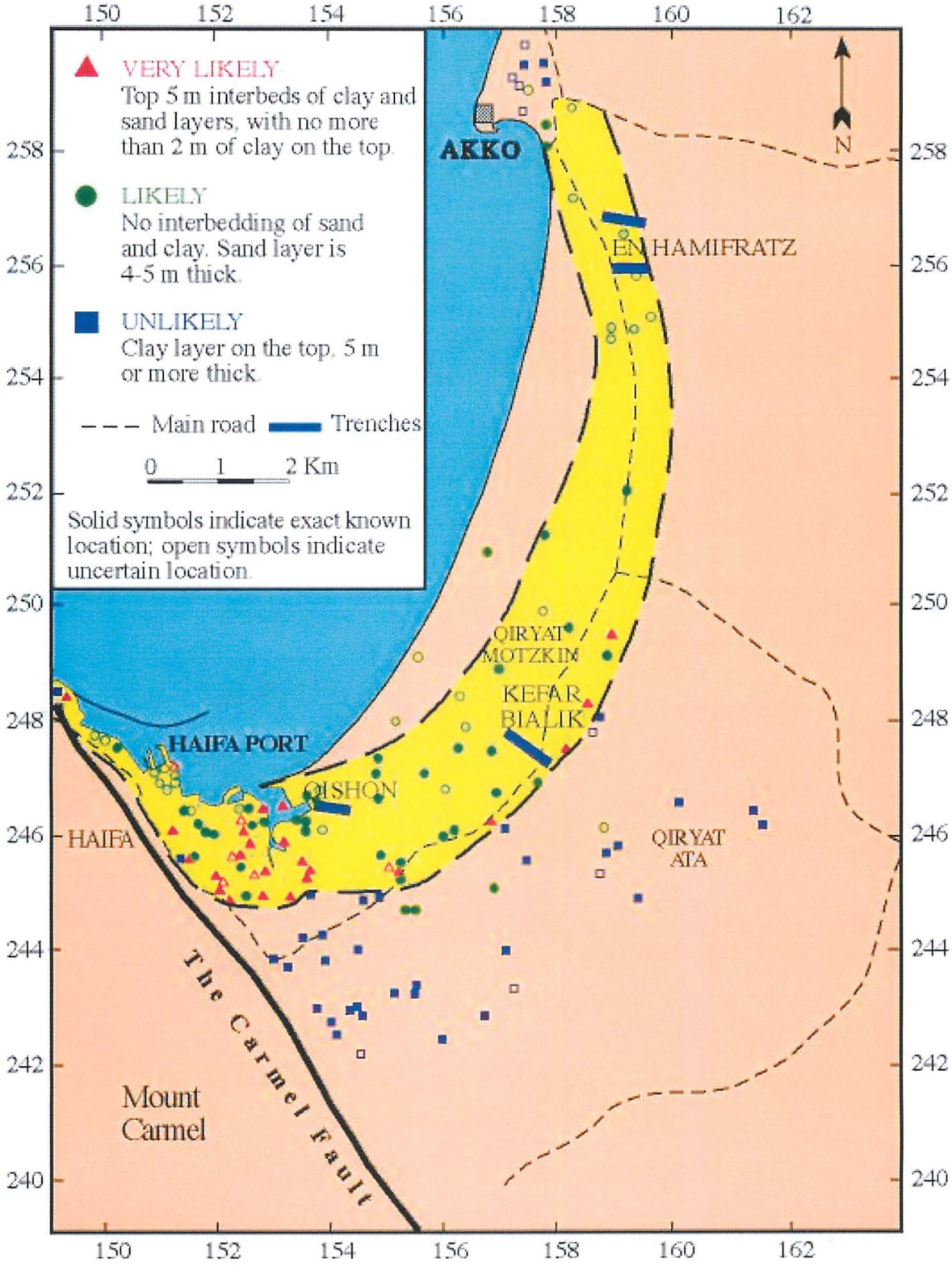

Figure 6.12. General likelihood for liquefaction in the Haifa Bay as deduced from shallow boreholes data. The yellow strip marks the most likely area for liquefaction.

6.3.1 Results of Trenching

6.3.1.1 En Hamifraz

En Hamifraz is located in the northern part of the Haifa Bay area (Figure 6.12). We have augered at that site and found that the upper part of the section is composed, in general, of three units:

(1) Topsoil – the top 30-90 cm

(2) A clay layer with sand and some pebbles – 50-250 cm thick

(3) Clean sand – 30-150 cm thick; the lower part of the exposed trench; above the water table and below it. The lower part of the unit is not exposed.

We excavated trenches at two sites in Kibbutz En Hamifraz.

A. North of the Kibbutz, 200 m NE of the barn, in the edge of the field. We excavated several parallel and crosscutting trenches over a total length of 200 m (Figures 6.13-6.16). The cross section of one of these trenches is described in Figure 6.17. We have divided the main three units into sub-units in order to get a better picture of the details. In this location an archaeological site was exposed when the trenches were opened, and numerous pieces of broken clay pottery were found. The archaeological site is from the six century C.E. (Motti Aviam, personal communication). The archaeological findings are located mainly in the eastern part of the site.

Figure 6.13. Ein HaMifratz Northeastern trench. The groundwater level is here at depth of 3 m.

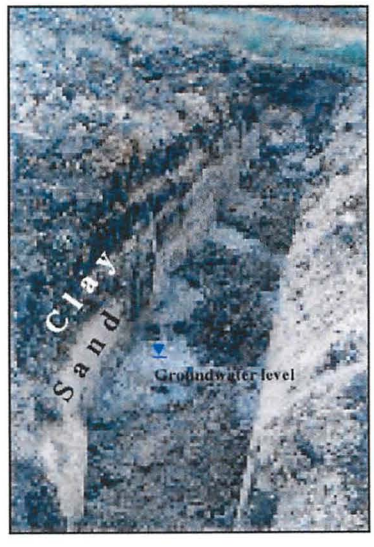

Figure 6.14. Ein HaMifratz North trench. The groundwater level is here at depth of 3.8 m. Clay covers the sandy section below.

Figure 6.15. En HaMifratz northern trench – general view. The sequence is composed of clean sand cover by soil. The transition is sharp. No paleoliquefaction features were found.

Figure 6.16. En HaMifratz northern trench. A clay insertion within the clean sand is visible. All of these features were found to be the result of bioturbation of the section.

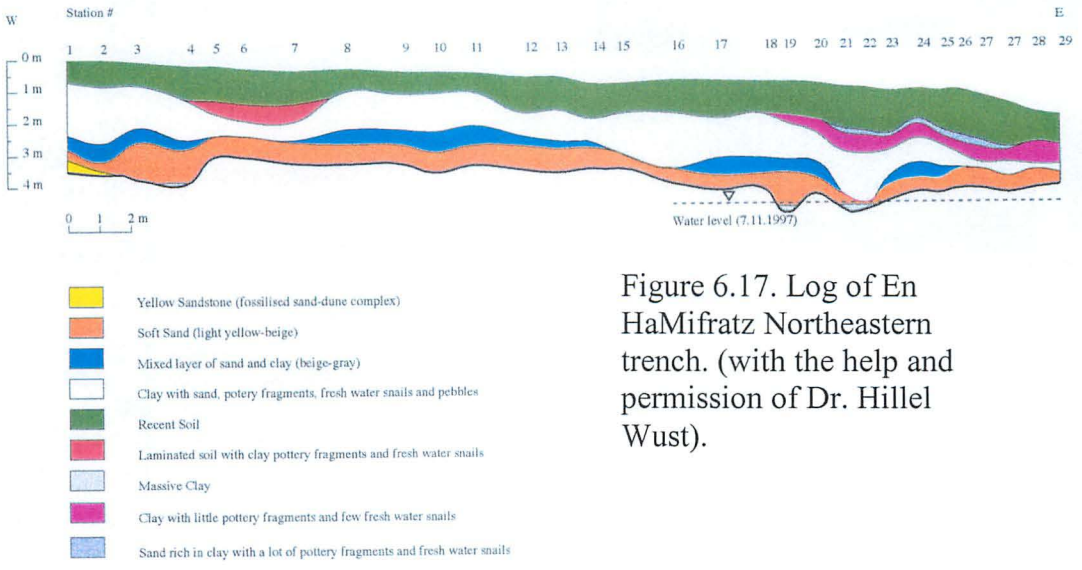

Figure 6.17. Log of En HaMifratz Northeastern trench. (with the help and permission of Dr. Hillel Wust).

B. South of the Kibbutz, near the "Wedding Garden". We have trenched here two parallel trenches over a total length of 250 m (Figures 6.18-6.21). In this case, the trenches were logged using the general division to the main three units (Figure 6.22).

Figure 6.18. Ein HaMifratz Southern trench.

Figure 6.19. Ein HaMifratz Southern trench. The sand here contains more clay but still is very clean. No liquefaction features were observed.

Figure 6.20. Ein HaMifratz southern trench. See the soil cover and the continuous section.

Figure 6.21. Ein HaMifratz southern trench. Some sea-water mega fossils were found in the section. The fossils were not indicative for dating.

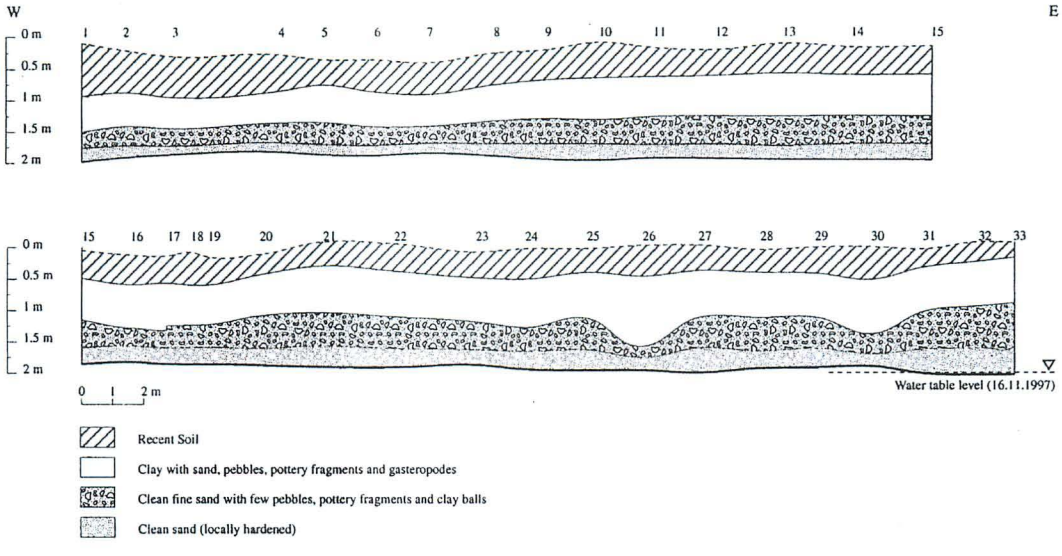

Figure 6.22. Log of the En HaMifratz southern trench (see text).

6.3.1.2 Kefar Bialik

Kefar Bialik is located on the eastern side of the strip that contains the potentially liquefiable area. East of this strip the upper part of the section contains at least 5 m of clay horizon. Therefore, we predicted that at Kefar Bialik we would find a site in which sand appears in the west, clay in the east, with an interfingering area in between. We first augered the site and then excavated several trenches in different directions, over a total length of 117 m. We logged several walls and carefully looked for paleoliquefaction features. A trench that was excavated from west to east showed the predicted soil profile (Figure 6.23).

The section in the western side of the site is the following (from top to bottom):

(1) Upper sandy layer, contains a lot of clay, with indications for a soil process – top 15 cm.

(2) White sand, small grain size, well consolidated. Few fossils – 30 cm.

(3) Yellow, clean sand. No fossils, unconsolidated – 125 cm above water table. 40 cm above the water table, a layer containing calcite concretions are found in most parts of the trench.

We augered in the bottom of the open trench into the unit which is at present below the water table. The augering was done through the center of a pipe to support the drillhole in order to prevent its collapse. 130 cm of the section below the water table was augered and the material was found to be clean, yellow sand.

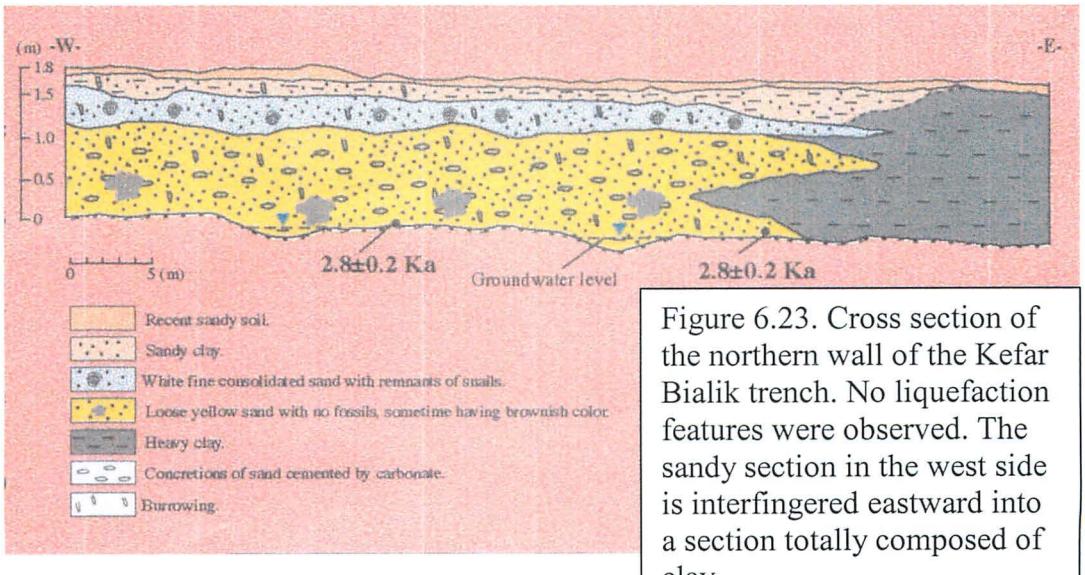

Figure 6.23. Cross section of the northern wall of the Kefar Bialik trench. No liquefaction features were observed. The sandy section in the west side is interfingered eastward into a section totally composed of clay.

6.3.1.3 Kishon Port

The Kishon Port is a relatively large area which is undisturbed. We located a site north of the Kishon River just south of the Port Authorities, which is not disturbed (Figure 6.24). Augering showed that the section is mostly sand and that the water table here is about 1 m deep. We trenched for a total of about 1000 m in order to look for liquefaction. We carefully surveyed the trenches, but did not log any as the section is the same everywhere.

Figure 6.24. One of the trenches in the Kishon site. The section is composed of loose sand. The ground water level is 1.4 m deep. Mount Carmel is in the background.

6.3.2 Paleoliquefaction findings

We have checked the trenches carefully in order to identify paleoliquefaction features. In several places, we noted that the section is not continuous, or has some clay insertions within the clean sand (e.g. Figure 6.16). We found all of these features as being the result of bioturbation of the section, but found no liquefaction features in any of these trenches.

6.3.3 OSL Dating

Samples from different trenches were dated using the OSL method by Dr. N. Porat from the Geological Survey. The results are:

Sample	Depth (m)	Water (%)	K KF (%)	K (%)	U (ppm)	Th (ppm)	Int. β	ext. α	ext. β	Ext. γ +cos.	De (Gy)	Total dose	Age (ka)
EM-1	2.1	20	11.5	0.2	1.3	0.9	527	87	249	347	4.4±0.2	1210±65	3.7±0.2
KBN-2	1.6	20	11.6	0.4	0.5	0.8	532	42	312	328	3.4±0.1	1214±64	2.8±0.2
KBS-2	1.6	18	11.0	0.4	0.4	0.7	504	35	312	318	3.3±0.2	1168±62	2.8±0.2
QSE	1.4	12	10.1	0.4	0.4	0.9	463	38	297	324	3.5±0.2	1122±53	3.2±0.2
QSW	1.4	18	11.6	0.5	0.4	0.9	532	38	358	346	3.2±0.2	1274±58	2.5±0.2

De measured using infrared stimulated luminescence on alkali feldspars and the Single Aliquot Added Dose protocol. Grain size for all samples is 150-177 μm. All dose rates are in μGy/a. γ calculated from radioisotope contents, the cosmic dose estimated from burial depth.

The sites are:

EM1: En HaMifratz, at the northern site (special hole, not in trench), depth 2.10 m.

KBN-2: Kefar Bialik, northern trench, two samples, depth 1.60 m.

QSE: Qishon Port, eastern trench, depth 1.40 m.

QSW: Qishon Port, western trench, depth 140.

At all sites samples were collected at the base of the trench.

According to the OSL dating of the sand in the bottom of the trenches is from the Upper Holocene, 3.7-2.5 ky.

6.3.4 Discussion

As shown above, we did not find any liquefaction features in any of the trenches that were examined. We checked three areas, which are located in the northern, central and southern part of the Haifa Bay, in the area that we concluded has the highest potential for liquefaction.

It should be emphasized that the trenched sections are about 3-4 meters deep, and not below the present water table. Therefore, we may have missed any liquefaction features that exist below the present water table. But, as the water table level changes, as can be seen from the section, we believe that the present exposed section has been, and still is at times, under water (which is essential for liquefaction to occur). Moreover, we believe that even if liquefaction had occurred at a depth greater than that of the trenched section, we would see liquefaction features above the liquefied layer.

Therefore, as we have not identified any liquefaction features at all the three locations (En Hamifraz, Kefar Bialik, Kishon Port), we assume that liquefaction did not occur, at least at these specific sites.

The age of the samples from the bottom of the trenches can assist in assuming the minimum age that the area did not suffer from liquefaction.

Therefore the En HaMifratz area did not suffer from liquefaction during the last 3.7 ky, the Kefar Bialik area did not suffer during 2.8 ky and the Kishon area during the last 3.2 ky. These are minimum ages. If we assume that the whole area would suffer from liquefaction whenever it occurs, then the maximum found age, 3.7 ky, would be the minimum period during which the Haifa Bay area did not suffer from liquefaction.

7 Geotechnical aspects

Geotechnical investigations were carried out both in Eilat and in the Haifa Bay area. In the following, the results of the studies performed at each site are reported separately, and then general comments and conclusions are presented.

7.1 Eilat

7.1.1 In-situ investigations

7.1.1.1 SPT borings

In an earlier investigation (Wachs and Zilberman, 1994), 12 exploration borings were carried out, at locations shown in Figure 7.1. Standard penetration tests (SPT) were performed at regular intervals in each of the borings, and disturbed samples were extracted for gradation testing in the laboratory.
It is recognized that liquefaction is most problematic in soils containing no fines, or a small amount of fines (Seed et al., 1985). Consequently, for the purposes of the present research, focus was placed on SPT tests carried in soils containing less than 20% fine soil (smaller than 74 microns). Figure 7.2 shows the percent of fines as a function of depth for each of the borings, as well as relative density, as implied by the SPT results, in the zones of less than 20% fines. Relative density, Dr, was implied from SPT blow counts using the correlations for clean sands developed by Gibbs and Holtz (1957), which were curve-fitted by Alpan (unpublished) to give the empirical relationship:

$$1000\ N = (0.00716 P_v' + 0.66)\ Dr^{2.24} \qquad (1)$$

where N is the SPT blow count, and P_v' is the overburden pressure in kPa.

The following observations may be made from Figure 7.2:

(a) The insitu soils generally include a significant percentage of fines, commonly more than 20%. In a number of the borings (B1, B2, B3, B4,

B8, B9, B11) the fines content increases with depth, starting from a depth of between 6 – 10 meters.

(b) For the relatively clean sands, implied relative densities show large variations; values greater than 100%, as shown in the figures, are obviously not relevant, and indicate the non-exact, empirical nature of the N – Dr correlation equation (1). At the same time, it is noted that 70% of the tests imply relative densities of greater than 80%, indicating that overall, the sands at the site would be considered to be dense.

(c) The lowest implied relative densities (about 55%) were observed at about 3.5 m depth in borings B3 and B5. Sands at this relative density could be potentially liquefiable. Implied relative densities of between 60% - 70% were also measured in borings B3 (at 3.9 m), B4 (at 5.6 m), B6 (at 7.3 m), B7 (at 6.3 m), and B12 (at 3.25 m, 8.22 m, and 8.72 m). All of these could, possibly, liquefy under a strong earthquake input. The most dangerous cases would be the shallower sands. Considering all of this data, it is noted that a number of relatively low implied densities were measured in the top 4 m of the profile, justifying further investigation of this zone.

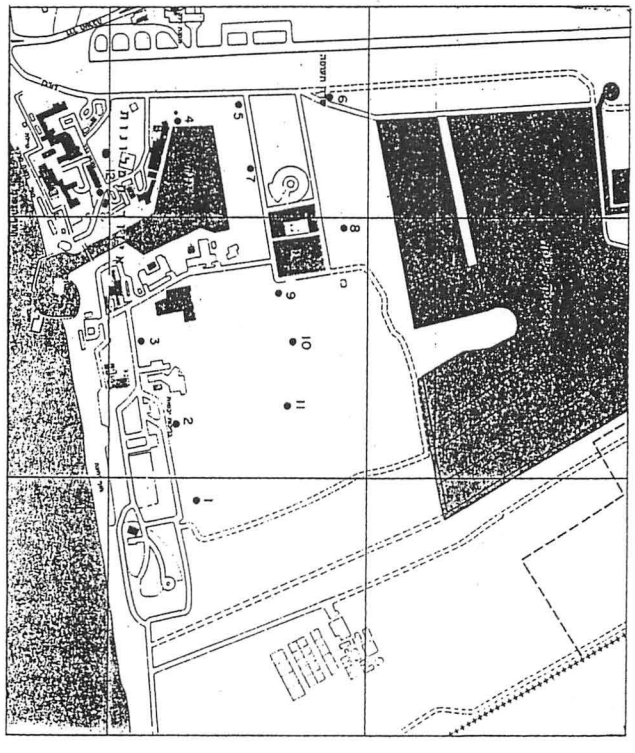

Figure 7.1. Location map of Standard penetration tests in the Hotels area in Eilat (from Wachs and Zilberman, 1994)

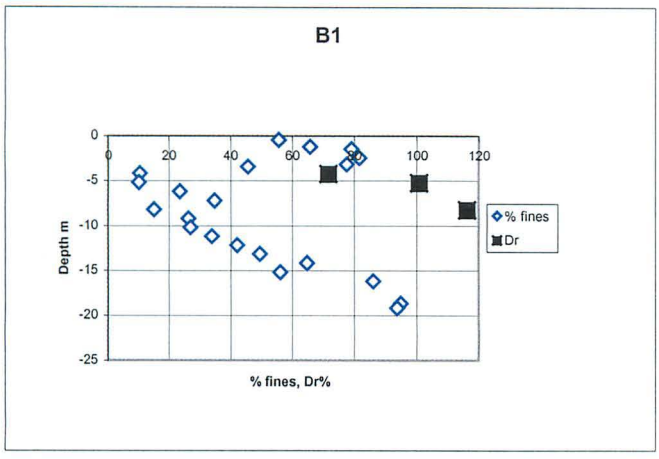
B1
0
0 20 40 60 80 100 120
-5
-10
-15
-20
-25
Depth m
% fines, Dr%
% fines
Dr

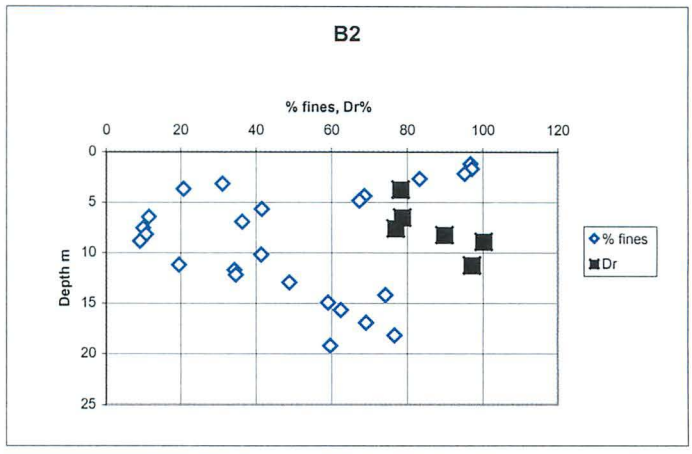
B2
% fines, Dr%
0 20 40 60 80 100 120
0
5
10
15
20
25
Depth m
% fines
Dr

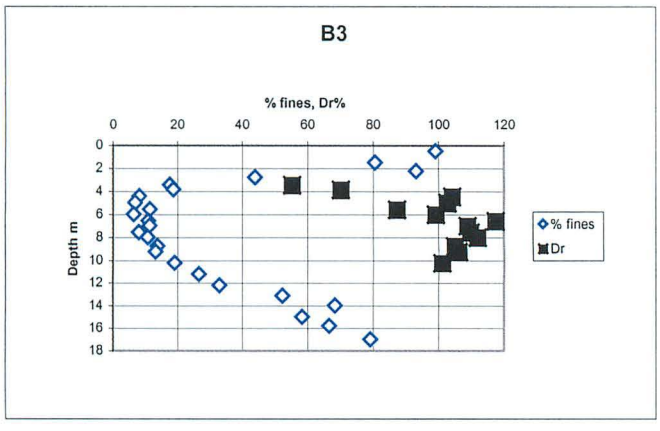
B3
% fines, Dr%
0 20 40 60 80 100 120
0 2 4 6 8 10 12 14 16 18
Depth m
% fines
Dr

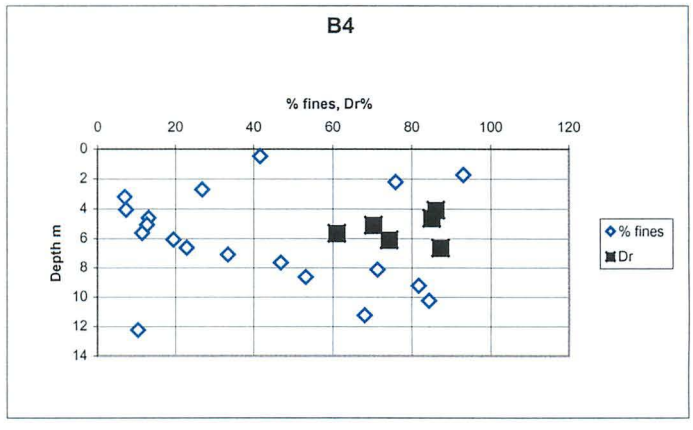
B4
% fines, Dr%
0 20 40 60 80 100 120
0 2 4 6 8 10 12 14
Depth m
% fines
Dr

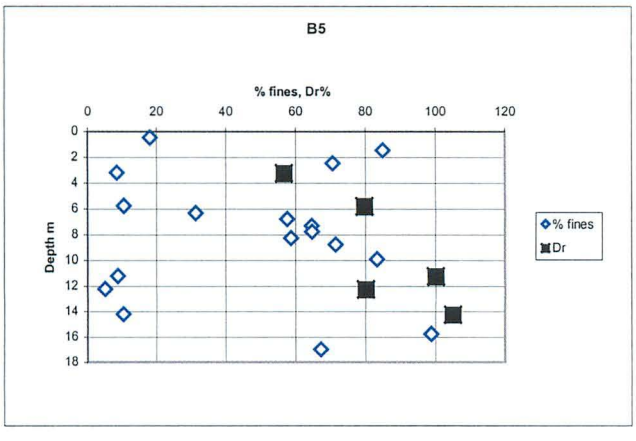
B5
% fines, Dr%
0 20 40 60 80 100 120
0 2 4 6 8 10 12 14 16 18
Depth m
% fines
Dr

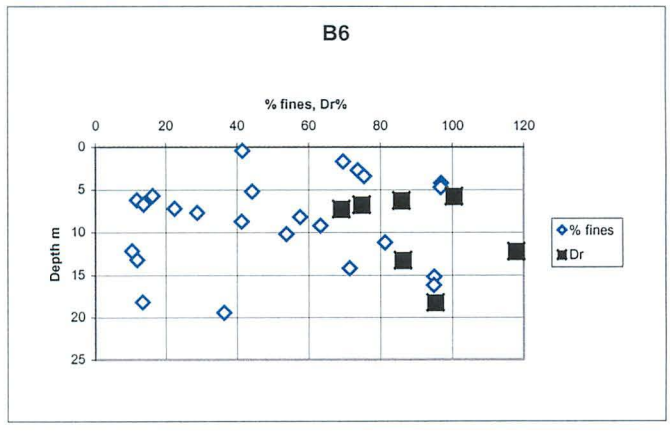
B6
% fines, Dr%
0 20 40 60 80 100 120
0 5 10 15 20 25
Depth m
% fines
Dr

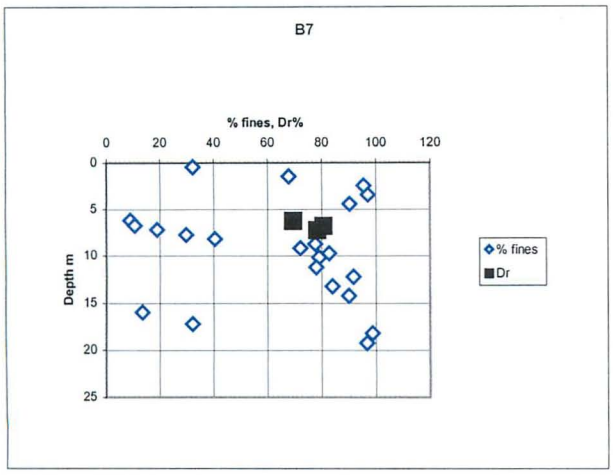

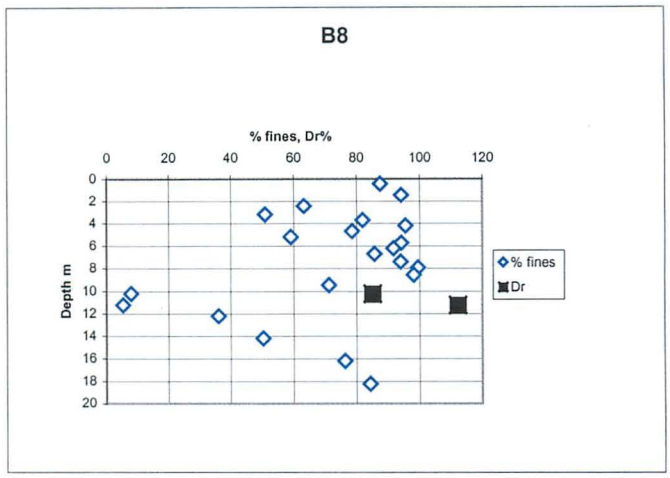

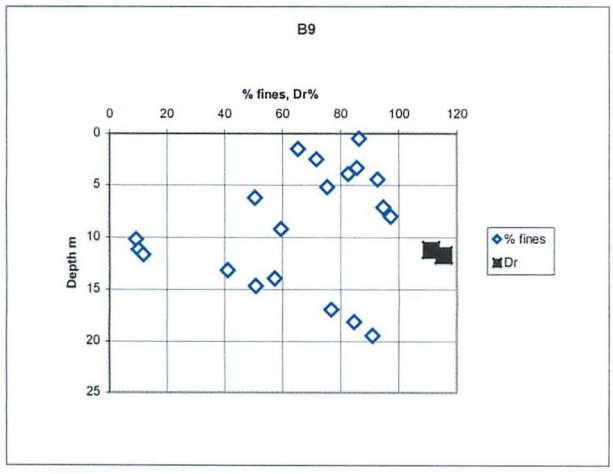

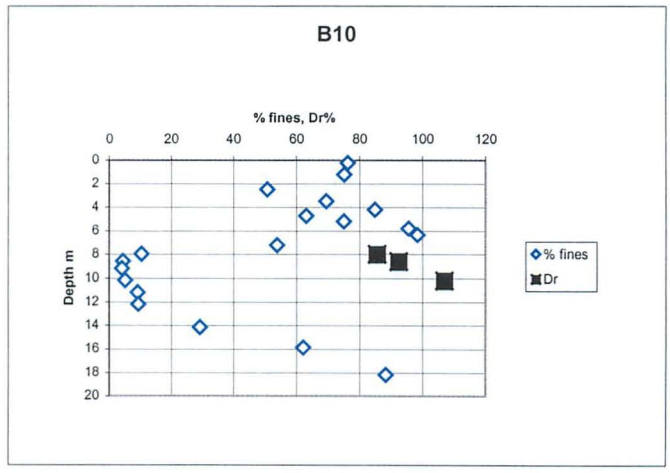

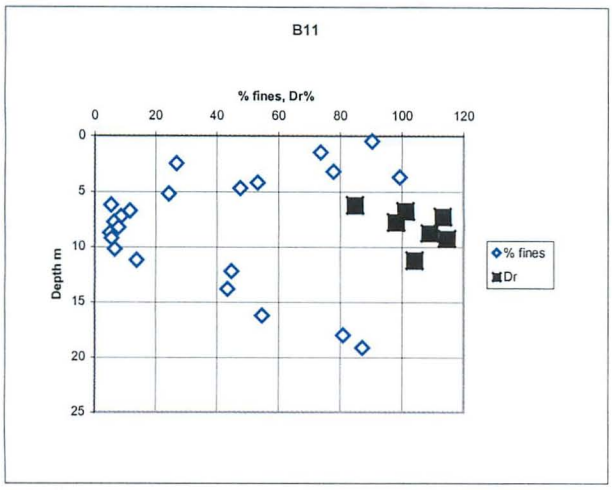

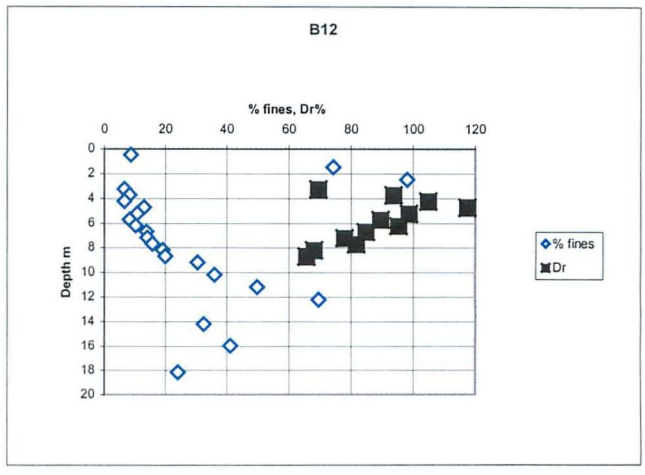

Figure 7.2 Percent fines and relative density - samples from borings at Eilat site

An alternative, and more quantative approach to the use of SPT data for estimating liquefaction potential was initiated by Seed et al. (1984). They compared the normalized SPT resistance, $(N_1)_{60}$, and the estimated cyclic stress ratio at sites where liquefaction was, or was not observed in earthquakes of M = 7.5, to determine the minimum cyclic stress ratio at which liquefaction could be expected for a given SPT resistance.

$(N_1)_{60}$ is defined as the standard penetration resistance normalized to an overburden pressure of 100 kPa, and to an energy ratio of 60% (the ratio of the actual energy delivered by the hammer to the theoretical free-fall energy). $(N_1)_{60}$ may be calculated from the SPT blow count, N, using the following formula:

$$(N_1)_{60} = N. C_N. ER/0.6 \qquad (2)$$

where CN is the overburden correction factor, given by Liao and Whitman (1986) as:

$$C_N = (p_a/p_v')^{0.5} \qquad (3)$$

Where p_a is atmospheric pressure, and p_v' is effective overburden pressure.

ER is the actual energy ratio specific to the SPT equipment being used. It is estimated that for the SPT equipment commonly used in Israel, the energy ratio is about 60%.

Figure 7.3(a) shows Seed et al's comparisons for clean sands, containing less than 5% fines; the curve divides between cases in which liquefaction did or did not occur. For any particular value of $(N_1)_{60}$, values of cyclic stress ratio falling right of the curve would not be expected to cause liquefaction, while points falling left of the curve would indicate potential liquefaction. Figure 7.3(b) shows similar (b) comparisons for cases of sands with up to 35% fines. Examination of these figures shows that for $(N_1)_{60} > 30$, no liquefaction would be expected for any sandy soils.

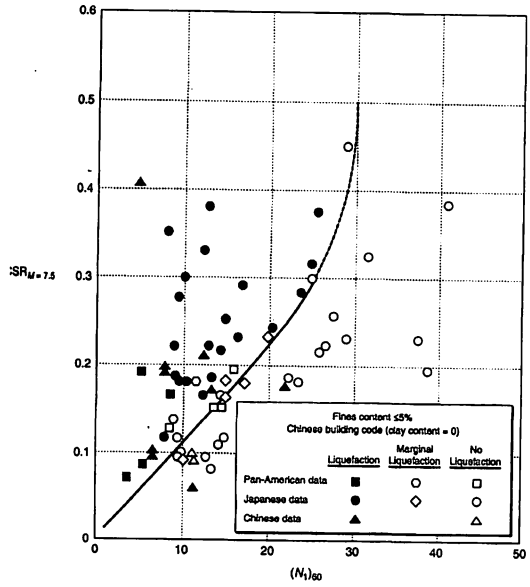

Figure 9.30 Relationship between cyclic stress ratios causing liquefaction and $(N_1)_{60}$ values for clean sands in $M = 7.5$ earthquakes. (After Seed et al. (1975). Influence of SPT procedures in soil liquefaction resistance evaluations, *Journal of Geotechnical Engineering*, Vol. 111, No. 12. Reprinted by permission of ASCE.)

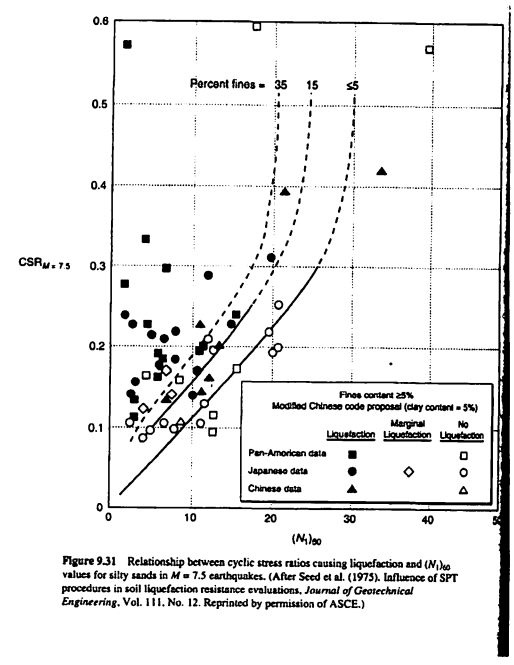

Figure 9.31 Relationship between cyclic stress ratios causing liquefaction and $(N_1)_{60}$ values for silty sands in $M = 7.5$ earthquakes. (After Seed et al. (1975). Influence of SPT procedures in soil liquefaction resistance evaluations, *Journal of Geotechnical Engineering*, Vol. 111, No. 12. Reprinted by permission of ASCE.)

Figure 7.3 Use of SPT for estimating liquefaction potential (Seed et al., 1984)

The data used to prepare Figures 7.3(a) and 7.3(b) has been updated since it was collected by Seed et al.; Youd and Idriss (2001) showed updated design curves (Figure 7.4). Rauch (quoted in Youd and Idriss, 2001) curve fitted the design curve for clean sand, obtaining the following equation, which is relevant for $(N_1)_{60} < 30$:

$$CRR_{7.5} = 1/[34-(N_1)_{60}] + (N_1)_{60}/135 + 50/[10(N_1)_{60} + 45]^2 - 1/200 \quad (4)$$

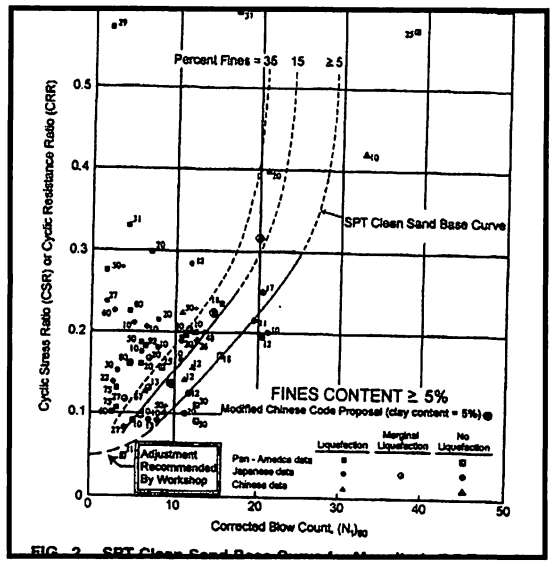

Figure 7.4. Use of SPT for estimating liquefaction potential (Youd & Idriss, 2001)

The effect of fines has been taken into account by Idriss and Seed (quoted in Youd and Idriss, 2001), who suggested the following relationship between the the actual value of $(N_1)_{60}$ for the sand with fines, and an equivalent value for clean sand, $(N_1)_{60cs}$:

$$(N_1)_{60cs} = \alpha + \beta(N_1)_{60} \qquad (5)$$

Idriss and Seed suggested the following values for α and β:

Fines content % (FC)	α	β
<5	0	1
5 - 35	$\text{Exp}[1.76-(190/FC^2)]$	$[0.99+(FC^{1.5}/1000)]$
>35	5	1.2

Figurs 7.3 and 7.4 were developed on the basis of data obtained from magnitude 7.5 earthquakes. Correction factors for other magnitudes have been suggested by several researchers, based on observations of occurrence or non-occurrence of liquefaction during earthquake events. Ambraseys (1988) suggested that the critical cyclic stress ratio, CRR, appearing in Figures 7.3 and 7.4 should be corrected by the following factors for other magnitude earthquakes:

Magnitude	Correction Factor
5.5	2.86
6.0	2.2
6.5	1.69
7.0	1.3
7.5	1.0
8.0	0.67

The equivalent, uniform cyclic stress ratio expected to develop at any depth during a given earthquake may be estimated, approximately, using a simplified approach suggested by Seed an Idriss (1971), from the following equation:

$$(\tau/\sigma_v') = 0.65(a_{max}/g)\,(\sigma_v/\sigma_v')\,r_d \qquad (6)$$

where τ is the cyclic shear stress, σ_v is the total overburden stress, σ_v' is the effective overburden stress, a_{max} is the peak ground acceleration, and r_d is a factor which accounts for the soil flexibility (see Figure 7.5). As is seen, there is a significant variation in r_d, depending on soil conditions, but no correlations are available expressing r_d in terms of soil properties. Consequently, it is common to use the average curve shown in Figure 7.5, and this has been fitted by the expressions:

$$r_d = 1.0 - 0.00765\,z \qquad (z < 9.15\text{ m}) \qquad (7a)$$

$$r_d = 1.174 - 0.0267\,z \qquad (9.15\text{ m} < z < 23\text{ m}) \qquad (7b)$$

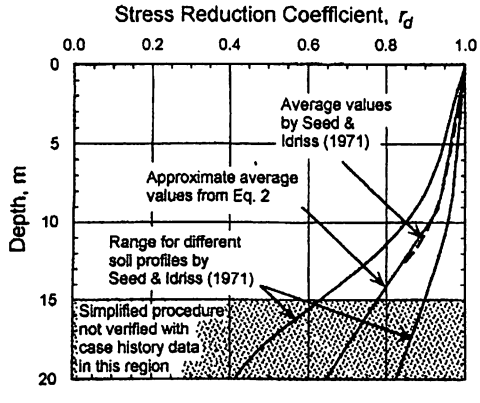

Figure 7.5. Soil flexibility factor, r_d, as a function of depth (Youd & Idriss, 2001)

The above expressions have been used to study the liquefaction potential of the soils on the Northern Shore site, based on the SPT results. Analysis was limited to those soils containing less than 20% fines, and cases in which $(N_1)_{60}$, as estimated from (2), was less than 30. The results of the analysis are shown in Figures. 7.6(a) – 7.6(c). In these figures, factor of safety against liquefaction is defined as the ratio between the critical cyclic stress ratio which would cause liquefaction (as obtained from equation (4), modified for fines content by equation (5)), to the expected cyclic stress ratio (from equation (6)). Figures 7.6(a), 7.6(b), and 7.6(c) refer to earthquake magnitudes 7.5, 7.0 and 7.0 respectively, and each figure shows factors of safety for the cases of maximum ground acceleration equal to 0.2g, 0.3g and 0.4g.

The following observations may be made from Figure 7.6:

(a) For a magnitude 7.5 earthquake, events causing a peak ground acceleration of 0.2g or greater could be expected to initiate liquefaction at various locations at the site. For a 0.2g peak ground acceleration, minimum factors of safety of 1.0 were obtained in 2 tests, at depths down to 6 m. For a peak ground acceleration of 0.3g and 0.4g, 8 tests and 17 tests, respectively, indicated likelihood of liquefaction.

(b) In the case of a magnitude 7.0 earthquake, no tests suggested liquefaction for a peak ground acceleration of 0.2g, although factors of safety less than 1.5 were indicated. Liquefaction could still be expected for events causing peak ground accelerations of 0.3 g or greater.

(c) In the case of a magnitude 6.5 earthquake, only events causing a peak ground acceleration of the order of 0.4g, or higher, would be expected to initiate liquefaction.

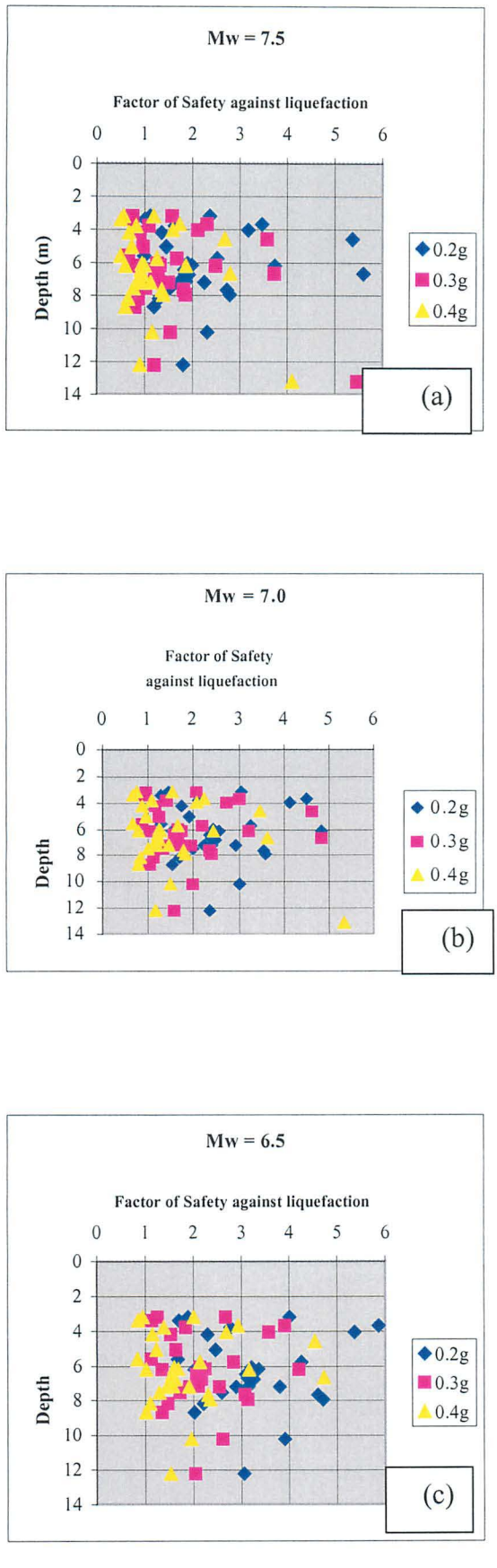

Figure 7.6. Liquefaction potential of Eilat site, based on SPT data.

7.1.1.2 DCP soundings

As part of the present investigation, two trenches were studied in the hotel area, at locations shown in Figure 7.7. During examination of these trenches, a series of dynamic cone penetrometer (DCP) tests was performed, and the results of these are summarized in the present section.

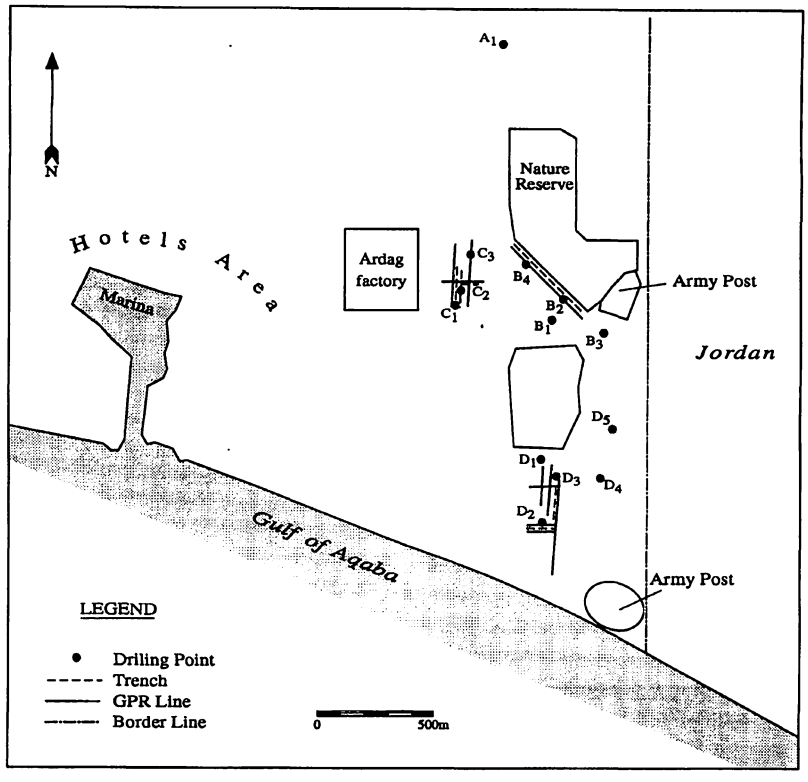

Figure 7.7. Location map of trenches in Eilat. Geotechnical studies were performed on trenches B and C.

The dynamic pone penetrometer is commonly used in Israel for site investigations related to pavement design. The instrument being used has a hammer weight of 8.0 kg, falling through a height of 57.5 cm on a rod of 16 mm diameter; the cone angle is 90°, and the cone base diameter is 20 mm. The advantage of the test method is that it provides a continuous record of soil "resistance" to penetration;

its disadvantage is that is can be used only to a depth of the order of 2 meters. From a correlation between SPT and DCP results presented by Livneh and Ishai. (1988), the following equation is suggested for relating between the two:

$N = (10{,}000/D)^{0.493}$ (8)

Where D = the DCP penetration in mm/blow, and N is the equivalent SPT blow count.

Seven DCP soundings were performed adjacent to trench no. 1, and three next to trench no. 2. The results were translated into equivalent SPT blow counts, using equation (8), and these were then analyzed in accordance with the procedure set out in the latter part of section 1.1.1, in order to estimate factors of safety against liquefaction. As no data was available for fines content corresponding to individual penetration readings, the effect of fines was ignored – as fines are believed to increase resistance to liquefaction, ignoring the presence of fines is conservative. Again, analyses were done only for cases of $(N_1)_{60}$ less than 30 blows. Figures 7.8 and 7.9 show the results of the analyses for the cases of earthquake magnitudes of 6.5, 7.0 and 7.5, and a peak ground acceleration of 0.3g, for trench 1 and trench 2, respectively.

It must be pointed out that the analyses were performed assuming that water level reached the soil surface. In fact, water level at the site is at a depth of about 2 – 2.5 m, and sand above water table would not liquefy. The purpose of the analyses was to consider the possible behavior of submerged sand, having the same density/penetration properties as that of the surface sands at the site, under earthquake conditions.

The figures indicate that for the existing sands in a submerged condition, a high potential for liquefaction exists in the depth range 0.6 – 2 m, in the case of a 7.5 magnitude earthquake, developing a peak ground acceleration of 0.3g. On the other hand, for a 6.5 magnitude event developing the same peak ground acceleration, there would be a considerably lower potential for liquefaction in this upper zone, although some liquefaction could take place.

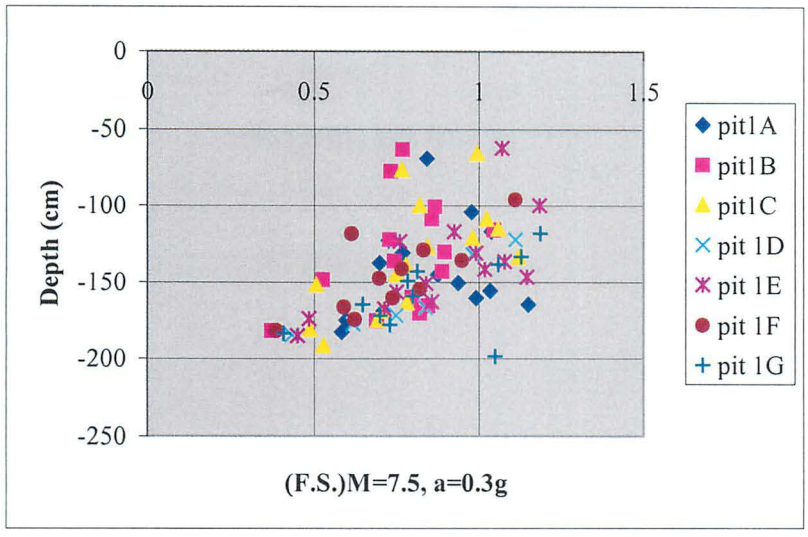

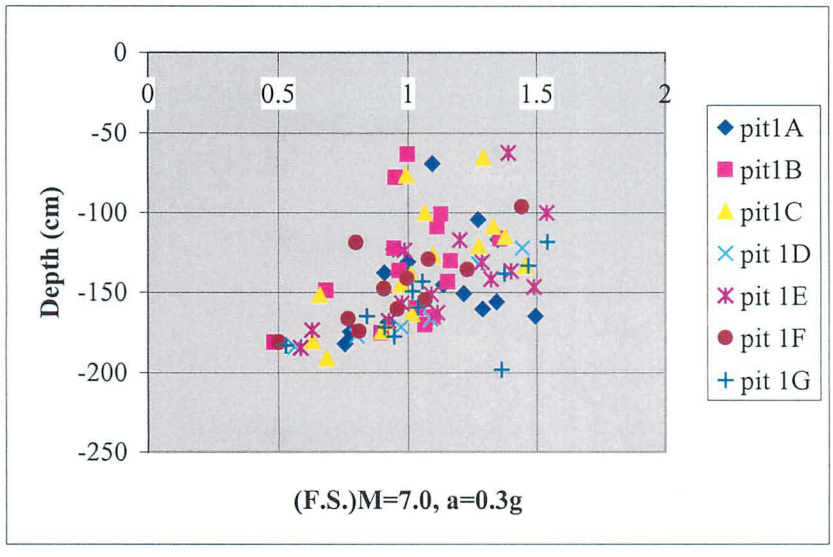

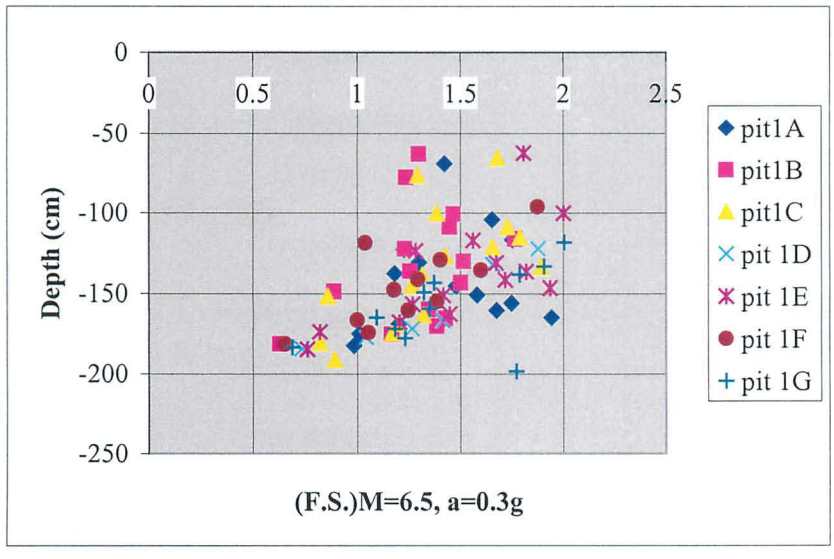

Figure 7.8. Liquefaction potential at Eilat trench 1, based on DCP data

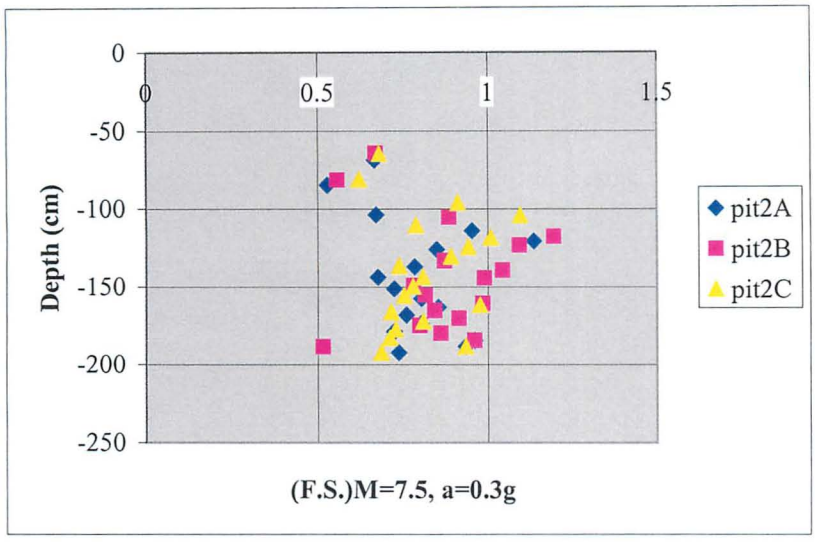

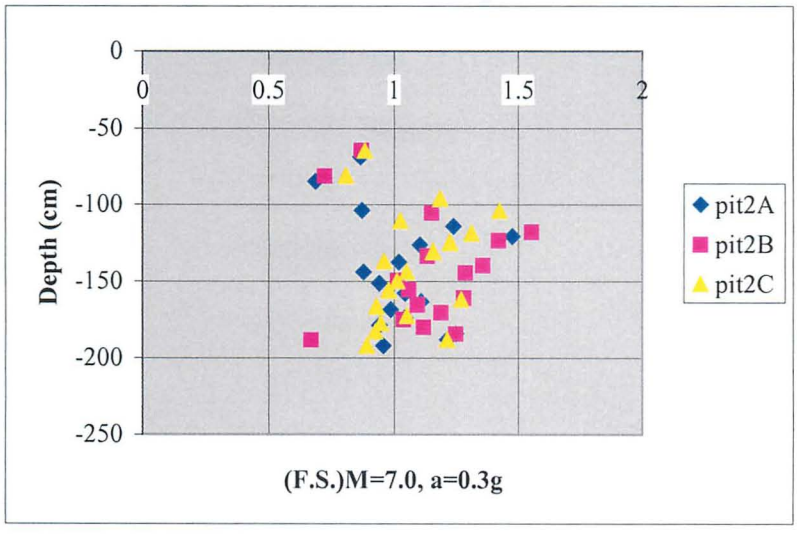

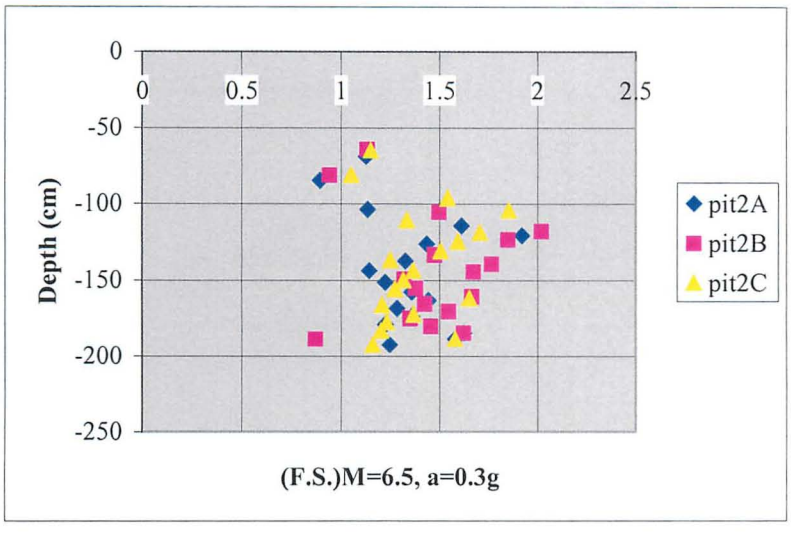

Figure 7.9. Liquefaction potential at Eilat trench 2, based on DCP data

7.1.2 Laboratory investigations

In addition to the geological investigation and the DCP soundings performed at the test trench the hotel area, block samples were extracted from a step excavated into the side of the trench, from a depth of 1.8 – 2.0 m. these block samples were used to prepare undisturbed cylindrical specimens for triaxial testing, as described below. Stages in the preparation of the block samples are shown in figs. 10.

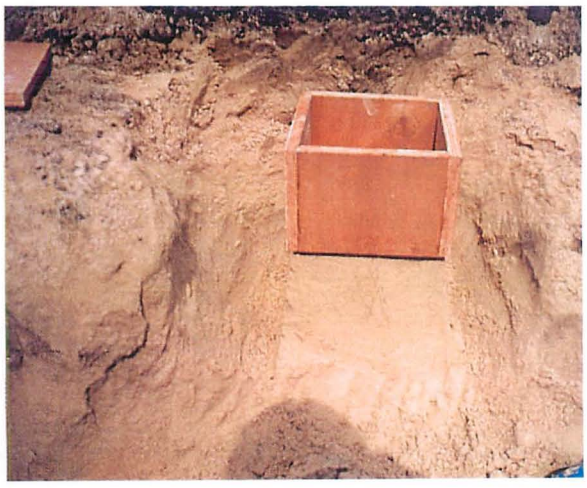

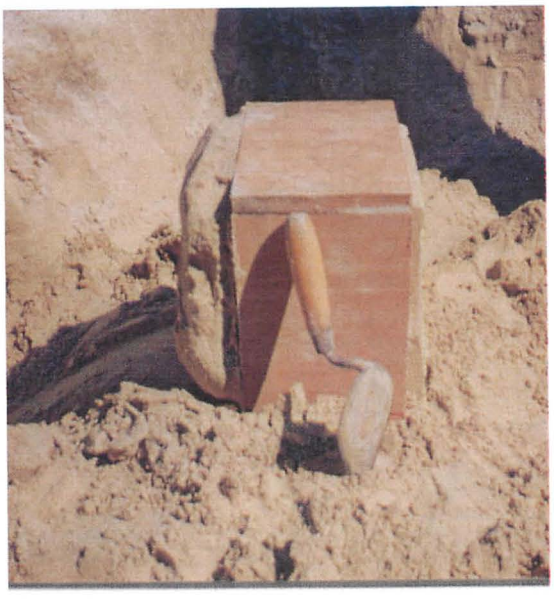

Figure 7.10. Stages in preparation of undisturbed block of sand

The samples were transferred to the laboratory, frozen in a deep-freezer at about -18°C, and then cored to produce cylindrical tests specimens. The frozen specimen was wrapped in a latex sleeve; placed in a triaxial cell, subjected to a low ambient cell pressure for support, and allowed to thaw. Triaxial testing was then performed.

The block samples tested were found to contain 27% fines, and the soil had a maximum dry density of 16.5 kN/m^3 and a minimum dry density of 14 kN/m^3. The natural dry density of the samples was 14.65 kN/m^3, corresponding to a relative density, D_r = 29%, and the moisture content was 6.5%. This is a very low relative density, and is in accordance with the predictions of a high potential for liquefaction presented in section 1.1.2. A relative density of this low magnitude would, almost certainly, cause liquefaction in a clean sand. The high fines content of the sand may have been responsible for the more optimistic predictions which were made in section 1.1.2, for the case of a lower magnitude (M = 6.5) event.

The triaxial testing program included drained and undrained monotonically loaded tests, as well as undrained cyclically loaded tests. The results of these tests are presented below.

7.1.2.1 Monotonic triaxial tests

Stress-strain and pore pressure or volume change – strain curves are shown in appendix 1. Stress paths followed in the various tests are shown in Figure 7.11. Drained tests were performed at cell pressures of 70, 120 and 200 kPa, while consolidated undrained tests were carried out at consolidation pressures of 35, 70 and 150 kPa.

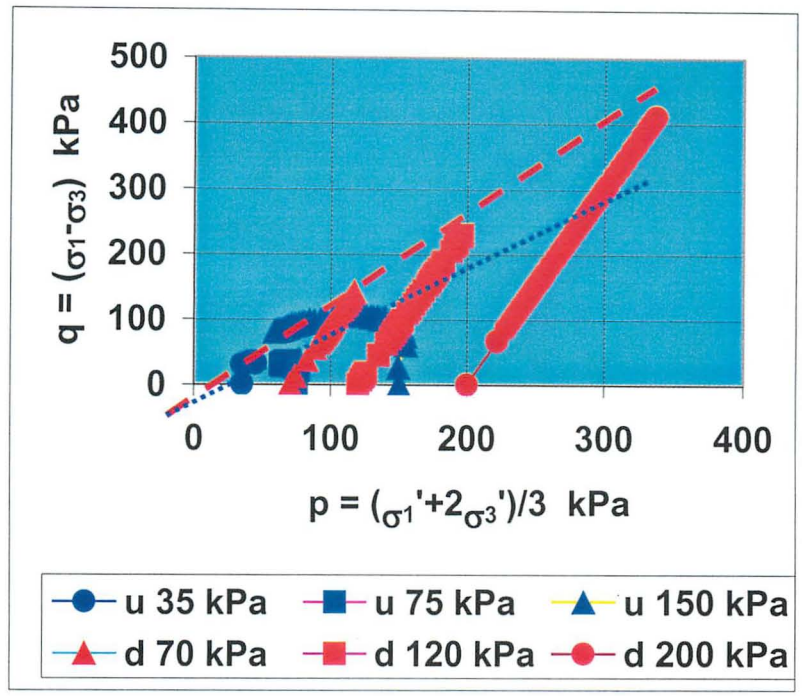

Figure 7.11. Stress paths followed in monotonic triaxial tests on Eilat samples (u = undrained; d = drained)

Of particular interest is the shape of the effective stress paths followed during the undrained tests. The decreasing mean effective stress results from an increasing pore pressure, indicating the contractive nature of the material, and its high potential for liquefaction. This is consistent with the low relative density of the material, and with the liquefaction potential estimates presented in section 1.1.2. The red dashed line in Figure 7.11, joining the ultimate points on the effective stress paths, indicates an effective friction angle, $\phi' = 33°$. The blue dotted line joins points of peak deviator stress on the undrained effective stress paths, and indicates that failure in undrained shear would correspond to a friction angle of 24.5°. The effective friction angle, $\phi' = 33°$, is extremely low for Israeli sand, and corresponds to the critical state value. Figure 7.12 shows data for Israeli sands, relating friction angle, ϕ', to relative density, D_r. The yellow dashed line represents a suggested relation between ϕ' and D_r. It is seen that the Eilat results correspond well with the collected data, and that the friction angle is at the lower end of measured values.

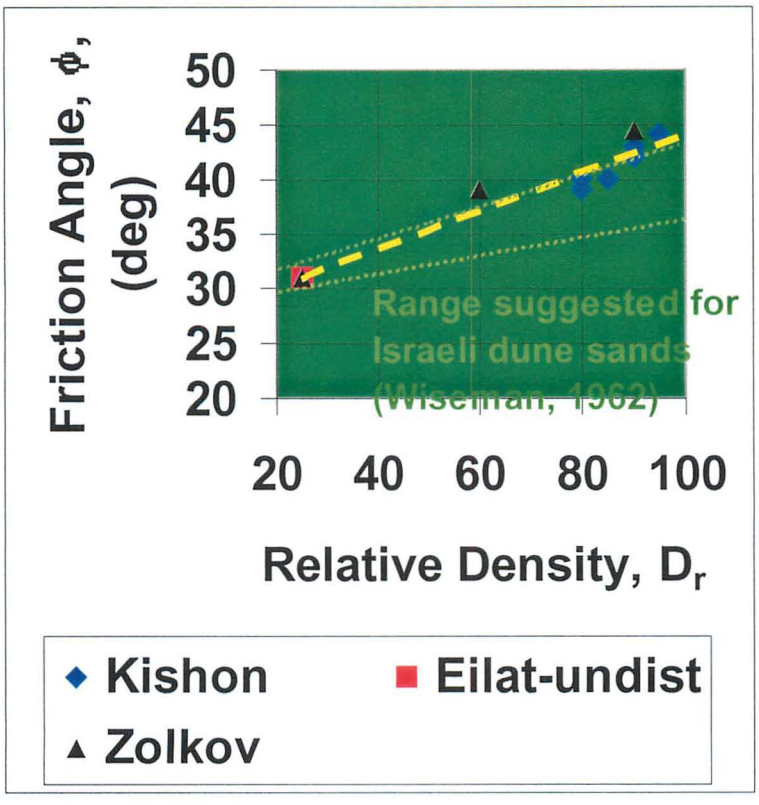

Figure 7.12. Relationship between friction angle, ϕ', and relative density, D_r, for Israeli sands (Frydman, 2000)

7.1.2.2 Cyclic triaxial tests

Two undrained, cyclic triaxial tests were performed, both at a consolidation pressure of 100 kPa. Cyclic stress ratio (SR = $\sigma_d/2\sigma_c$) was 0.25 and 0.3, where σ_d is the deviator stress, cycled about the isotropic consolidation stress, σ_c.

The results of the tests with SR = 0.25 are shown in Figures 7.13 and 7.14. Figure 7.13 shows cyclic stress strain curves; Figure 7.13(a) shows the development of strain over the complete test duration, while Figure 7.13(b) concentrates on the first cycles. Figures 7.14(a) and 7.14(b) similarly show the development of pore pressure against axial strain during the cycling. Figures 7.15 and 7.16 are similar curves, for tests with SR = 0.30.

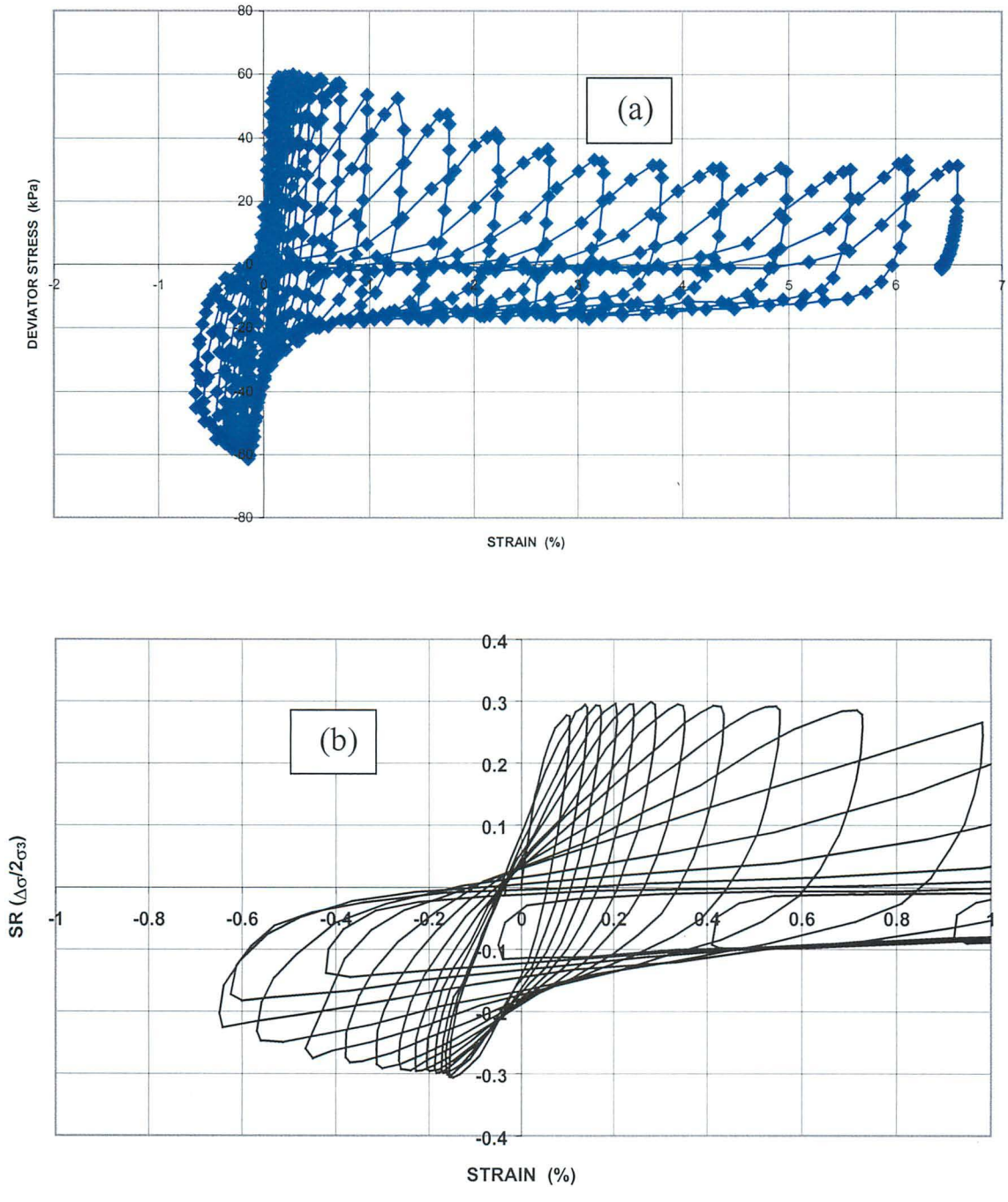

Figure 7.13. Cyclic stress-strain curves for Eilat sand, SR = 0.25

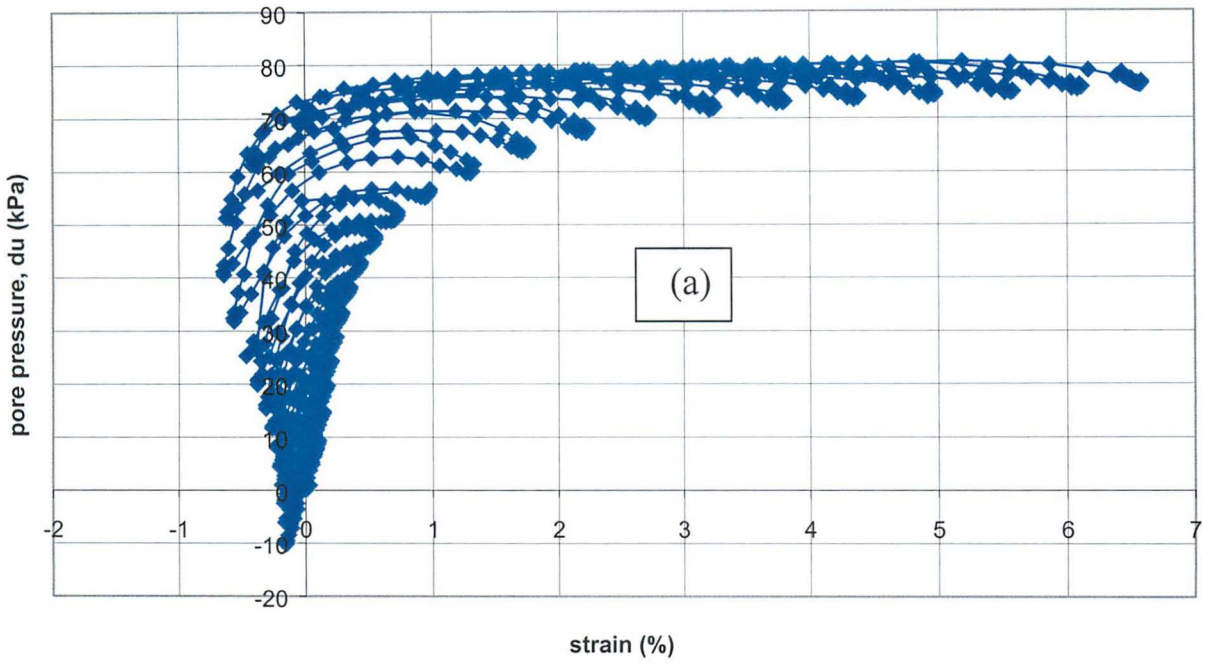

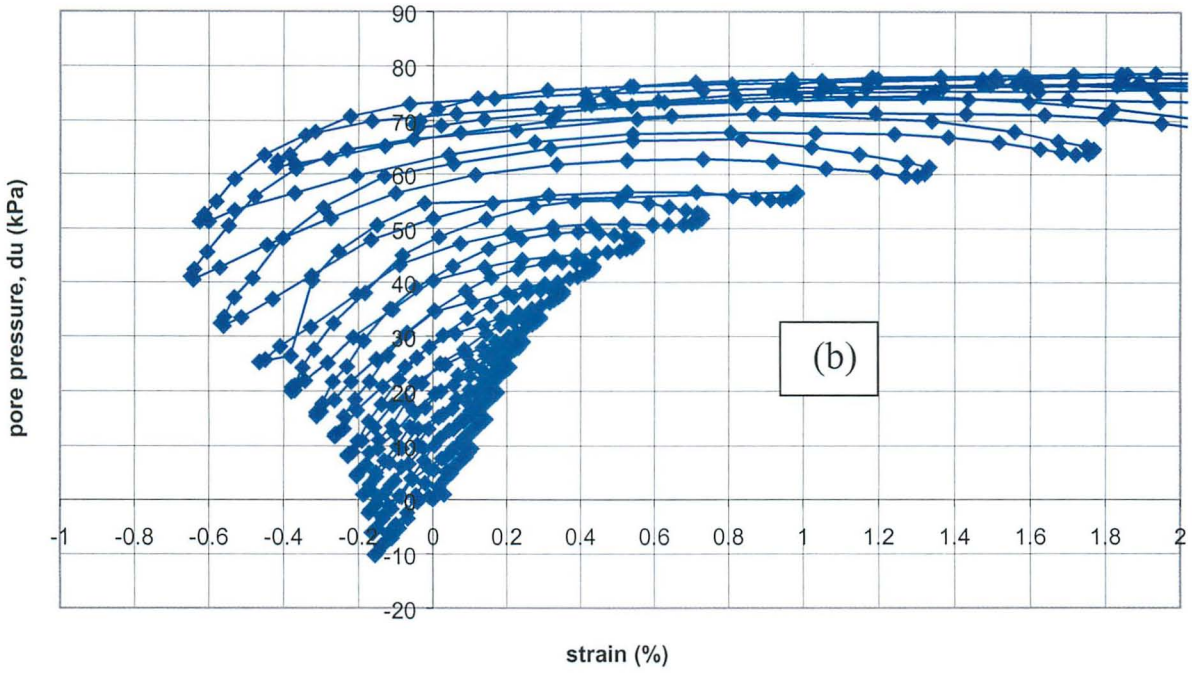

Figure 7.14. Cyclic pore pressure development for Eilat sand, SR = 0.25

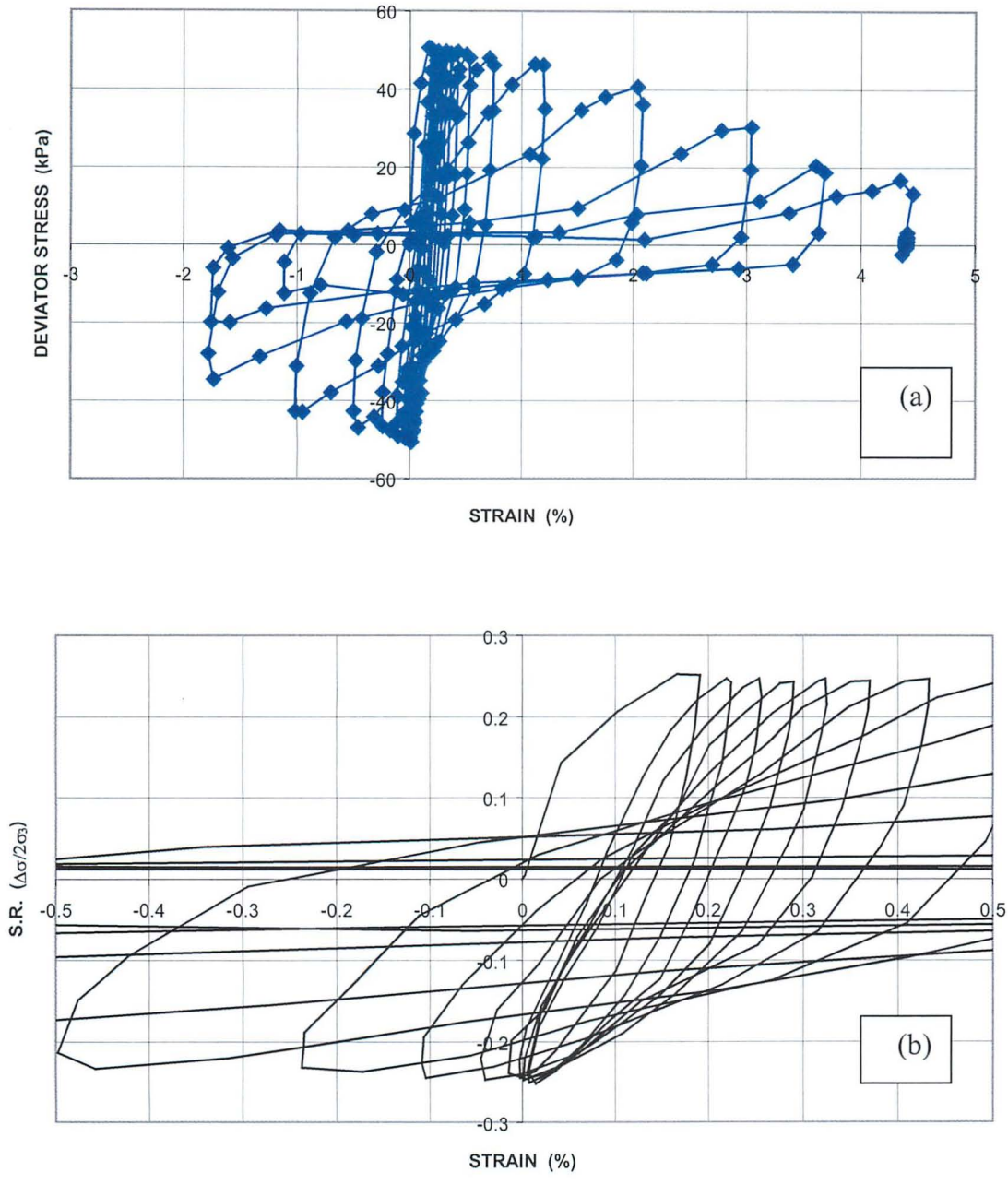

Figure 7.15. Cyclic stress-strain curves for Eilat sand, SR = 0.30

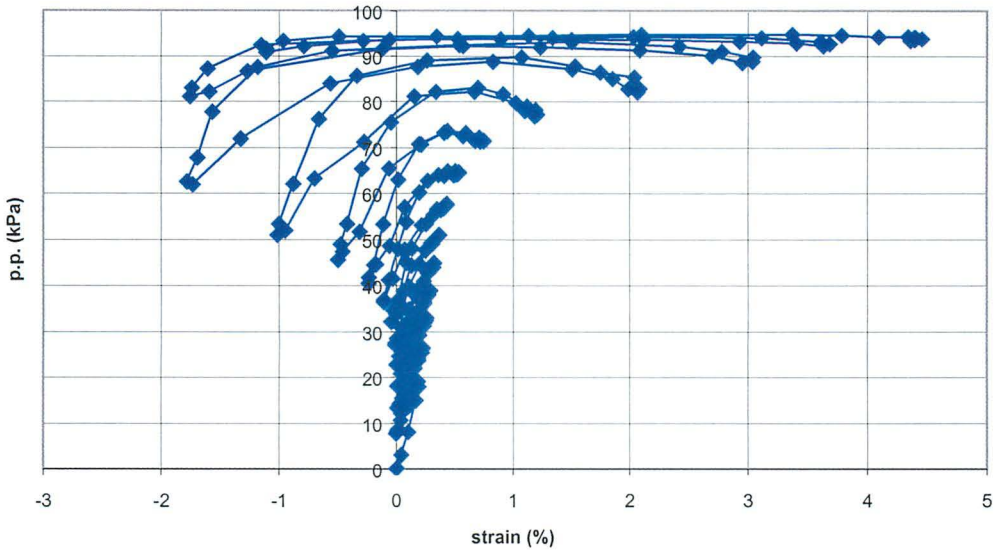

Figure 7.16. Cyclic pore pressure development for Eilat sand, SR = 0.0.30

It is difficult to define the onset of liquefaction during cyclic triaxial tests. For practical purposes, this should be defined as the stage at which strains and pore pressures increase at an accelerated rate. From a study of Figures 7.13 – 7.16, this condition is estimated to occur after 9 – 10 cycles for SR = 0.25, and after 7 – 8 cycles for SR = 0.3. These values are extremely low, again indicating the high liquefaction potential of the soil. For comparison, Figure 7.17 shows the relationship between stress ratio, SR, and number of cycles for initial liquefaction, as found for a number of soils. The black points on the figure represent values obtained from undisturbed samples of dune sands and kurkar-sands; the lower dashed curve represents a suggested lower bound to these results. The upper dashed curve was obtained for reconstituted samples of Monterey 0 sand, tested at a relative density of 60%. The Eilat results are shown as red triangles. Data for undisturbed samples from the Kishon are also shown, and will be discussed in section 2 of this report. It is noted that the Eilat results fall below, and close to the lower bound suggested for Israeli dune sands and kurkar sands; they are well below the results obtained for Monterey sand at 60% relative density.

Estimates of the equivalent stress ratio likely to develop in the upper part of the soil profile in a submerged condition, for a peak ground acceleration of 0.3g (using equation (6)) indicate values of the order of SR = 0.38. Referring to Figure 7.17, it is seen that this soil could probably only resist 3 – 4 cycles of such a stress ratio. Seed et al. (1975) estimated that a magnitude 6 earthquake would apply the equivalent of about 5 uniform loading cycles, and a magnitude 7 earthquake the equivalent of about 10 uniform loading cycles. The high danger for liquefaction in the upper portion of the Eilat profile if it is submerged, is, therefore, clear.

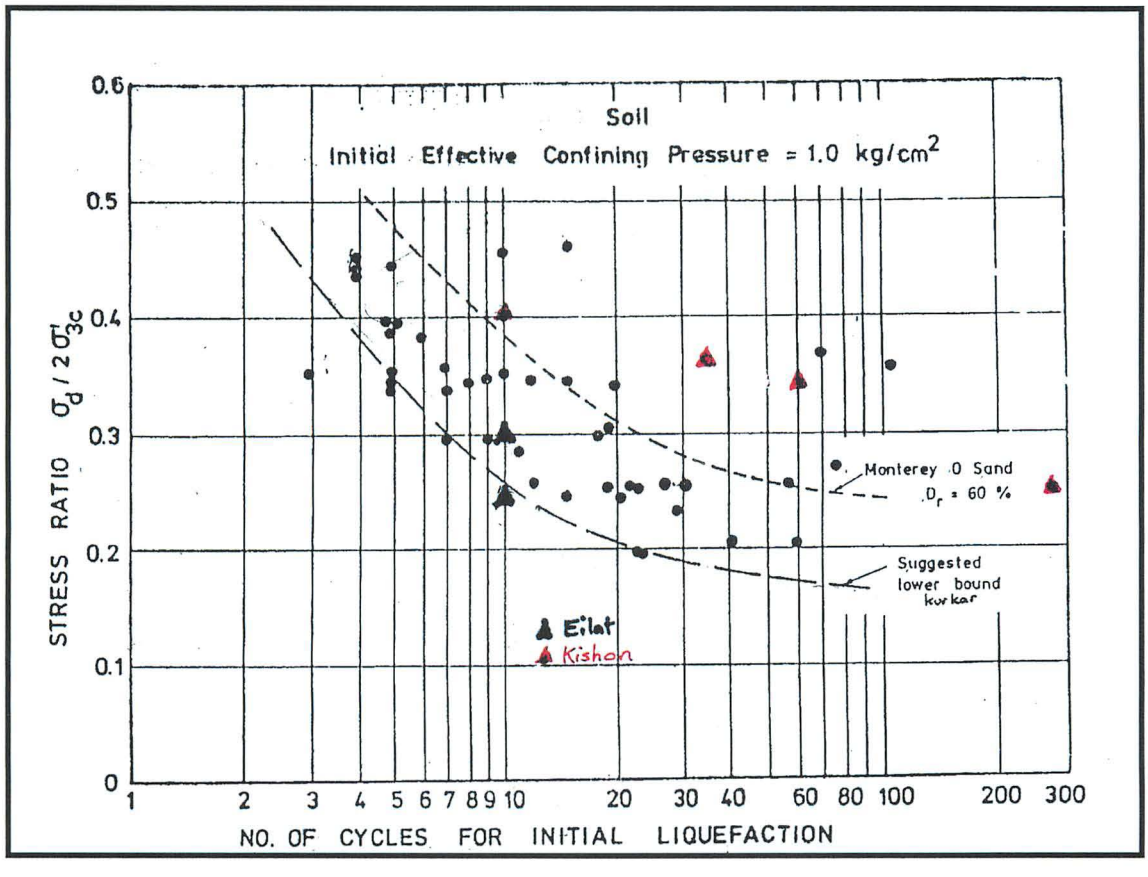

Figure 7.17. No. of cycles for liquefaction versus stress ratio

7.1.3 Summary of information related to the Eilat site

Summarizing all the data presented in section 1, it is clear that the danger of liquefaction at the Eilat site is highly dependent on the magnitude and proximity of the earthquake, and level of the ground water table at the site. Both field tests and laboratory studies show that the in-situ sand in portions of the profile has a very low relative density, and would be expected to liquefy under strong earthquake input. The field tests suggest that a magnitude 6.5 earthquake, applying a peak ground acceleration of 0.3 may result in some liquefaction, and this would be higher spread for stronger events. The triaxial tests, performed on samples taken from the top 2 meters of the profile, reinforce this conclusion, showing that only a few cycles (3 – 4) of a magnitude 6 or more earthquake causing a peak ground acceleration of at least 0.3 g. may result in liquefaction in the upper two meters at the site, if they were submerged. With regards the portion of the profile presently below water table, a magnitude 7.0 event at least, causing a peak ground acceleration of 0.3g or more, would appear to be required to cause liquefaction.

7.2 Haifa Bay

Bag samples, and undisturbed, block samples were extracted from the trenches excavated at the three Haifa Bay sites – Ein Hamifratz, Kfar Bialik and Kishon. The block sampling procedure was similar to that described above, for the Eilat site, and test specimens were prepared using the same freezing technique as described previously. Triaxial testing programs were carried out on specimens from the Kishon site, as the sand at this site was found to be clean of fines, and having a density lower than that at the other sites.

7.2.1 Basic tests

The bag samples were used to test the particle size distribution of the soil, and the result is shown in Figure 7.18. It is noted that the sand is essentially free of fines, and is a uniform sand, with about 90% of its particles in the size range 0.1 – 0.3 mm. Relative density of samples varied between 60% - 75%.

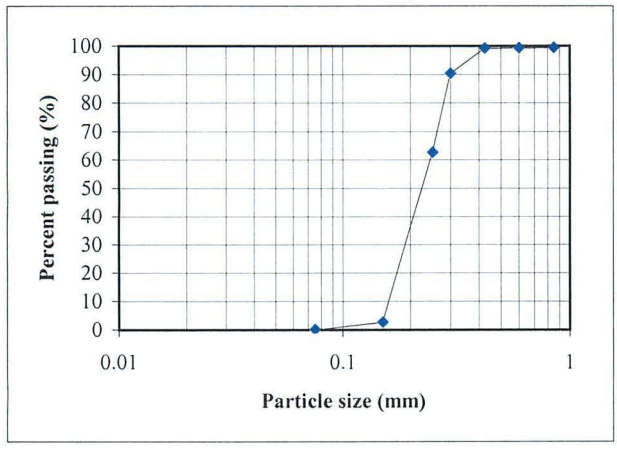

Figure 7.18. Particle size distribution of Kishon sand

7.2.2 Monotonic triaxial tests

The monotonic triaxial testing program, included both drained and undrained tests, and was aimed at studying the following features:

(a) Comparison of behavior of undisturbed samples to that of samples reconstituted to the same density using different preparation methods – underwater pluviation, and dynamic compaction.

(b) Isotropic/anisotropic behavior of specimens cored perpendicular and parallel to the in-situ horizontal plane.

The testing program was inspired by the fact that most laboratory testing for analysis and prediction of liquefaction in sands is currently performed on reconstituted specimens. It was, therefore, considered desirable, in the framework of the present research, to investigate the comparative behavior of undisturbed and reconstituted specimens of the in-situ sands. As standard liquefaction testing is performed in triaxial equipment, with the in-situ horizontal plane modeled by a plane at 45° to the horizontal in the test specimen, the influence of anisotropy may be significant, and so this represented a second feature studied in these tests.

Although a large number of tests was carried out, the following presents some typical results, and the major observations and conclusions.

Figure 7.19 shows typical stress-strain-volume change relationships from drained tests.

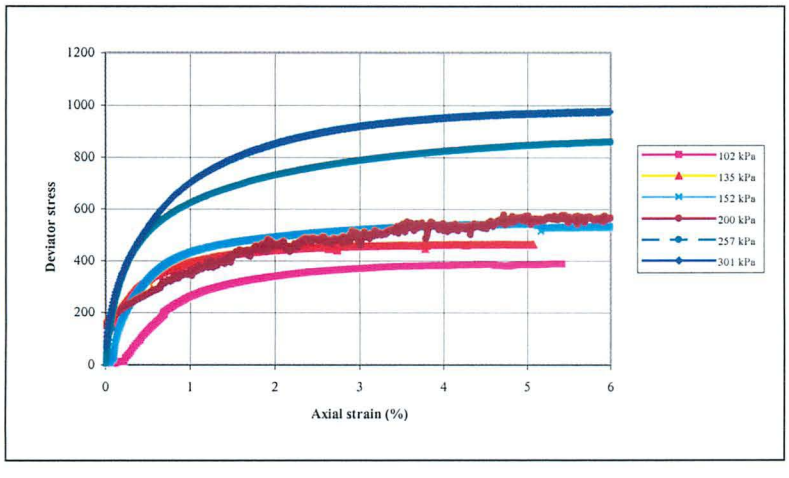

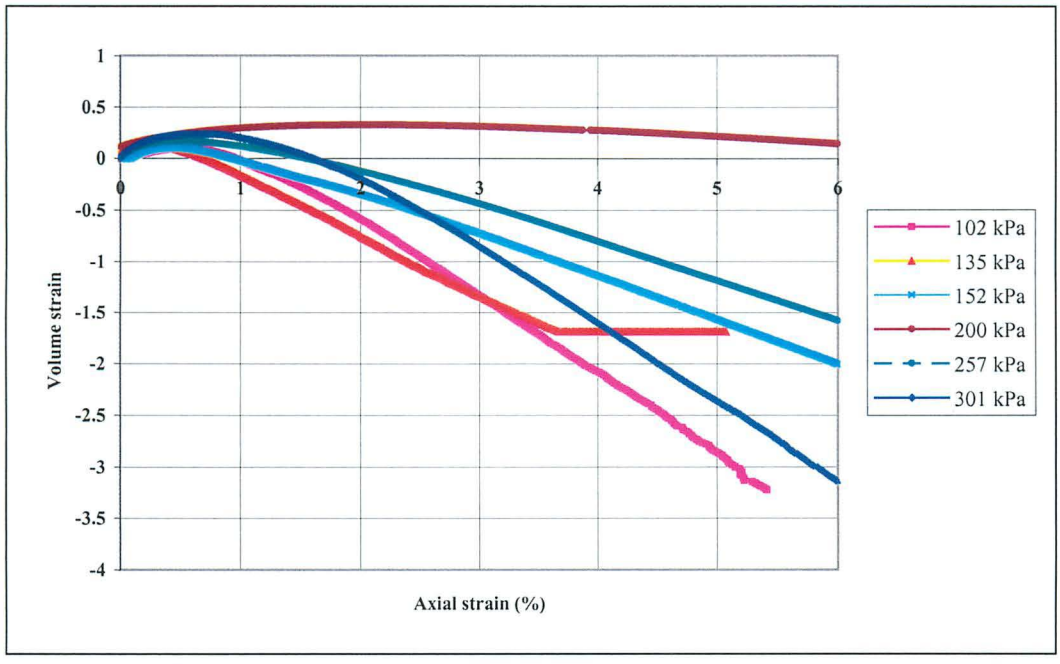

Figure 7.19. Stress-strain-volume change behavior of drained, undisturbed samples of Kishon sand.

The most significant observation from these results is the dilative nature of the material. Although relative densities varied from the order of 60% to 75%, all the specimens (with the possible exception of the test performed at cell pressure 200 kPa) showed clearly dilative behavior. This is in contrast to the contractive behavior of the Eilat material, and would suggest a higher resistance to liquefaction.

Figure 7.20 shows effective stress paths followed in consolidated undrained tests.

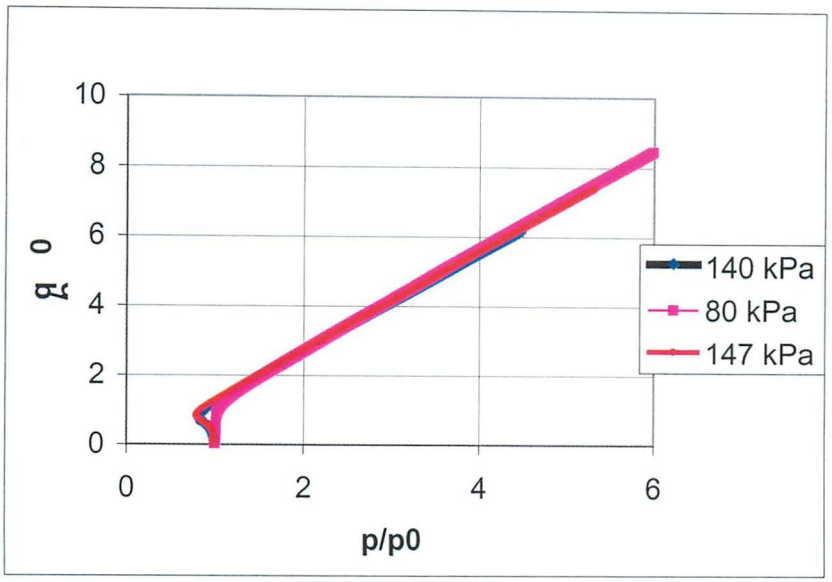

Figure 7.20. Normalized effective stress paths in undrained tests on undisturbed samples of Kishon sand.

It is noted that the three test paths shown coincide almost precisely, showing very slight contractive behavior at the start of shearing, but rapidly developing dilative behavior. The increase in p/p_0 along the stress path results from decreasing pore pressure, which is a consequence of the dilative nature of the soil. This behavior is consistent with the dilative behavior shown in the drained tests, as seen in Figure 7.19, and is in contrast to the behavior of the Eilat samples, as shown by the blue curves in Figure 7.10.

Figure 7.21 shows normalized effective stress paths from tests on undisturbed samples cored vertically and horizontally, a pluviated sample, and a compacted sample. Again it is seen that the stress paths coincide almost precisely, suggesting that natural structural effects in this soil is not of major significance, and, consequently, reconstituted samples could reasonably be employed in order to study the behavior of the undisturbed material. The stress paths are again seen to show the highly dilative behavior demonstrated in the drained tests.

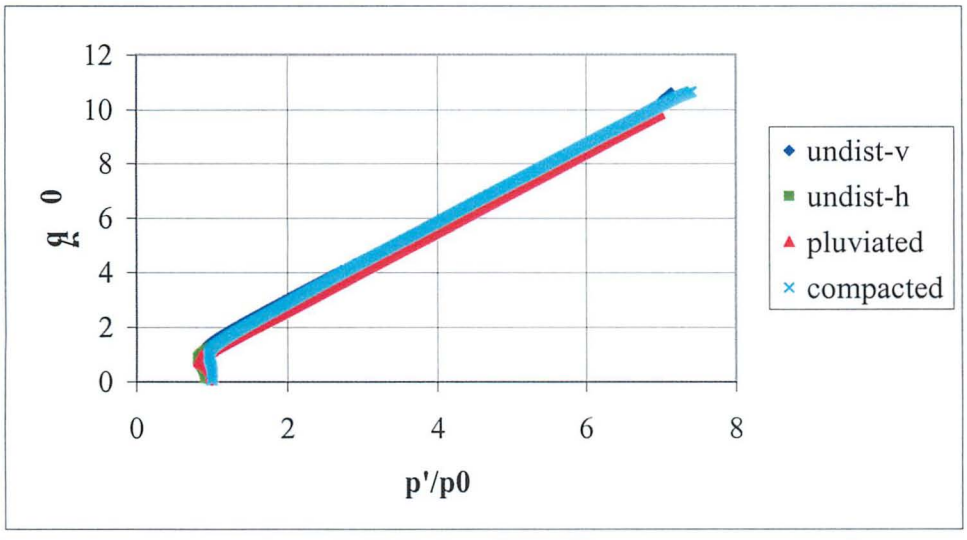

Figure 7.21. Effective stress paths for Kishon samples prepared in different ways

In summary, the response of the undisturbed Kishon sand to monotonic shear loading suggests that this material would be significantly less prone to liquefaction than the Eilat soil.

7.2.3 Cyclic triaxial tests

Four cyclic triaxial tests were performed on undisturbed samples of the Kishon sand. All tests were carried out at an effective consolidation pressure of 100 kPa; stress ratios applied were S.R. = 0.25, 0.35, 0.37 and 0.41.

A typical set of cyclic stress-strain curves, as obtained from the test carried out with a stress ratio of 0.35, is shown in Figure 7.22. The low-strain part of the figure, showing the first 30 cycles, up to a strain of 1%, is shown in Figure 7.23.

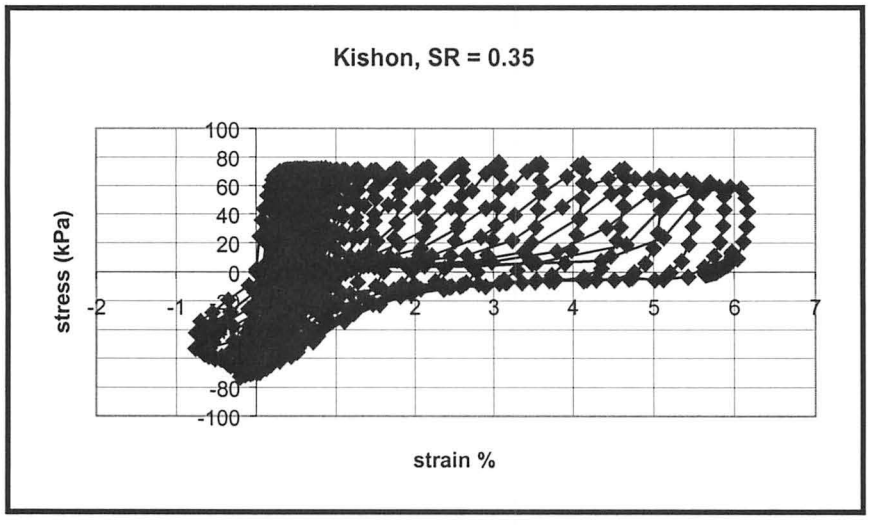

Figure 7.22. Stress-strain cycles – Kishon sand, SR = 0.35

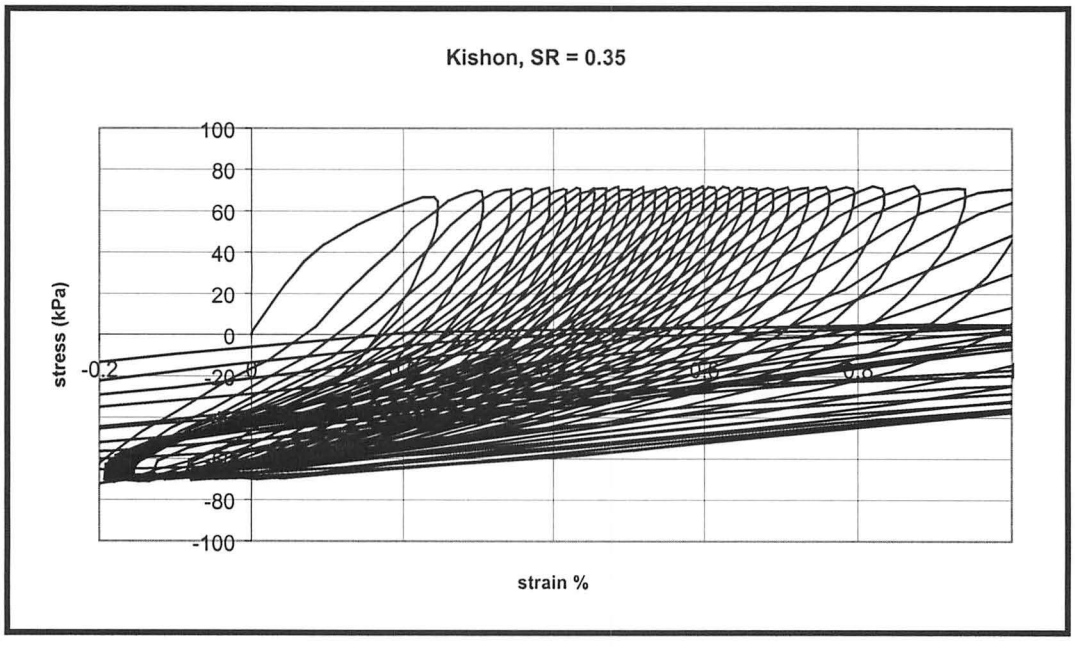

Figure 7.23 Stress-strain cycles – Kishon sand, SR = 0.35; first 30 cycles.

Comparing Figure 7.23 for the Kishon sand to Figure 7.13 for the Eilat sand, the significant difference between the two sites is immediately evident. The Eilat sample, under a cyclic stress ratio of 0.25, developed 1% strain after 11 loading cycles, whereas the Kishon sand, under a higher stress ratio of 0.35, withstood 30 load cycles before developing the same strain.

Figure 7.24 shows the development of pore pressure as a function of number of loading cycles for the Kishon sand. Figure 7.25 shows the same plot, using a log scale for no. of cycles – the development of pore pressure during the first cycles is seen clearer here.

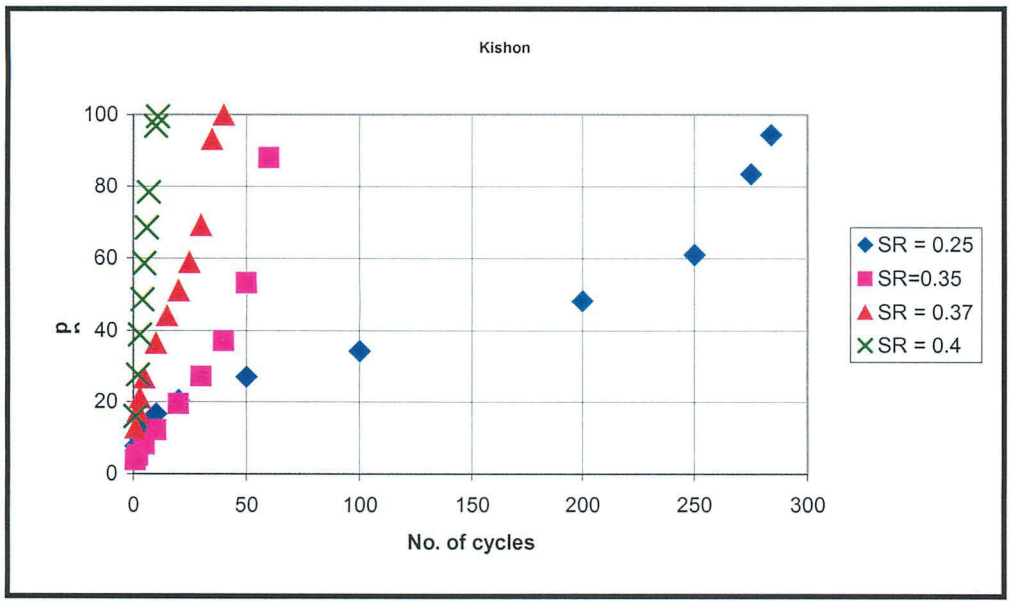

Figure 7.24(a). Development of pore pressure with loading cycles, Kishon sand

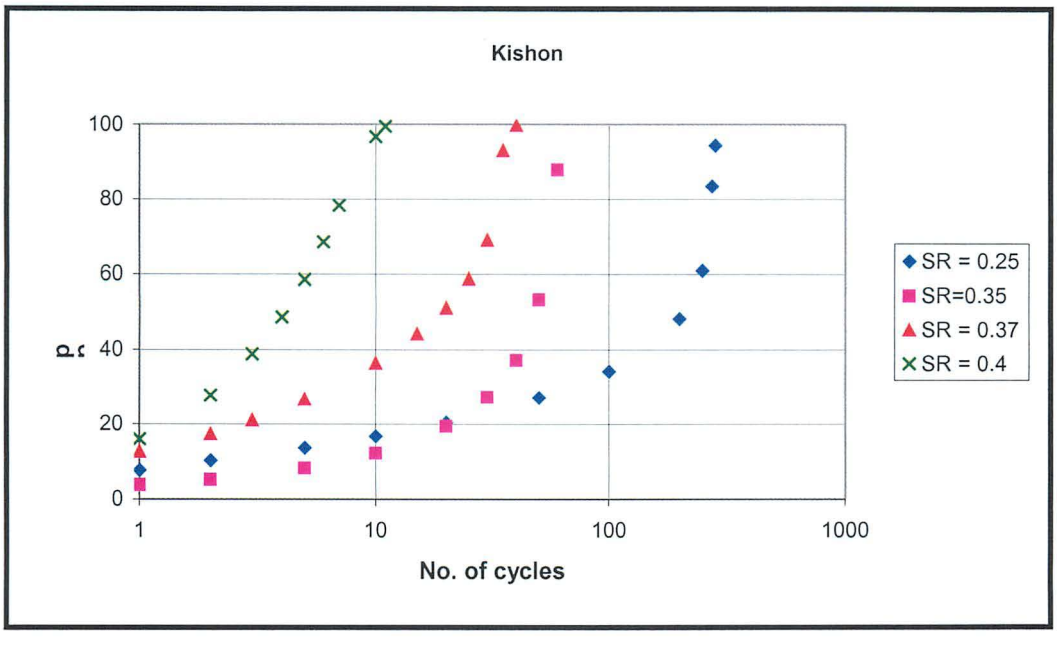

Figure 7.24(b). Development of pore pressure with loading cycles, Kishon sand

Figure 7.25 shows the change in secant modulus of elasticity, E, of the Kishon sand with loading cycles. The well-known decrease in E with cycles is noted, resulting from the increasing pore pressure and strain with loading cycles.

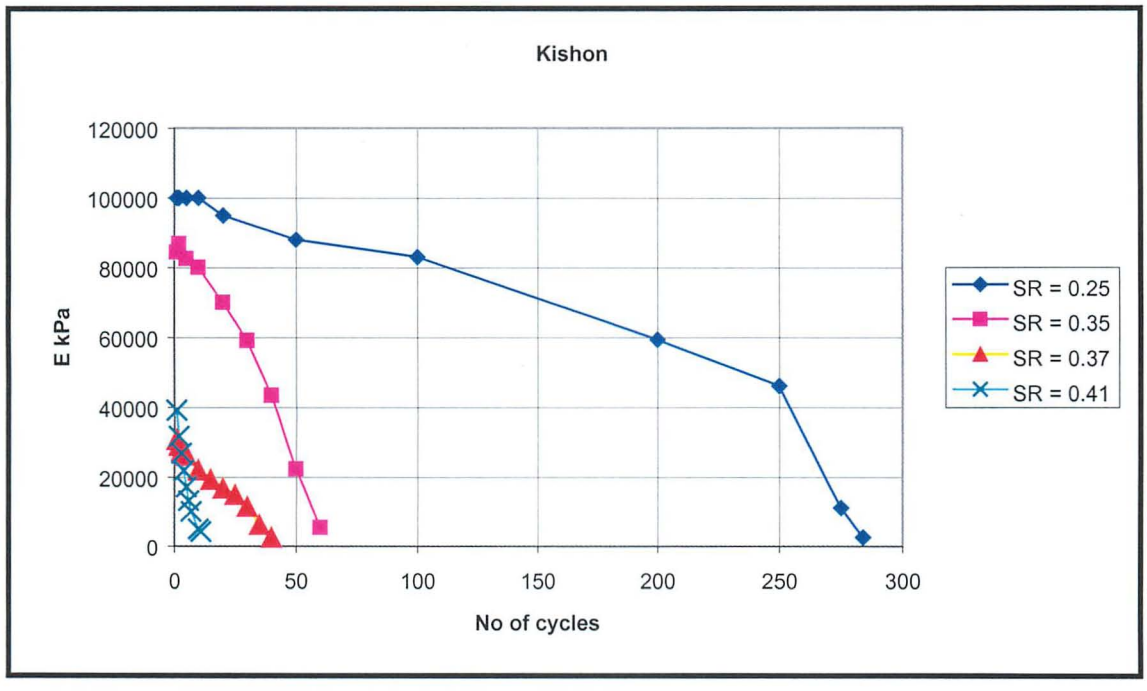

Figure 7.25. Secant modulus of elasticity as a function of loading cycles, Kishon sand

7.2.4 Comparison of results of cyclic tests on Eilat, Kishon samples

Figures 7.26 and 7.27 show comparisons between the results of cyclic triaxial tests on undisturbed samples of Eilat and Kishon sands. Figure 7.26 shows the increase of normalized pore pressure, with loading cycles. It is seen that the pore pressure developed significantly faster in the Eilat samples than in the Kishon samples. For example, for a stress ratio of SR = 0.25, u is seen to reach 100% of its maximum value after about 12 cycles in the Eilat samples, while in the case of Kishon sand, only 36% of maximum pore pressure was developed after 100 loading cycles.

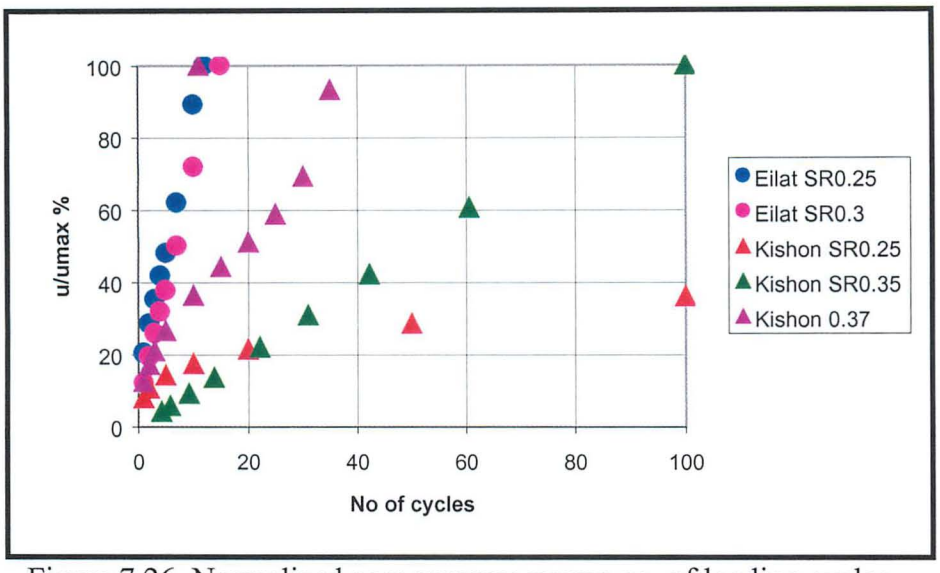

Figure 7.26. Normalized pore pressure versus no. of loading cycles

Figure 7.27 similarly compares the change in secant elastic modulus with loading cycles.

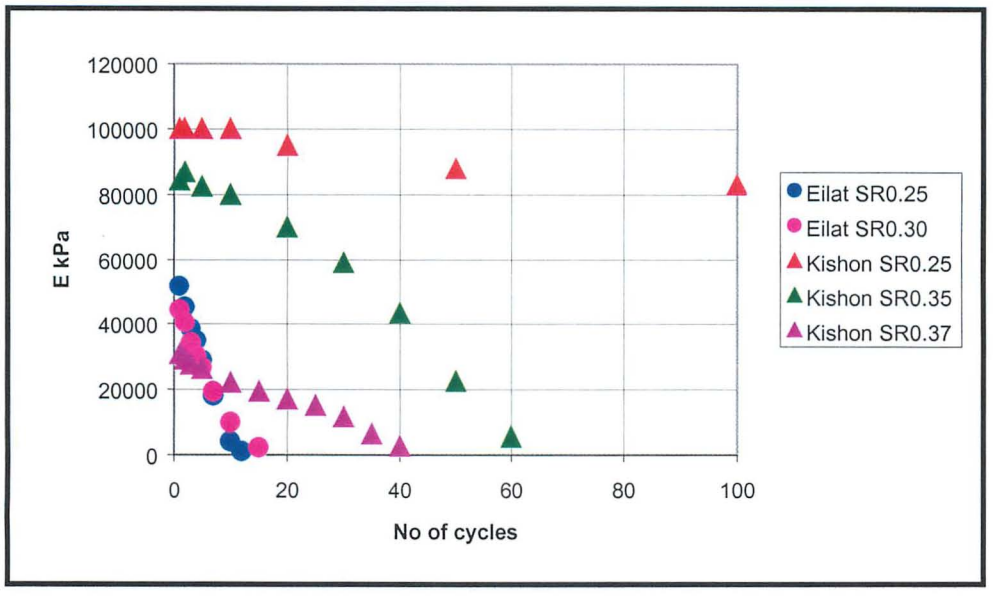

Figure 7.27 Secant elastic modulus versus no. of loading cycles

The stiffer behavior of the Kishon sand is again seen in Figure 7.27, the most obvious indication being a comparison of behavior of the 2 samples tested at a stress ratio of SR = 0.25. Even the Kishon sample tested at a stress ratio of 0.35

showed stiffer behavior and less pore pressure development than the Eilat sample under a stress ratio of 0.25.

Figure 7.17, presented previously, shows cyclic stress ratio versus the number of cycles required for liquefaction. The black circles are results of tests performed on undisturbed samples of kurkar-sand from the Nitzanim site, with the lower dashed curve shown as a suggested, reasonable lower bound (Frydman et al., 1980). The upper dashed curve is a relationship presented by Seed and Lee for reconstituted samples of Monterey 0 sand at 60% relative density. The red triangles are the results of the tests on the undisturbed samples of Kishon sand, while the blue triangles are the results of the tests on the undisturbed samples of Eilat sand. It is seen that the Kishon results lie close to the upper limit of the Nitzanim kurkar-sand, and above the Monterey sand , whereas the Eilat results lie close to the lower bound suggested for the kurkar-sand, and significantly below the curve for the Monterey sand. The Kishon results indicate that a peak ground acceleration of 0.3g, corresponding to an equivalent stress ratio in the upper part of the profile of about 0.38, would require 15 – 20 loading cycles in order to cause liquefaction. A magnitude 7.5 earthquake would be required in order to develop such conditions.

7.3 Conclusions from Geotechnical studies

The geotechnical studies described in the above sections have indicated a significant difference between the liquefaction potential of the Eilat and Kishon sites. The Eilat site appears to have a potential for liquefaction under the action of an earthquake of magnitude 6.0 or greater, producing a peak ground acceleration of 0.3g or more. On the other hand, at the Kishon site, a peak ground acceleration of 0.3g would only be expected to cause liquefaction if it resulted from an earthquake of magnitude about 7.5. It is not surprising, therefore, that no signs of paleoliquefaction are evident at the Kishon site. On the other hand, such signs may have been expected at the Eilat site, since magnitude 6 events, developing peak ground accelerations of 0.3g, may conceivably have occurred in the past.

8 Paleoseismology and Morphologic Evidence of Young Tectonic Activity along the Carmel Fault

8.1 Introduction

Mount Carmel is an isolated hilly belt in northern Israel (Figure 8.1) which exposes upper Cretaceous rocks (Kashai, 1966) with volcanic syn-sedimentary rocks (Sass, 1957; Sass, 1980). Most of the stratigraphic section of the Carmel belongs to the Judean group from the age of Albian to Turonian and composed of limestone, dolomite, chalk, and marl (Figure 8.2). Senoian, Eocene to Pleistocene and Holocene sediments are also present in the stratigraphic sequence.

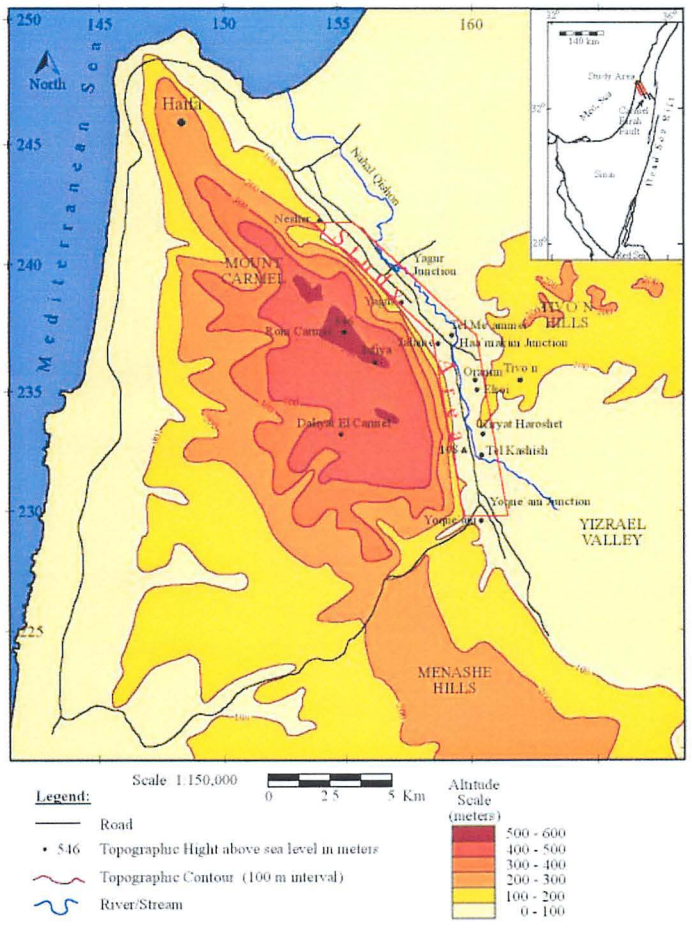

Figure 8.1. Location map of the Carmel

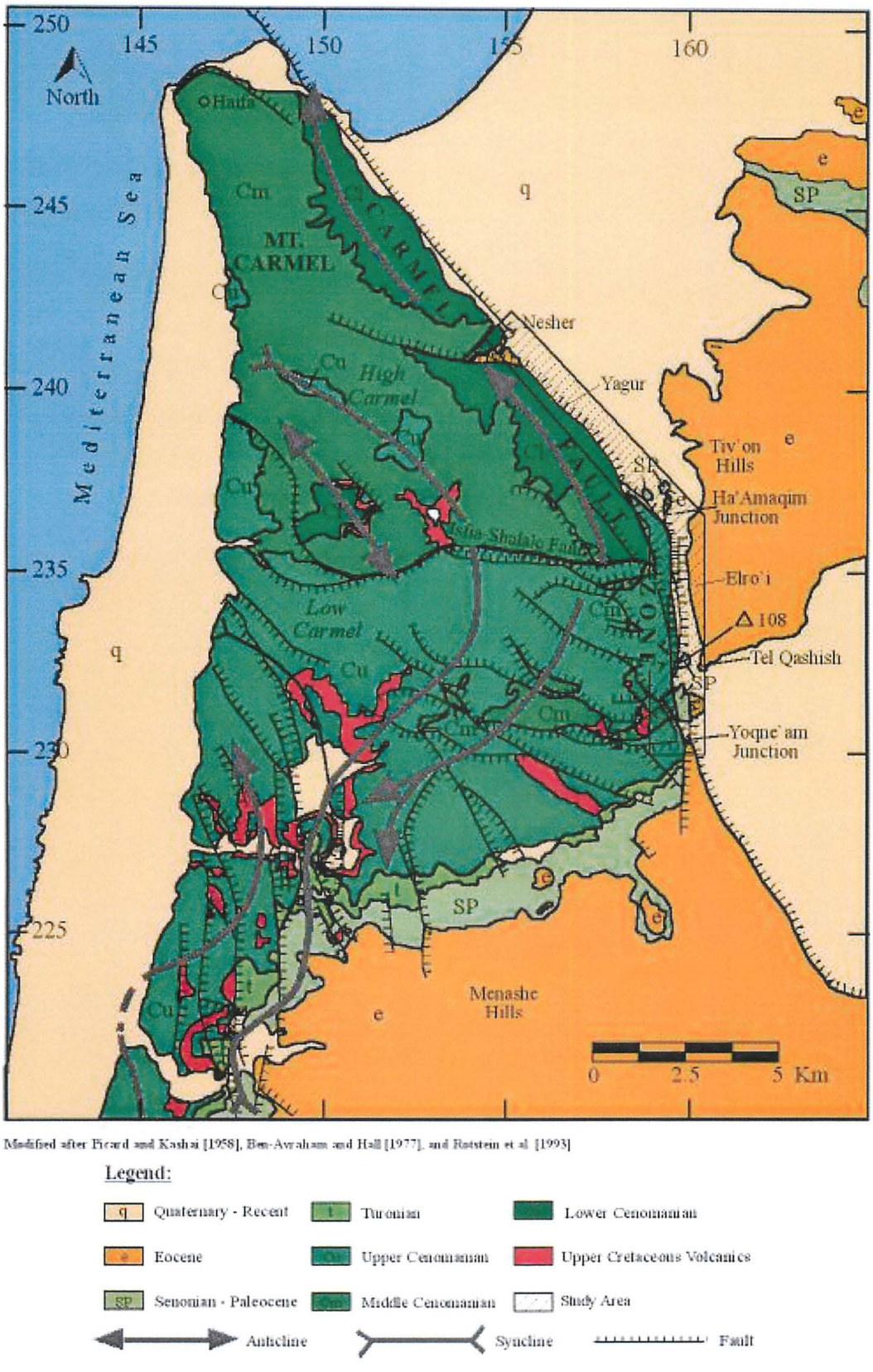

Figure 8.2. Geological map of the Carmel area (after Ben-Avraham and Hall, 1977).

The northern and eastern boundary of the Carmel follows the fault line of the Carmel Fault (Karcz, 1959; Kashai, 1966) which creates a significant morphotectonic border in northern Israel (Rotstein et al., 1993; Achmon and Ben-Avraham, 1997). This border is part of the Carmel – Tirtza fault system which splays from the Dead Sea Transform to the continental shelf in the eastern Mediterranean (Freund, 1965; Ben-Avraham and Hall, 1977) (Figure 8.2). Great differences appear in topographic features, structural style, seismic activity, crustal structure and other geological characteristics, between north of this fault system and south of it (Achmon and Ben-Avraham, 1997). The Carmel block is associated with relatively positive magnetic and gravity anomaly (Dmozalski, 1967; Folkman, 1976; Achmon and Ben-Avraham, 1997). Ben-Menahem and Aboody (1981), Shapira and Feldman (1987), Rotstein and Arieh (1986) and VanEck and Hofstetter (1990) showed that the Carmel Fault zone is characterized by microseismic activity, which is as high as that of the Dead Sea Rift itself. Focal plane solutions show mainly a left slip with a minor component of thrusting associated with the activity of this fault zone (Ron et al., 1990).

The Carmel Fault is divided clearly into two main sections (Figure 8.2): (1) The northern section, that trends NW-SE, extends from the area of Haa`makim junction to the continental shelf on the northwest (Ben-Avraham and Hall, 1977; Achmon, 1986), and (2) The southern section, trends N-S and extends from the area of Yoqneam to the Haa`makim junction area (e.g Picard and Kashai, 1958; Kashai, 1966; Achmon, 1986). It is clear though, that there is a strong connection between the two sections, which creates the same morphological and structural sequence (Achmon, 1986).

Previous works (reffered above) discussed the structure, the characteristics and the development of the Carmel between the Triassic and the Pleistocene (e.g. Achmon, 1986; Achmon and Ben-Avraham, 1997 and references therein). The recent faulting (Upper Pleistocene and Holocene) along the Carmel Fault was almost neglected and is therefore somewhat unclear. Achmon (1986) presented river channels offset, which indicate a sub-recent sinistral lateral motion.

Microseismicity indicates that the Carmel Fault is active (Ben-Menahem and Aboody, 1981; Rotstein and Arieh, 1986; Shapira and Feldman, 1987; VanEck and Hofstetter, 1990). Focal plane solutions show mainly left slip with a minor component of thrusting associated with the activity of this fault zone (Ron et al., 1990). The objective of this study is therefore, to determine how active was the Carmel Fault during the Upper Pleistocene and Holocene and to evaluate the seismic hazard that derived from its Quaternary activity. In order to do that we used paleoseismic methods that included mapping of the fault, seismic lines, trenching, dating and geomorphic studies. The study area extends from Yoqneam to Nesher on the eastern and northern piedmont of Mount Carmel (Figure 8.2).

8.2 Methods

In order to evaluate the paleoseismic activity of the Carmel Fault during the Upper Pleistocene and Holocene we searched for traces of deformed young sediments. We searched at the base of the mountain front that the Carmel Fault formed and inside it, at sites where thick soils and colluvial profiles, that would have been record deformation if occurred, are found. The research included: (1) mapping from air-photos lineaments and morphological scarps that might be fault scarps. We also recorded offset alluvial fans or stream channels along those lineaments; (2) Trenching across some lineaments and mapping and describing the stratigraphy exposed on the walls of the trenches; and (3) running a seismic line across the morphological scarps at the southern part of the Carmel Fault.

8.3 Geological Setting

8.3.1 Structure

The Carmel block is uplifted and tilted to the southwest, with a border faults system on its northeastern side (Karcz, 1959; Kafri, 1970; Achmon, 1986; Rotstein et al., 1993). The structure of Mount Carmel can be best described as a main, fifty-kilometer long, asymmetrical anticlinal ridge. The main anticlinal structure is built from two anticlines, the anticline of the low Carmel, which

trends northeast, and the anticline of the high Carmel, which trends northwest (Kashai, 1966). There are also several smaller anticlinal and synclinal structures, which are parallel or sub-parallel to the main anticline (Picard and Kashai, 1958; Kashai, 1966) (Figure 8.2).

The E-W trending Isfiya-Shallale Fault separates the structure of the northern high Carmel from the southern low Carmel (Figure 8.2). There is a significant difference in the internal faulting pattern north and south of this fault. The northern Carmel is faulted only by a few small faults with a vertical separation of just several meters. The southern Carmel is faulted by significant faults, having tens of meters of vertical separation and which are arranged in a fan pattern system. The faults strikes trend from N-S in the west, to E-W in the east (Kashai, 1966; Ron et al., 1984; Achmon, 1986; Ron et al., 1990) (Figure 8.2). On the basis of Cretaceous volcanic structures, Sass et al. (1977) and Sass (1980) suggested the existence of a strike-slip displacement upon the faults in the southern Mount Carmel. Ron et al. (1984; 1990) estimated 1,300 to 2,900 meters of left lateral displacement. The movement on these faults was caused by a rotation of rigid blocks. The amount of rotation increases southwestward from 10°-15° clockwise of the southern Carmel in the Ha`amaqim Junction area to 35° in Zihron-Ya`aqov area. In contrast, the northern Carmel is rotated only by not more than 10° clockwise. Therefore, no significant internal faulting occurred in that area (Ron et al., 1984; Achmon, 1986; Ron et al., 1990).

8.3.2 The Carmel Fault system

The eastern and northeastern border of the Carmel structure is a complex structural system, having a few hundred meters width. The deformation features include the main and major faults, many small faults, flexures and strong tilts of the bedding, detached blocks and widespread brecciation. The Carmel Fault creates a significant morphotectonic border in Northern Israel (Achmon, 1986). Freund (1965) proposed that The Carmel-Farah fault system is an important secondary structure of the Dead Sea Rift fault system, and that it is taking up some of the transform motion along the Arabia-Africa boundary (Ben-Menahem et al., 1976).

The sense and magnitude of fault displacement on the Carmel Fault was the subject of many studies: Picard and Kashai (1958), Karcz (1958), De-Sitter (1962), Arad (1965), Freund (1965), Kashai (1966), Freund (1970), Achmon (1986), Ron et al. (1984; 1990). It is agreed that there is a major sinistral movement along the Carmel Fault but the exact amount is not known.

Table 1 summarizes the amount of vertical and sinistral movement along the Carmel Fault according to these authors.

Table 1. The amount of vertical and sinistral movement along the Carmel Fault as was suggested in previous works.

Author	**Through (m)**		**Assumption based on:**
	Vertical	**Lateral**	
Picard and Kashai (1958) Kartz (1958) Kashai (1966)	1,000		Stratigraphic displacement in the Nesher area
De-Sitter (1962)		10,000	The axis of Dvora anticline related to the Um-El-Fahem anticline
Arad (1965) Freund (1965)		10,000	The displacement of the Turonian formations in the Western Galilee related to the Carmel
Freund (1970)		3,000 - 4,000	Slickensides and stratigraphy
Achmon (1986)	300-400 in the Southern part and 1,000 in the Northern part	Total of 1,000 – 1,500 with 300 in the Pleistocene	Lateral: - The displacement of the Senonian formation (3,000m), and the Turonian formation (1,500m)
Ron (1984; 1990)		1,300 – 2,900 inside the southern Carmel	- Displaced volcanic bodies - Block rotation (≈35°)

Picard and Kashai (1958), Karcz (1958) and Kashai (1966) estimated the maximum stratigraphic vertical displacement to be 1,000 meters near Nesher. This is based on field relationship showing the Eocene Zora` formation displaced against the Albian-Cenomanian Yagur formation. Achmon (1986) determined the amount of vertical displacement by stratigraphic displacement in the southern part of the Carmel Fault to 300 to 500 meters (Figure 8.12).

De-Sitter (1962) was the first to suggest a strike-slip motion on the eastern border fault of the Carmel (the "Carmel Fault"). He estimated a left lateral displacement of 10 kilometers. This estimation was based on the displacement of the Dvora anticline axis relative to the axis of Um-El-Fahem anticline, which he thought to be a single structure. Freund (1965) and Arad (1965) also suggested a left lateral displacement of 10 kilometers, but they based their estimation on the amount of displacement between the Turonian formation in the western Galilee and the Carmel. Shahar (1966), following Freund (1965), mentioned that there is a component of strike-slip movement, but he did not mention to what extent. Freund (1970) estimated a left lateral displacement of 3 to 4 kilometers. He based his estimation on the direction of the slip on slickensides, which trends 25° to the northwest, and upon the vertical stratigraphic displacement in the quarry near Neve-Sha`anan. Schulman and Weiler (1972) claimed that there is no proof of lateral offset on the Carmel Fault.

Achmon (1986) discussed the amount of vertical and lateral movement on the Carmel Fault in detail. He showed that most of the fault planes, the main faults and the small faults, are either vertical or subvertical. The strikes of the small faults are oblique to the strike of the main faults. These field relations fit a situation where the main faults have a significant component of sinistral strike-slip movement. Achmon (1986) estimated 300 meters of left lateral displacement in the region between Yoqneam to Jalame junction. This estimation of the displacement was based on the change in the direction of dry stream channels. It seems that it represents only the latest stages of the lateral movement. Achmon (1986) showed that there are slickensides in different directions, therefore, he claimed that it is not possible to estimate the amount of lateral offset as Freund (1970) had suggested.

An attempt to estimate the total amount of lateral displacement on the Carmel Fault was made by Achmon (1986) based on displaced rock units from both sides of the fault. West of the fault, the most northern exposure of the Ein-Zeitim formation is in the Yoqneam area, whereas east of it, the most southern exposure of these rocks appears near triangulation point 108 (coordinate 15980/23255). These two outcrops are 3,000 meters away from each other. The northern exposure of the Dalya formation, west of the fault, appears up to latitude 235, whereas in the Jalame area it appears in the quarry (latitude 236) and north of it. These Dalya formation outcrops are separated by 1,500 meters. Achmon (1986) pointed out an oblique movement; he estimated the lateral component to be 1,000 meters of left lateral displacement. Rotstein et al. (1993) accept the amount of lateral offset on the exposed faults that Achmon (1986) suggested, but, claimed that the total lateral offset is more than 3 to 4 kilometers. They drew that conclusion from high-resolution imaging of the Carmel Fault.

The recognition of the border fault between Yoqneam and the Jalame Junction as a large sinistral strike-slip fault fits well within a general model of the deformation in the southern Carmel. According to this, the eastern border fault of the Carmel is the eastern border of the clockwise rotating region. Therefore, a relatively large amount of sinistral movement is exist on this part of the fault (Achmon, 1986). Rotstein et al., (1993) suggested that the movement on the Carmel Fault is a pure strike-slip where the fault strikes northwest – southeast, and has a reverse component where the fault strikes north – south.

The main activity on the northeastern border faults of the Carmel occurred after the formation of the internal folds of the Carmel (Kashai, 1966). Picard (1943) suggested that the faulting occurred at the Pleistocene, whereas Karcz (1959) claimed that they occurred at the Late Tertiary to Quaternary. Ron et al. (1984) showed that the main phase of the strike-slip faulting in the Galilee and in the Carmel region occurred at the period between the Late Miocene to Early Pliocene.

The mountain piedmont is built of young sediments from the Pleistocene to Holocene periods. The units are composed mainly of conglomerate and clays. The

conglomerate is composed of pebbles and cobbles from the mountain front rock units. The clays are red to brown clay from the flood plain of the Kishon River and from the mountain front. Above these young sediments there is 0.5 to 1 meter of recent soil. Achmon (1986) detected two "steps" about 2 m high on the mountain piedmont 3 km north of Yoqneam Junction. He suggested that these steps are young fault scarps. Seismic activity along the Carmel Fault indicates that the Fault is active (Ben-Menahem and Aboody, 1981; Rotstein and Arieh, 1986; Shapira and Feldman, 1987; VanEck and Hofstetter, 1990). Focal plane solutions reveal sinistral strike slip with a small compression component (Ron et al., 1990). The August 1984 earthquake (M=5.1) having such a focal plane solution is a good example for the general nature of earthquakes along the Carmel Fault (Ron et al., 1990; Amiran et al., 1994).

8.4 Geomorphology and Tectonic Geomorphology

The northern boundary of Mount Carmel is a steep slope associated with the Carmel Fault zone, which creates a significant mountain front. The water divide is passing through the eastern part of the high Carmel. The character of the streams is asymmetric on both sides of the water divide. East of the water divide there are short steep slopes and gullies, whereas to the west, there are long streams with a relatively moderate gradient. The short and steep gullies and streams that trend eastward, are young morphological features, which were probably formed only with the development of the mountain front. In contrast, the streams that flow to the west have a v-shaped valley, which indicate a long history of development. Near Isfiya, the water divide is located west of the anticlinal ridge. It is possible, that in the past, the water divide was located at the anticlinal ridge. Possibly, it migrated westward towards the moderate slopes, because of the proximity of the base level, the Kishon River, east of the ridge (Kashai, 1966).

The base of the mountain front can be divided to two morphologic districts: (1) The southern district from Tel-Kashish to the Ha`amaqim Junction, along the section where the Carmel Fault trends north – south; and (2) The northern section from the Ha`amaqim Junction to the Mediterranean Sea where the Carmel Fault

trend SE-NW. A 5 km long and about 800 m wide valley between the Tivon Hills and the mountain front of the Carmel characterizes the southern district. Within this district the Kishon River flows generally in strait direction with some small meanders. The northern district is characterized by a very wide valley that delimited on the south by the Carmel mountain front. In this section the Kishon River flows in wide meanders pattern.

In the study area, the steep and uniform escarpment along the hard rocks units, and the steep gullies with dry waterfalls, create an indication for young uplifting. Along the base of the mountain front there are small step-like escarpments, relatively straight, that can be suspected as fault scarps. Achmon (1986) suggested that small scarps at the base of the mountain front are recent fault scarps. He also showed that the main faults of the Carmel Fault system that trending N-S in the section from Yoqne'am to the Ha'amakim Junction offset the courses of dry stream channels by as much as 300 meters in a sinistral direction. This faulting, that offsets the course of the dry streams, is subsequent to the development of the main drainage system that was caused by the uplifting. In the section between Jalame and Nesher the stream courses are relatively straight. This implies that there was no significant lateral movement on the Carmel Fault in this section in the near past.

Few alluvial fans that act as shutter ridges are located 500 m north-west of Kibbutz Yagur (Figure 8.3) where the Carmel Fault trends NW-SE. The head of each alluvial fan is not connected to the stream that used to feed it. These displaced alluvial fans caused the blockage of the streams in theirs course. As a result the streams found their way around the alluvial fans (Figure 8.4). All the blocking alluvial fans are shifted at the same direction and thus it seems that left lateral movement along the Carmel Fault caused this displacement. The estimated total lateral displacement is about 50 to 80 m. This estimation was measured by the stream channels that flows around the alluvial fans, and when possible by the heads of the alluvial. It should be remembered that this is an estimation and in some cases might represent an exaggeration of the real amount of displacement.

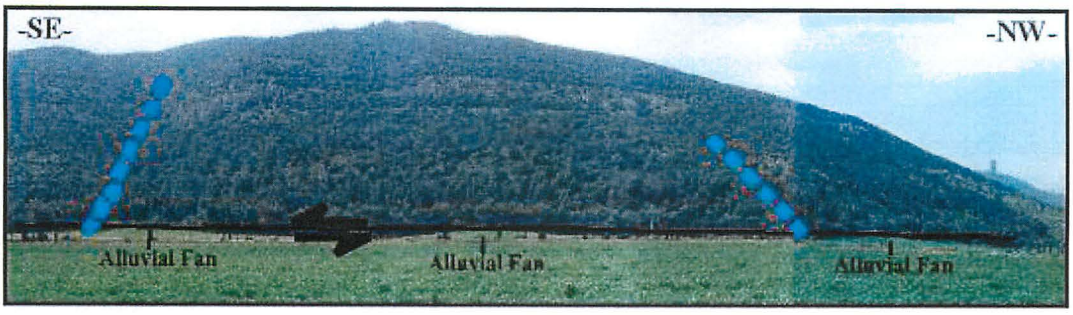

Figure 8.3. Offset alluvial fans and stream channels north-west of Kibbutz Yagur. There is 50 to 80 m of sinistral movement of these features.

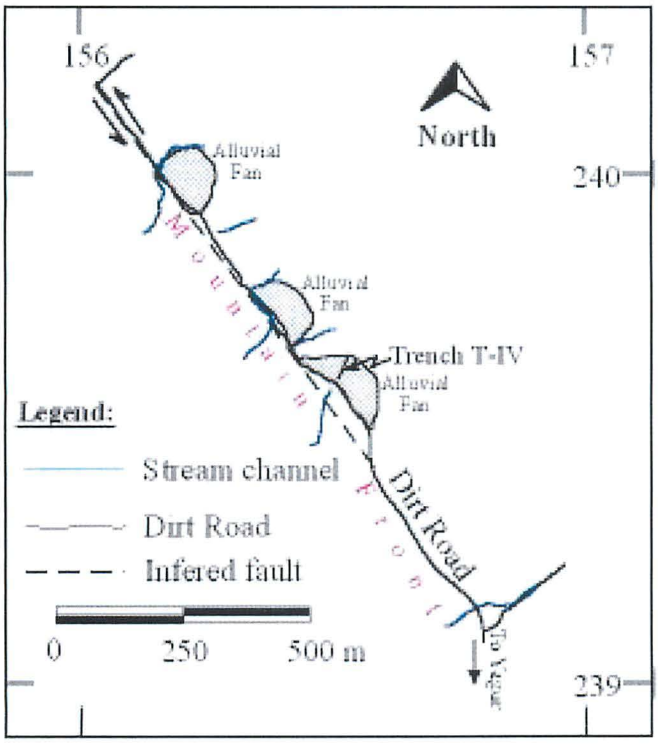

Figure 8.4. Offset alluvial fans at the base of the mountain front 500 m north-west of Kibbutz Yagur where the Carmel Fault trends SE-NW.

The relation of stream size to their channel size is different between the Yoqne'am – Jalame section, where the Carmel Fault trends north – south, to the Jalame – Nesher section, where the fault trends northwest – southeast. In both sections the streams are fairly wide with an opening of few hundred meters, which indicates a long time of development. In the Yagur area the channels are few meters wide,

filled with gravel and silt, and they fit the size of the streams. In contrast to the Yagur area, the channels in the section between Yoqneam to Jalame are very narrow, usually not more than one meter wide. It seems that these channels are evidence of a young tectonic interruption in the geomorphic development of the drainage system, probably due to the lateral offset of the channels courses (Achmon, 1986) and to rapid uplifting of the mountain front in this section.

In the southern part and in the northern part of the Kishon valley, where the Carmel Fault trends north – south, there are two hills on both side of the Kishon River. The hills are triangulation point 108 and Tel-Kashish in the southern edge, and in the northern edge, Tel-Mua`mar and Tel-Jalame (Figure 8.1, 8.2). An intense deformation is clear in the southern hills (Figure 8.5(a)) and less clear in the northern ones. The existence of these hills may be explained by their specific location at the base of the mountain front, in the section where the Carmel Fault trends north – south. The reason for their appearance may be either compression at this part of the Carmel Fault like Rotstein et al. (1993) suggested, or more likely, by dextral stepping associated with sinistral movement that creates push up swells. This might explain the different dips of the hills (Figure 8.5(b)).

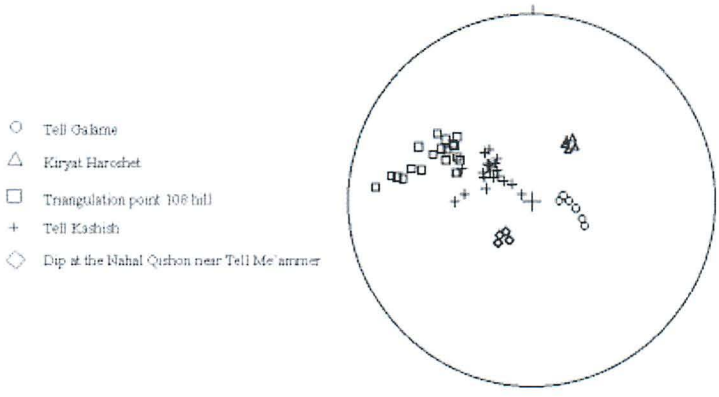

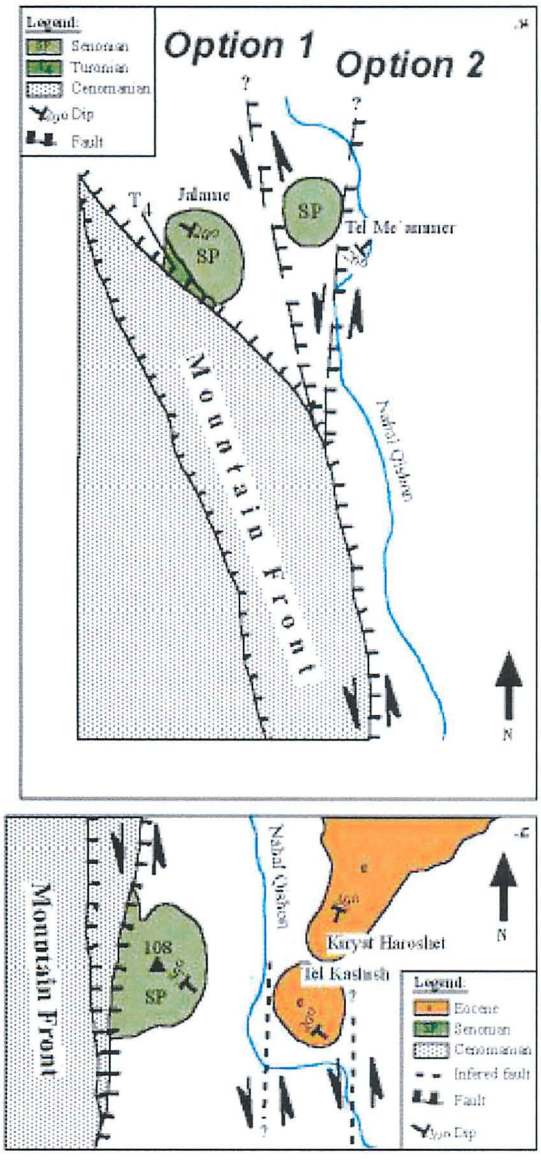

Figure 8.5. (a) Stereogram of the tilted layers of the Hills at the Qishon Valley in the southern district of the Carmel Fault. (b) Two Schematic models of the formation of the hills at the mountain front of the Carmel.

8.5 Paleoseismology

The paleoseismology study along the Carmel Fault involved running seismic line and trenching across suspected fault scarps.

Mapping of lineaments along the southern part of the Carmel Fault was done using air photos dated from 1944 (Figure 8.6). This is the section where Achmon (1986) noticed the offset stream channels within the mountain range. We found that steam channels located east of the mountain front where also offset (Figure 8.6). These displaced stream channels are sinistral offset by about 45 to 140 meters (Figure 8.6) (From north to south - 80, 135, 50, and 140 m.) It seems that the three southern streams are offset on the path of the road. Because in 1944 this road was still a dirt road and there is no evidence of artificial diversion of the stream channels we conclude that sinistral movement of the Carmel Fault caused the offset these stream channels.

In this region around coordinate 15975/23335 there are clear two linear scarps that form clear morphological steps at the base of the mountain front. These scarps were suspected as a degraded fault scarp. A high-resolution seismic line was done across these lineaments. This was done with the help of the Geophysical Institute of Israel (Dr. Ilan Brunner).

The interpretation of the seismic line shows few faults (Figure 8.7). As the seismic line is do not provide data about the upper few meters it was not clear at that time if the faults reach the surface. Evidence of deformation were found in three zones: at the 60^{th}, 120^{th}, and 170^{th} meter. The deformed zones in the 60^{th} and 120^{th} meter are in accordance with the morphological scarps. In order to better understand the nature of the deformation zone and the faults we excavated trenches across the morphological scarp and the sites where the faults might reach the surface.

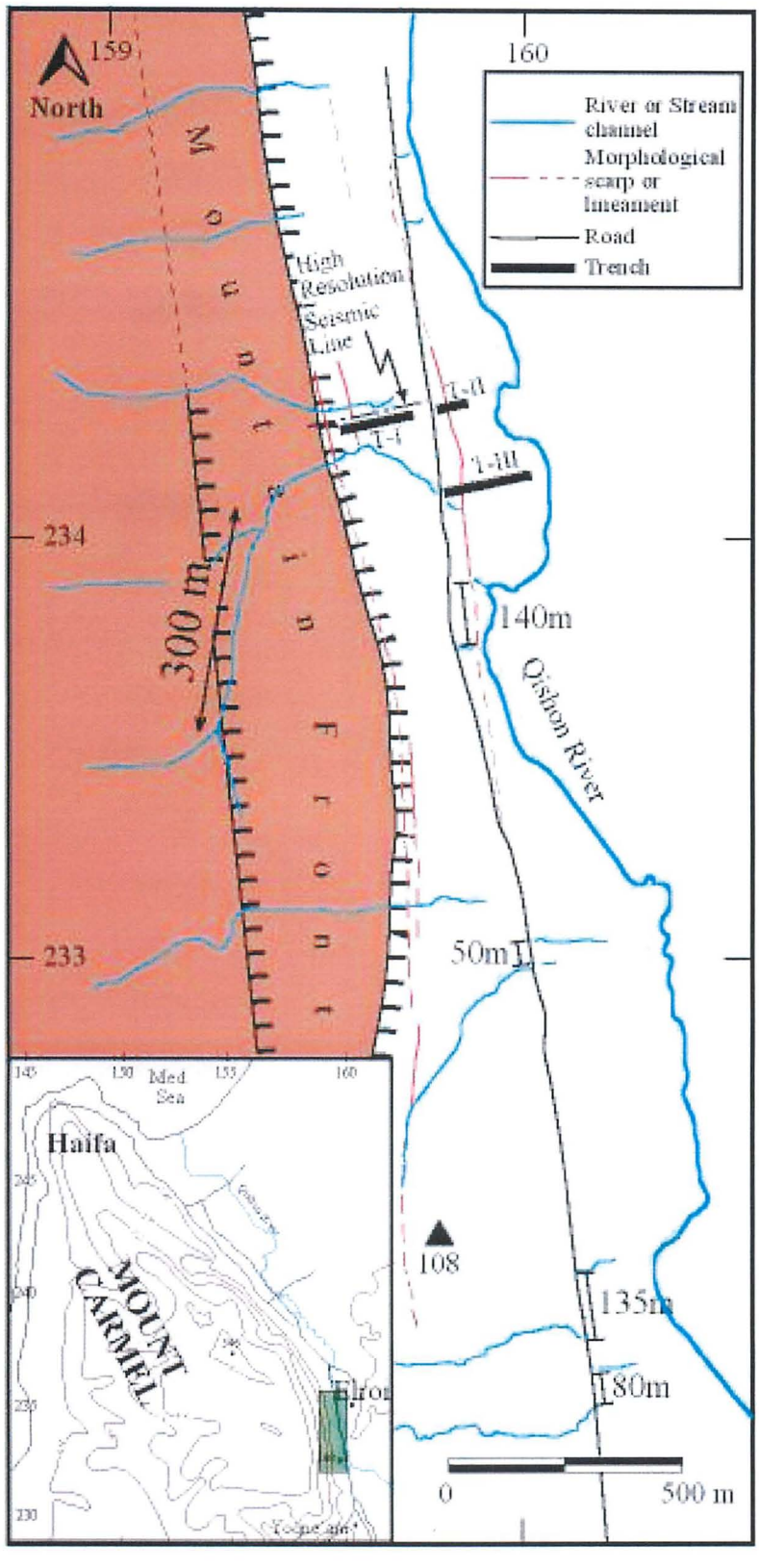

Figure 8.6. Map of morphological scarps and suspected lineament as fault trace along the southern part of the Carmel Fault.

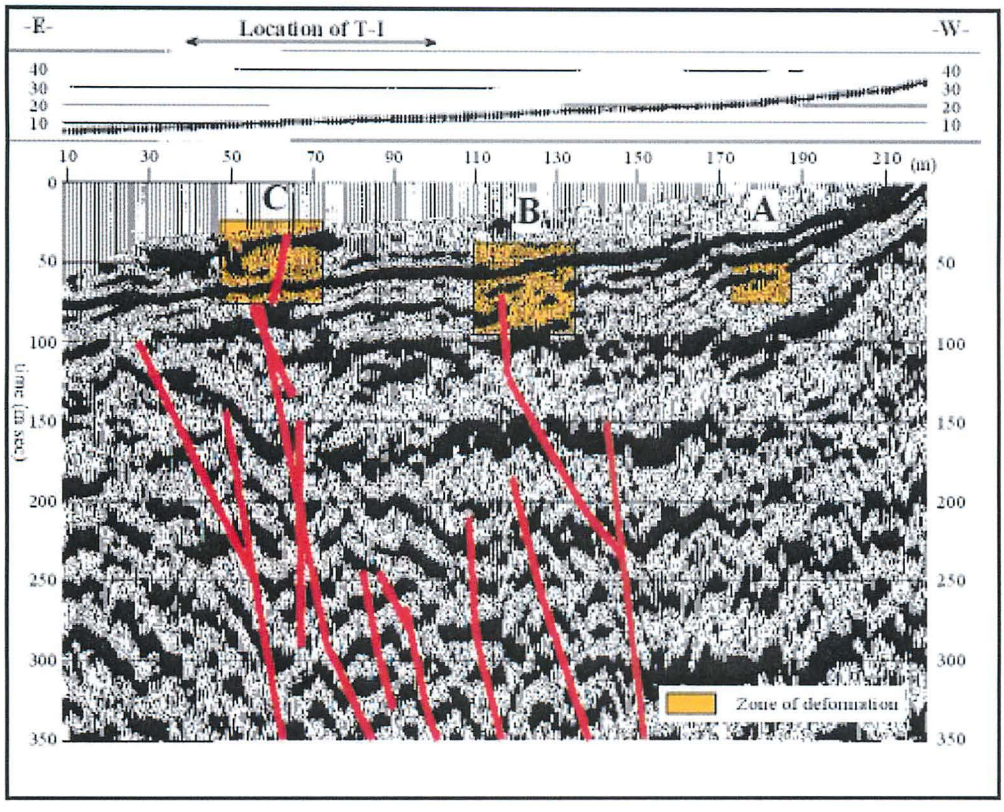

Figure 8.7. High-resolution seismic line at the base of the mountain front in the southern part of the Carmel Fault. The line crosses the lower morphological step (fault scarp?) that was mapped in Figure 8.6.

We excavated a trench (T-1) through the lower scarp and mapped the wall of the trench in details (Figure 8.8). The stratigraphic sequence in the trench includes six main units (Figure 8.8). Unit DF is a debris flow composed of carbonate fragments 0.5 to 20 cm in a red clay matrix. Unit CL1 is brown clay with small carbonate fragments (5 to 7 cm). Units B1 and B2 are conglomerates that composed of the exposed formations in the mountain front nearby; unit M1 is mixed of unit CL1, B2 and surface soil; and unit CL2 is clean dark brown clay (Figure 8.8). Several units were dated using the OSL method by Dr. N. Porat from the Geological Survey of Israel. Unit DF was dated to 80.0±10Ka and unit CL1 was dated to 20.6±2.3Ka. At the 85th meter of the trench a Neolithic site is present inside unit B2 (Figure 8.8). Its age is estimated to 7 Ka (Personal comment by Nigel Goring, The Institute of Archeology, the Hebrew University). It seems that

the stratigraphic sequence in the section between the 60th meter to the 80th meter was undergone a significant deformation. There is some order in the stratigraphic sequence but in small scale this part of the trench is not in an order as the sequence at the rest of the trench. This area of the deformed section coincides with the morphological scarp found on the surface.

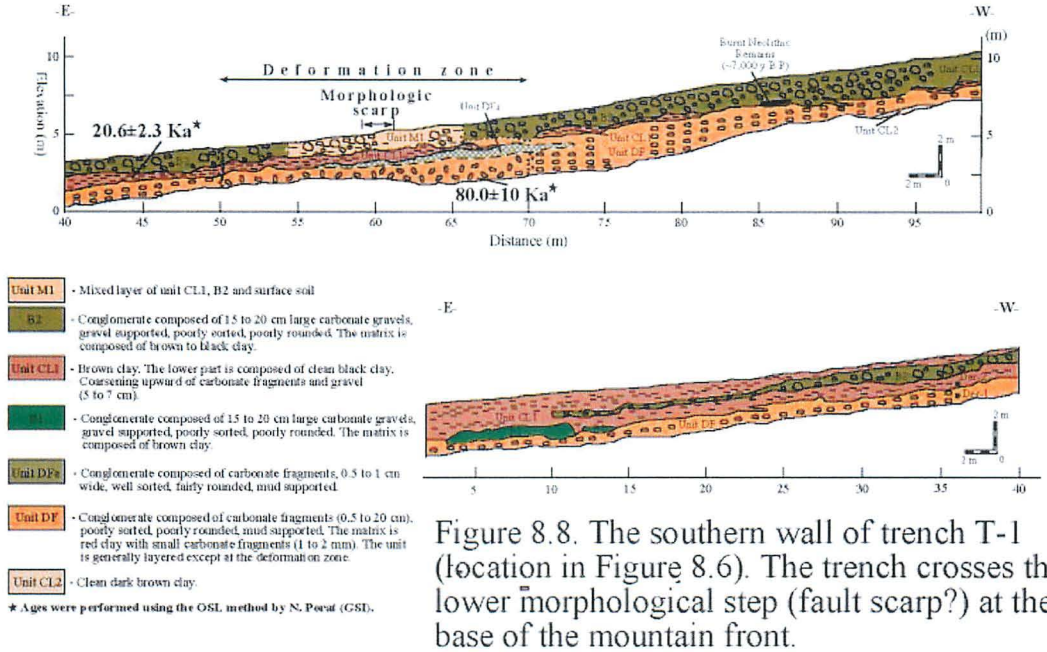

Figure 8.8. The southern wall of trench T-1 (location in Figure 8.6). The trench crosses the lower morphological step (fault scarp?) at the base of the mountain front.

Two more trenches were excavated across the major lineament that was suspected to be a fault trace on the 1944 air photo (T-2 and T-3 east of the road, Figure 8.6). Small offset of stream channels were located along this lineament. Five stratigraphic units are exposed in the trench T-2 (Figure 8.9): Unit 1 is composed of poorly sorted conglomerate (10-15 cm). The boulders are mud supported by dark brown clay. Unit 2 contains dark brownish clay. Unit 3 composed of moderately sorted boulders (10-15 cm). Unit 4 contains reddish brown clay. Unit 5 composed of poorly sorted boulders up to 20 cm big. The unit contains about 30% cobbles; the boulders are mud supported by reddish clay. Above unit 5 there is 0.5 to 1 m thick soil (Figure 8.9). It seems that the units in trench T-2 are similar to the units exposed in trench T-1. It is most likely therefore that the ages of the units in T-2 are similar to the age of the same units in trench T-1. There was no evidence to any kind of deformation or faulting in this trench.

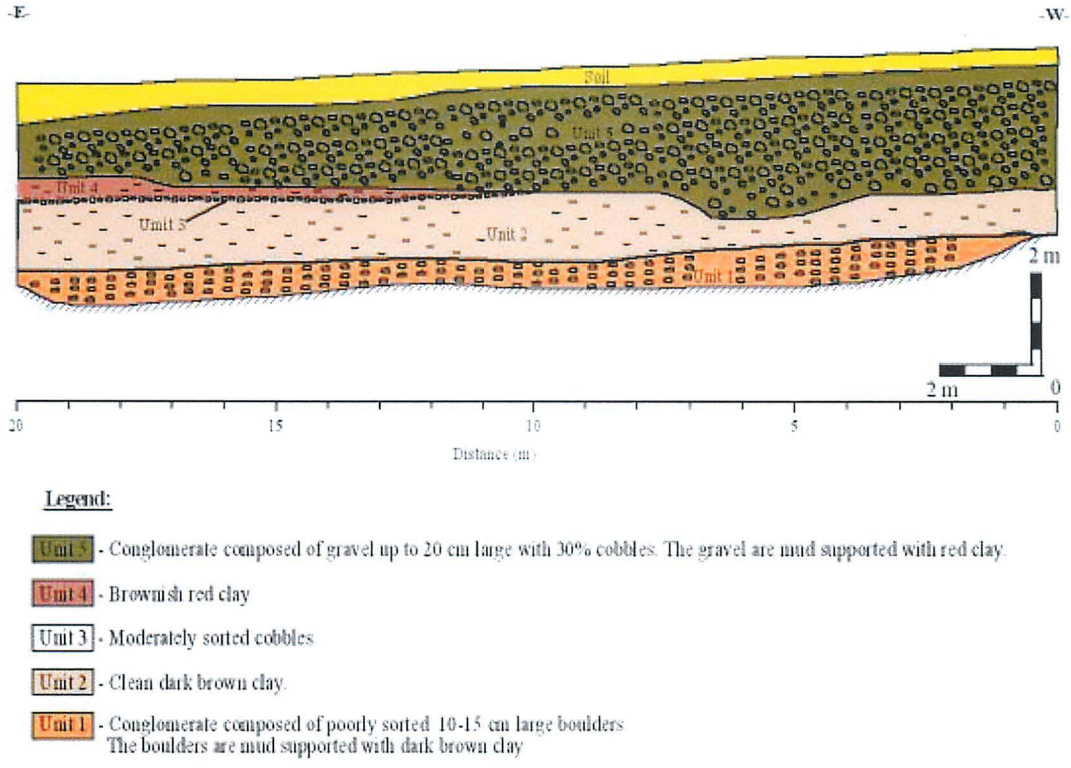

Figure 8.9. The southern wall of trench T-2. The trench crosses a significant lineament that was mapped on the air photo from 1944 that was suspected to be a fault trace at the surface (Figure 8.6).

Trench T-3 was excavated about 300 m south of trench T-2. There are six stratigraphic units exposed in this trench (Figure 8.10): Unit 1 composed of dark brown clay. Unit 2 contains poorly sorted conglomerate with boulders up to 25 cm big. The boulders are mud supported by brown clay, and in places there is presence of granules and cobbles. Unit 3 contains clean dark brownish clay with no boulders presented except one boulders horizon in the middle of the unit. Unit 4 contains granules, cobbles and boulders up to 15 cm long. Unit 5 composed of brown clay. Unit 6 contains cobbles and boulders up to 10 cm long. The gravels are mud supported by reddish clay. At the western part of the trench there is an outcrop of the stream channel that cross the road opposite of the trench (Figure 8.6). The stratigraphic sequence of trench T-3 is quite similar to the sequence exposed in trenches T-1 and T-2. No significant deformation or faulting was observed in the channel.

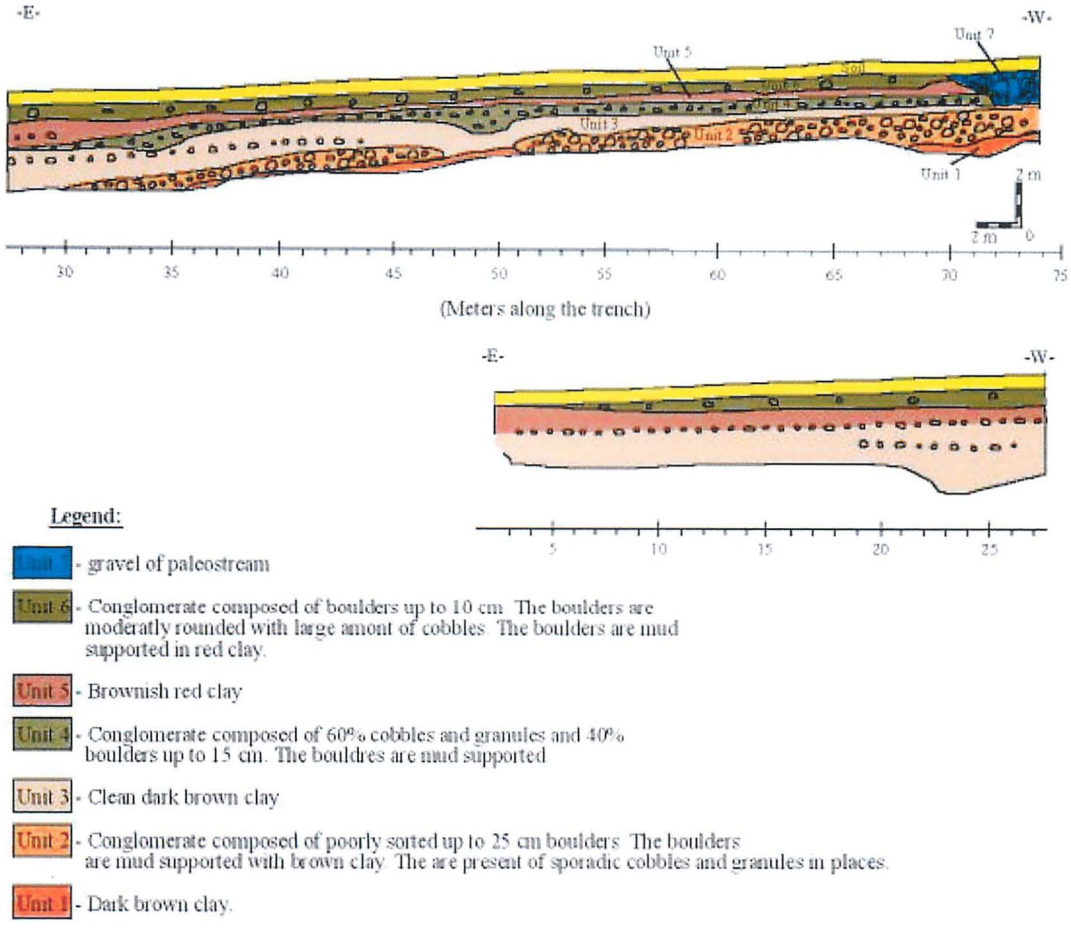

Figure 8.10. The southern wall of trench T-3. The trench crosses a significant lineament that was mapped on the air photo from 1944 that was suspected to be a fault trace at the surface (Figure 8.6).

About 1 km north of Kibbutz Yagur Feigin (1994) performed a ground penetrating radar (GPR) along a dirt road perpendicular to the Carmel Fault at the base of the mountain front. Feigin (1994) recognized few shallow faults along the line. We excavated a 50 m long and 4 m deep trench along this dirt road in order to detect these faults (Figure 8.3). The stratigraphic sequence in the trench includes five main units. Units 1,2,3 and 5 are composed of brown clay with variable amount and size of carbonate fragments and dolomite pebbles whereas unit 4 is composed of conglomerate of dolomite pebbles of the Yagur formation. There is presence of big boulders (≈1.5m×1.5m×2m) along the trench, which

might roll from the mountain front during big earthquakes. We dated unit 1 to 18.5±2.5Ka, unit 3 to 26.8±3.2Ka, unit 4 to 43.6±5.0Ka, and unit 5 to 33.5±5.1Ka using the OSL method. At the 36th meter of the trench there is abrupt discontinuation of about 1m in unit 4 and the unit continues to the NE 20 cm lower. A fault plane was not presented but this discontinuation may represent a fault at the base of the trench that displayed only the lower units exposed in the trench. Feigin (1994) showed a fault at this location in the GPR line but there is no evidence in the trench for the rest of the faults that he located. This displacement probably occurred about 35,000 years ago and since then there was no further displacement on this fault.

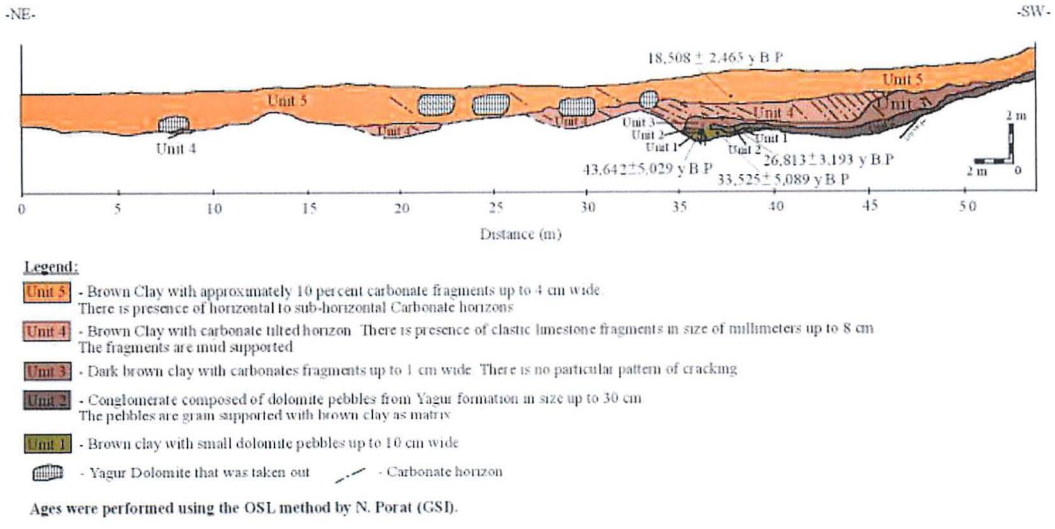

Figure 8.11. The southern wall of the trench north-west of Kibbutz Yagur. Notice the small fault at the base of the trench.

8.6 Discussion

Tectonic activity along the Carmel Fault was observed from the Miocene to the Pleistocene and is well defined in the geological record (e.g Kartz, 1958; Picard and Kashai, 1958; Kashai, 1966; Kafri, 1971; Ben-Avraham and Hall, 1977; Kafri and Folkman, 1981; Achmon, 1986; Ron et al., 1990; Rotstein et al., 1993; Achmon and Ben-Avraham, 1997). The Carmel Fault is seismically active at the present as is recorded by the Israeli network (Ron et al., 1990; Amiran et al., 1994; Hofstetter et al., 1996). Still, there is a gap of information about the activity of the fault from the Upper Pleistocene to the Holocene. In the present work we looked along the Carmel Fault for displaced alluvial fans and offset stream channels along the mountain front piedmont, and recent faulting. In the following chapter we will discuss the possibility of seismic activity and faulting during the Upper Pleistocene and Holocene.

The displacement of the alluvial fans at the northern part of the Carmel Fault and the offset stream channels at the southern part happened in a sequence of earthquakes, with a magnitude larger than M=5.5. This occurred in that way, as the amount of displacement is larger than could occur in a single surface rupture and as it is agreed that the minimum magnitude of an earthquake that will cause surface rupture is about 5.5 (Wells and Coppersmith, 1994). It is clear, therefore, that the sinistral offset of tens of meters should occur in more than one earthquake but still, we did not find features that would allow us to separate the total amount of displacement to different events. The time of the displacement of the offset stream channels at the southern part of the Carmel Fault is delimited by the age of the sediments in trenches T-1, T-2, and T-3. In case that the age of the lower units in trenches T-2 and T-3 are the same as unit DF in trench T-1 (80.0±10Ka) this displacement occurred before 80,000 years ago. The absence of significant deformation along the lineament that offset the stream channels may be regard to the dominant of clays in the stratigraphic sequence present in the trenches. The nature of the clay and its ability to "flow" probably erased any fault plane or other deformation that might have been present in the trench.

The scarp that was located along the lineament at the foothill of the Carmel can be explain either by a neotectonic activity or by the activity of the Kishon River.
The geological sequence that is derived from trench T-1 does not give conspicuous evidence of a simple surface rupture that had happened during an earthquake event. Although there is no clear evidence for any earthquake, we think that there are still enough data to conclude that this scarp is the result of a tectonic activity:
(1) The lineament is a straight line which is not the case in river margins. More than that: The formation of the scarp at the surface occurred after 20 Ka (the age of unit CL1 in trench T-1). During that period, the mean sea level height was few tens of meters below the sea level height of today. This data implies that the Kishon River was also lower at least in few tens of meters than today and that the source of these sediments is not the Kishon River but probably the mountain front. If that so, it is not possible that the scarp was formed by activity of the Kishon River, but it was formed by tectonic activity.
(2) the seismic line that was conducted perpendicular to the scarp show clearly few faults one of them at the exact location of the scarp.
(3) The data from the trench show a clear deformed zone right below the scarp.

The deformed zone in trench T-1 located beyond the morphological step (scarp) and above the deformation zone in the seismic line. Each major type of faulting – strike-slip, normal-slip and reverse-slip - produces a characteristic assemblage of landforms. Normal and reveres faults generally produce different geomorphic features because they reflect either crustal extension or contraction, respectively. Geomorphic features associated with reveres and thrust faults are more subtle and difficult to recognize than those of strike-slip and normal-slip faults. Much of this difficulty lies in the fact that reveres and thrust faults may not rupture the Earth's surface. Where surface rupture does occur, the resultant scarps have complex, sinuous patterns and may be broad and poorly developed. Overthrusting of the hanging wall block commonly forms a "bulldozed" appearance of the scarp, with complex shuttering of the surface of the uplifted side of the fault. Where rupture does not reach the surface, repeated displacements along the fault produce warping, tilting and/or folding of deposits in the upthrown block of the fault

(Lettis and Kelson, 1998). It may be that the deformed zone in trench T-1 is the expression of faulting at the subsurface that cause the deformed zone in the trench and the scarp on the surface.

A model for the development of the Carmel was presented by Rotstein et al. (1993). According to this model, a phase of tension that caused a normal faulting in Yisra`el Graben, was followed by lateral motion on the Carmel Fault at the middle Miocene. In the Late Miocene, the Kishon Graben was starting to form, while the lateral motion continues on the Carmel Fault. At this stage, there was a motion with normal component on the section of the Carmel Fault that trend southeast - northwest, whereas at the section that trend north - south, there was a pure left lateral motion. At the Pliocene, subsequent to the rotation of 30° of the southern Carmel, the section of the Carmel Fault that trends north - south was locked to lateral motion, and a compression, uplifting and tilting to the southwest began. A pure left lateral motion occurred on the section that trends southeast - northwest, while on the section that trends north - south, a reverse motion with a small component of left lateral motion occurred. They claimed that the total lateral motion upon the Carmel Fault continues until today. Focal plane solution of the earthquake in 1984 sows also a strike slip motion with compression at the southern part of the fault (Ron et al., 1990). It is conceivable that the compression component is taking place as a reverse or thrust fault at the mountain piedmont.

The model suggested by Rotstein et al. (1993) may fit the observation that we found along the base of the mountain front. It might be that the scarps in the section of the fault from Yoqneam to the Ha`amaqim Junction, where the fault trends north – south, are folds or warps that were formed as consequence of reveres or thrust fault at the subsurface. This might explain the absence of evidence of faulting in trenches T-1, T-2, and T-3. Further more, if the alluvial fans north of Kibbutz Yagur are really lateral displaced, it agrees with this model for the recent motion upon the Carmel Fault: a compression on the north – south segment, and a left lateral movement on the northwest – southeast segment.

The form of faulting along the Carmel Fault might be explained in terms of strain partitioning. This model suggests that the motion along major strike slip faults

partitioned on different faults. The vertical component occurs on tilted fault planes and the lateral component occurs on vertical fault planes (Lettis and Hanson, 1991). Along the southern part of the Carmel Fault it may be appropriate to describe the faulting with this model. The sinistral strike slip motion occurred on the faults inside the mountain front (Achmon (1986) offset streams) and the vertical component occurs on the base of the mountain front. Thus, the faulting at the base of the mountain front is a reverse faulting. It is noticeable though that the offset stream channels in this section of the fault are in discordance with this model.

Heimann et al. (1999) tried to find evidence of faulting in the form of paleoliquefaction of the soils at the Haifa bay area (For details see other chapter in this report). They excavated tens of trenches with a total length of more than 1 km in a few locations from Akko to Haifa. Heimann et al. (1999) did not find any positive evidence for paleoliquefaction in these trenches.

It is possible therefore to conclude that although the Carmel Fault is seismically active and it displaced Pleistocene features such as alluvial fans and stream channels, there was no surface rupture in the last few tens of thousands of years along it. This may happened because during this time the Carmel Fault did not form earthquakes with magnitude M>5.5. Nur and Walder (1992) suggested that the recurrence time of earthquakes depends on the pore pressure and it could be in the scale of 10^3 to 10^5 years. It may be that the recurrence time of earthquakes that cause surface rupture on the Carmel Fault is longer than tens thousands of years. Still, as suggested above, although no fault rupture occurred, thrusting and deformation of the surface might occurred during that period.

9 Discussion

The cities of Haifa and Eilat, and their neighboring cities, are sited on the active Dead Sea Transform Fault and its major branch the Carmel Fault. Earthquakes of magnitude 7 and above in the Eilat area, and 6 and above in the Haifa Bay area are possible. Thus, and as both cities form areas with large populations, their seismic hazard is high.

In the present study we tried to evaluate some components of the seismic hazards of the areas. We surveyed both areas for paleoliquefaction features, we made a geotechnical study, and in the Haifa area studied the neotectonic and paleoseismology of the Carmel Fault.

Using boreholes data of upper subsurface sequences we recognized the northern shore of the Eilat Bay and a strip from Akko to the Kishon (with a width of a few km) as sites of high potential for liquefaction. We opened trenches at a few sites in these areas in order to identify paleoliquefaction features. A precise survey was carried in trenches with total length of about 2 km. No evidence for paleoliquefaction features was found.

It should be emphasized that the trenched sections are only about 3-4 meters deep, and are not below the present water table. Therefore, we may have missed any liquefaction features that exist below the present water table. But, as the water table level changes, as can be seen from the section, we believe that the present exposed sections have been, and still are, at times, under water (which is essential for liquefaction to occur). Moreover, we believe that even if liquefaction had occurred at a depth greater than that of the trenched section, we would see liquefaction features above the liquefied layer.

Therefore, as we have not identified any liquefaction features at any of the checked locations (En Hamifraz, Kefar Bialik, Kishon Port in Haifa and the Hotel area in Eilat), we assume that liquefaction did not occur, at least at these specific sites.

The age of the samples from the bottom of the trenches (in Haifa) can assist in estimating the minimum period during which the areas did not suffer from liquefaction.

Therefore the En HaMifratz area did not suffer from liquefaction during the last 3.7 ky, the Kefar Bialik area during the last 2.8 ky, and the Kishon area during the last 3.2 ky. These are minimum ages. If we assume that the whole area would experience liquefaction when it occurs at any site, then the maximum found age, 3.7 ky, is the minimum age for the period that the Haifa Bay area did not suffer from liquefaction.

Geotechnical studies were carried out in Eilat and in the Haifa bay areas. Summarizing the data from Eilat, it is clear that the danger of liquefaction at the Eilat site is highly dependent on the magnitude and proximity of the earthquake, and level of the ground water table at the site. Both field tests and laboratory studies show that the in-situ sand in portions of the profile has a very low relative density, and would be expected to liquefy under strong earthquake input. The field tests suggest that a magnitude 6.5 earthquake, applying a peak ground acceleration of 0.3 may result in some liquefaction, and this would be higher spread for stronger events. Cyclic triaxial tests, performed on samples taken from the top 2 meters of the profile, reinforce this conclusion, showing that only a few cycles (3 – 4) of a magnitude 6 or more earthquake causing a peak ground acceleration of at least 0.3 g. may result in liquefaction in the upper two meters at the site, if they were submerged. With regards the portion of the profile presently below water table, a magnitude 7.0 event at least, causing a peak ground acceleration of 0.3g or more, would appear to be required to cause liquefaction.

In the sand of the Kishon we found that the relative density is of the order of 70%. The stress-strain curves, and effective stress paths observed in triaxial tests on undisturbed and reconstituted samples coincide almost precisely, suggesting that natural structural effects in this soil is not of major significance, and, consequently, reconstituted samples could reasonably be employed in order to study the behavior of the undisturbed material. The effective stress paths obtained from undrained tests are seen to show the highly dilative behavior demonstrated in the drained tests. The response of the undisturbed Kishon sand to monotonic shear loading suggests that this material would be significantly less prone to liquefaction than the Eilat soil.

A significant difference between the Eilat and Kishon sites is evident. The Eilat sample, under a cyclic stress ratio of 0.25, developed 1% strain after 11 loading cycles of 0.25 stress ratio, whereas the Kishon sand, under a higher stress ratio of

0.35, withstood 30 load cycles before developing the same strain. The pore pressure developed significantly faster in the Eilat samples than in the Kishon samples. For example, for a stress ratio of SR = 0.25, u is seen to reach 100% of its maximum value after about 12 cycles in the Eilat samples, while in the case of Kishon sand, only 36% of maximum pore pressure was developed after 100 loading cycles. The Kishon sample tested at a stress ratio of 0.35 showed stiffer behavior and less pore pressure development than the Eilat sample under a stress ratio of 0.25.

We compared the cyclic stress ratio versus the number of cycles required for liquefaction for Eilat the Kishon and of kurkar-sand from the Nitzanim site and Monterey sand. The Kishon results lie close to the upper limit of the Nitzanim kurkar-sand, and above the Monterey sand, whereas the Eilat results lie close to the lower bound suggested for the kurkar-sand, and significantly below the curve for the Monterey sand. The Kishon results indicate that a peak ground acceleration of 0.3g, corresponding to an equivalent stress ratio in the upper part of the profile of about 0.38, would require 15 – 20 loading cycles in order to cause liquefaction. A magnitude 7.5 earthquake would be required in order to develop such conditions.

Tectonic activity along the Carmel Fault was observed from the Miocene to the Pleistocene and is well defined in the geological record. The Carmel Fault is seismically active at the present as is recorded by the Israeli network. Still, there is a gap of information about the activity of the fault from the Upper Pleistocene to the Holocene. In the present work we looked along the Carmel Fault for displaced alluvial fans and offset stream channels along the mountain front piedmont, and recent faulting.

The displacement of the alluvial fans at the northern part of the Carmel Fault and the offset stream channels at the southern part happened in a sequence of earthquakes, with a magnitude larger than M=5.5. This is evident since the amount of displacement is larger than could occur in a single surface rupture. The time of the displacement of the offset stream channels at the southern part of the Carmel Fault is delimited by the age of the sediments in trenches (80.0±10Ka) and thus, this displacement occurred more than 80,000 years ago. The absence of significant deformation along the lineament that offset the stream channels may be due to the dominance of clays in the stratigraphic sequence present in the

trenches. The nature of the clay and its ability to "flow" probably erased any fault plane or other deformation that might have been present in the trench.

The deformed zone in trench T-1 is located beyond the morphological step (scarp) and above the deformation zone in the seismic line. Each major type of faulting – strike-slip, normal-slip and reverse-slip - produces a characteristic assemblage of landforms. Normal and reverse faults generally produce different geomorphic features because they reflect either crustal extension or contraction, respectively. Geomorphic features associated with reverse and thrust faults are more subtle and difficult to recognize than those of strike-slip and normal-slip faults. Much of this difficulty lies in the fact that reverse and thrust faults may not rupture the Earth's surface. Where surface rupture does occur, the resultant scarps have complex, sinuous patterns and may be broad and poorly developed. Where rupture does not reach the surface, repeated displacements along the fault produce warping, tilting and/or folding of deposits in the upthrown block of the fault. It may be that the deformed zone in trench T-1 is the expression of faulting at the subsurface that caused the deformed zone in the trench and the scarp on the surface.

We observed that the scarps in the section of the fault from Yoqneam to the Ha`amaqim Junction, where the fault trends north – south, are folds or warps that were formed as a consequence of reverse, or thrust fault at the subsurface. This might explain the absence of evidence of faulting in trenches T-1, T-2, and T-3. Further more, if the alluvial fans north of Kibbutz Yagur are really lateral displaced, it agrees with this model for the recent motion upon the Carmel Fault: a compression on the north – south segment, and a left lateral movement on the northwest – southeast segment (as suggested also by Rotstein et al., 1993).

It is possible therefore to conclude that although the Carmel Fault is seismically active and it displaced Pleistocene features such as alluvial fans and stream channels, there was no surface rupture along it in the last few tens of thousands of years. This may be because during this time the Carmel Fault did not initiate earthquakes with magnitude M>5.5. Nur and Walder [1992] suggested that the recurrence time of earthquakes depends on the pore pressure and it could be in the scale of 10^3 to 10^5 years. It may be that the recurrence time of earthquakes that cause surface rupture on the Carmel Fault is longer than tens of thousands of years. Still, as suggested above, although no fault rupture occurred, thrusting and deformation of the surface might have occurred during that period.

10 Summary and Conclusions

1. No liquefaction features were observed in sites in the Haifa and Eilat Bay areas although these sites had the potential to have such features.
2. The Carmel Fault is seismically active and it displaced Pleistocene features such as alluvial fans and stream channels.
3. No evidence for surface rupture was detected in the trenches opened along the Carmel Fault although faults were located in a seismic line. A zone of deformation was located in the trench underneath the fault scarp directly above one of the faults identified in the seismic line. This could be interpreted as a blind fault.
4. It is possible therefore to conclude that although the Carmel Fault is seismically active and it displaced Pleistocene features such as alluvial fans and stream channels, there was no surface rupture in the last few tens of thousands of years along it. This may be because during this time the Carmel Fault did not initiate earthquakes with magnitude M>5.5. It may be that the recurrence time of earthquakes that cause surface rupture on the Carmel Fault is longer than tens of thousands of years. Still, as suggested above, although no fault rupture occurred, thrusting and deformation of the surface might have occurred during that period.
5. The geotechnical studies indicated a significant difference between the liquefaction potential of the Eilat and Kishon sites. The Eilat site appears to have a potential for liquefaction under the action of an earthquake of magnitude 6.0 or greater, producing a peak ground acceleration of 0.3g or more. On the other hand, at the Kishon site, a peak ground acceleration of 0.3g would only be expected to cause liquefaction if it resulted from an earthquake of magnitude about 7.5. It is not surprising, therefore, that no signs of paleoliquefaction are evident at the Kishon site. On the other hand, such signs may have been expected at the Eilat site, since magnitude 6 events, developing peak ground accelerations of 0.3g or more, may conceivably have occurred in the past.
6. It seems, therefore, that an earthquake with magnitude of 6 and above (that ruptured the surface) did not occur along the Carmel Fault in the last few

tens of thousand of years. The geotechnical information suggest that liquefaction in the Haifa Bay would occur as a result of an earthquake greater than 7.5, but such an event has not occurred on the Carmel Fault for a very long time and thus the non-finding of paleoliquefaction features is not surprising. It is therefore suggested that the seismic hazard due to surface rupture or liquefaction in the Haifa Bay area is not high.

7. In Eilat, an area producing earthquakes with magnitudes higher than 7, the geotechnical studies indicate that liquefaction may be expected to occur as a result of an earthquake of magnitude 6 or higher. Therefore, the non-finding of paleoliquefaction features is surprising. We suggest that the seismic hazard of Eilat, due to potential liquefaction must be regarded as high.

11 References

Achmon, M., 1986. The Carmel border fault between Yoqneam and Nesher [Ms.C Thesis]. Hebrew University, Jerusalem (in Hebrew, English abst.), 86 p.

Achmon, M. and Z. Ben-Avraham, 1997. The deep structure of the Carmel Fault zone, northern Israel, from gravity field analysis. Tectonics, 16 (3), 563-569.

Achmon, M., Ron, H., and Ben-Avraham, Z., 1994. Geophysical research of the Carmel-Yizre'el-Jordan fault zone. Earth Sci. Adm. Rep., ES-68-93, 1-21.

Aitkin, M. J., 1985. Thermoluminescence dating. London, Academic Press.

Aitkin, M.J., 1998. An introduction to optical dating: the dating of Quaternary sediments by the use of photon-stimulated luminescence. Oxford Univ. Press, Oxford, UK.

Ambraseys, N.N., 1988. Engineering seismology. Earthquake Eng. and Struct. Dynamics, 17, 1-105.

Ambraseys, N.N. and Karcz, I., 1992. The earthquake of 1546 in the Holy Land. Terra Nova, 253-262.

Amick, D. and Gelinas, R., 1991. The search for evidence of large prehistoric earthquake along the Atlantic Seaboard. Science, 251, 655-658.

Amick, D., Maurath, G., Gelinas, R. and Canavello, D., 1990. Identification of paleoliquefaction features using ground penetrating radar techniques. Proceedings of Fourth U.S. national conference on earthquake engineering, May 20-24, Palm Spring, California, 1, 629-638.

Amiran, D.H.K., Arieh, E. and Turcotte, T., 1994. Earthquakes in Israel and adjacent areas; macroseismic observations since 100 B.C.E. Israel Exploration Journal, 44 (3-4), 260-305.

Ansal, A.M., 1994. Cyclic behavior of cohesive soils, liquefaction, soil amplification and a case study on the effects of geotechnical factors in Erzincan 1992 eathquake. In: Rutenberg, A., ed., Earthquake

Engineering [Proceedings of the seventeenth regional European Seminar ed.], Rotterdam, A.A. Balkema, 121-132.

Arad, A., 1965. Geological outline of the Ramot Menashe region (northern Israel). Isr. Jour. of Earth Sci., 14, 18-32.

Bartov, Y., Steinitz, G., Eyal, M. and Eyal, Y., 1980. Sinistral movement along the Gulf of Aqaba, its age and relation to the opening of the Red Sea. Nature, 285, 220-221.

Ben-Avraham, Z. and Ginzburg, A., 1990. Displacement terranes and crustal evolution of the Levant and the Eastern Mediterranean. Tectonics, 9, 613-622.

Ben-Avraham, Z. and Hall, J. K., 1977. Geophysical survey of Mount Carmel structure and its extension into the eastern Mediterranean. Jour. of Geophys. Res., 82, 793-802.

Ben-Menachem, A., 1979. Earthquake catalogue for the Middle East, 92BC-1980AD. Boll. Geofis. Teor. Appl., 21, 245-310.

Ben-Menachem, A., Nur, A. and Vered, M., 1976. Tectonics, seismicity and structure of the Afro-Eurasian junction - the breaking of an incoherent plate. Phis. Earth. Planet. Interior., 12, 1-50.

Ben-Menahem, A. and E. Aboody, 1981. Micro and Macroseismicity of the Dead Sea rift and off coast Eastern Mediterranean. Tectonophysics, 80, 199-233.

De-Sitter, L.U., 1962 .Structural development of the Arabian Shield in Palestine. Geol. En. Mijnb., 45, 116-124.

Dmozalski, W., 1967. Aeromagnetic survey of Israel interpretation. Inst. for Petrol. Res. and Geophys. report SMA/482/67.

Elgamal, A. W., Amer, M. and Adalier, K., 1993. Liquefaction during the October 12, 1992 Egyptian Dahshure earthquake. Proceedings of the Third International Conference on case histories in geotechnical engineering. St. Lois, Missouri.

Enzel, Y., Amit, R., Harrison, J.B.J. and Porat, N., 1994. Morphologic dating of fault scarps and terrace risers in the southern Arava, Israel: comparison to other age-dating techniques and implications for paleoseismicity. Isr. Jour. of Earth Sci., 43, 91-104.

Feigin, D., 1994. High resolution seismic refraction study of young faults [Ms.C Thesis]. Tel Aviv University, Tel Aviv, 103 p.

Folkman, Y., 1976. Magnetic and Gravity investigation of the crustal structure in Israel. Ph.D. thesis, Tel-Aviv University, Tel-Aviv (in Hebrew).

Freund, R., 1965. A model of the structural development of Israel and adjacent areas since Upper Cretaceous times. Geol. Mag., 102, 189-205.

Freund, R., 1965. A model for the development of Israel and adjacent areas since the Upper Cretaceous times. Geol. Mag., 102, 189-205.

Freund, R., Garfunkel, Z., Zak, I., Goldberg, M., Weissbrod, T. and Derin, B., 1970. The shear along the Dead Sea Rift: Phil. Trans. of the Royal Soc. of London, Series A, 267, 107-130.

Freund, R., 1970. The geometry of faulting in the Galilee. Isr. J. Earth Sci., 19, 117-140.

Frydman, S., 1993. The effect of local soil conditions on earthquake response. Proc. 17th European Seminar on Earthquake Engineering, Haifa, 133-145.

Frydman, S., 1994. The effect of local soil conditions on earthquake response. Proc., 17th Regional European Seminar on Earthquake Engineering, Balkema, Rotterdam, 133-145.

Frydman, S., 2000. The shear strength of Israeli soils. Isr. J. Earth Sci., 49, 55-64

Frydman, S., Hendron, D., Horn, H., Steinbach, J., Baker, R. and Sha'al, B., 1980. Liquefaction study of cemented sand. Jnl. Geotech Eng. Div., ASCE, 106(GT3), 275-297.

Frydman, S., Hendron, D., Horn, H., Steinbach, J., Baker, R. and Sha'al, B., (1980). Liquefaction study of cemented sand. Jnl. Geotech. Eng. Div., Proc. ASCE, 106(GT3), 275-297.

Galanti, I., Inbar, M. and Raban, A., 1990. The evolution of the Qishon Delta during the Holocene. In Lavie, H., Schick, A., and Yair, A., eds., Notes of the geomorphology of the Negev - Ran Gerson book: Haifa, The Israeli Geog. Soc., 133-146.

Garfunkel, Z., Zak, I. and Freund, R., 1981. Active faulting along the Dead Sea transform (rift). Tectonophysics, 80, 1-26.

Gerson, R., Grossman, S., Amit, R. and Greenbaum, N., 1993. Indicators of faulting events and periods of quiescence in desert alluvial fans. Earth Surface Proc. and Landforms, 18, 181-202.

Gibbs, H.J. and Holtz, W.G., 1957. Research on determining the density of sands by spoon penetration testing. 4th Internatnl Conf. on SMFE, London, 1, 35-39.

Grant, L.B., and Sieh, K., 1994. Paleoseismic evidence of clustered earthquakes on the San Andreas Fault in the Carrizo Plain, California. Jour. of Geophys. Res., 99, 6819-6841.

Hajic, E.R., Obermeier, S.F., Munson, P., Wiant, M.D., Tankersley, K.B. and Garniewicz, R.C., 1994. Distribution and dating of prehistoric earthquake liquefaction in southeastern Illinois, central US. Geol. Soc. of Ame., Abst. and Program, 1994, 24-27.

Heimann, A. and Wachs, D., 1995. Identifying paleoliquefaction features in the northern shore of the Elat Bay: Abst. of the Isr. Geol. Soc., Annu. Meet., p. 48.

Heimann, A., 1990, The development of the Dead Sea Rift and its margins in northern Israel during the Pliocene and the Pleistocene [Ph.D. Dissertation]: The Hebrew University, Jerusalem, 114 p.

Heimann, A., Wachs, D., Frydman, S., Gluck, D. and Talwani, P., 1999. Evaluation of the seismic hazard of the Haifa Bay area, Israel. In Amr. Geophys. Union annual meeting.

Hofstetter, A., vanEck, T. and Shapira, A., 1996. Seismic activity along fault branches of the Dead Sea Jordan transform system: The Carmel-Tirtza fault system. Tectonophysics, 267 (1-4), 317-330.

Holzer, T.L., and Clark, M.M., 1993. Sand boils without earthquakes. Geology, 21, 873-876.

Inst. Petrol. Res. Geophys., 1982-1992. Earthquakes in and around Israel. Seismological Bulletins, v. 1-11.

Kadan, G., Eyal, Y. and Enzel, Y., 1995. Dead-Sea fluctuations and tectonic events in the Holocene fan-delta of Nahal Darga. Abst. of the Isr. Geol. Soc., Annu. Meet., p. 52.

Kafri, U. and Folkman, Y., 1981. Multiphase reverse vertical tectonic displacement across major fault in northern Israel. Earth and Planetary Sci. Let., 53, 343-348.

Kafri, U., 1970. Pleistocene tectonic movements in the coastal area, Isr. J. Earth Sci., 19, 147-152.

Kafri, U., 1971. Pleistocene tectonic movements in the coastal plain of Israel emphasizing the Mount Carmel area. Isr. J. Earth Sci., 20, 133-134.

Kartz, Y., 1958. The geology of the northwestern Mount Carmel. MS.c. thesis, Hebrew University, Jerusalem, (in Hebrew).

Karcz, Y., 1959. The structure of the northern Carmel: Bull. Res. Counc. Isr., v. 8G, 119-130.

Kashai, E., 1966. The geology of the eastern and southwestern Mount Carmel. Ph.D. thesis, Hebrew University, Jerusalem, (in Hebrew).

Lettis, W.R. and K.I. Kelson, 1988. Applying geochronology in paleoseismology. In: Dating and Earthquakes: Review of Quaternary geochronology and its application to paleoseismology, edited by J.M. Sowers, J.S. Noller, and W.R. Lettis, pp. 3-26, U. S. Nuclear Regulatory Commission.

Lettis, W.R. and Hanson, K.L., 1991. Crustal strain partitioning-implication for seismic hazard assessment in western California. Geology, 19, 559-562.

Livneh, M. and Ishai, I., 1988. The relationship between in-situ CBR and various penetration tests. Penetration Testing, A.A. Balkema, Rotterdam, 445-452.

Marco, S. and Agnon, A., 1995. Prehistoric earthquake deformations near Masad, Dead Sea Graben. Geology, 23, 695-698.

Munson, P.J., Munson, C.A. and Pond, E.C., 1995. Paleoliquefaction evidnece for a strong Holocene earthquake in south-central Indiana. Geology, 23, 325-328.

Nur, A. and Walder, J., 1992. Hydraulic pulses in the Earth's crust. In: Fault mechanics and transport properties of rocks; a festschrift in honor of W.F. Brace., edited by B. Evans, and T.F. Wong, pp. 461-474, Acad. Press, San Diego, CA, United States.

Obermeier, G.S., Weems, R.E., Gelinas, R.L. and Rubin, M., 1985. Geologic evidence for recurrent moderate to large earthquakes near Charleston, South Carolina. Science, 227, 408-411.

Obermeier, S.F., Bleuer, N.R., Munson, C.A., Munson, P.J., Martin, W.S., McWilliams, K.M., Tabaczynski, D.A., Odum, J.K., Rubin, M. and Eggert, D.L., 1991. Evidence of strong earthquake shaking in the lower Wabash Valley from prehistoric liquefaction features. Science, 251, 1061-1063.

Obermeier, S.F., Jacobson, R.B., Smoot, J.P., Weems, R.E., Gohn, G.S., Monroe, J.E. and Powars, D.S., 1990. Earthquake-induced liquefaction features in the coastal setting of South Carolina and in the fluvial setting of the New Madrid seismic zone. US. Geol. Surv. prof. Paper, 1504, 44 p.

Pardee, J.T., 1926. The Montana earthquake of June 27, 1925. U.S. Geol. Surv., Prof. Pap. 147-B.

Picard, L., and Kashai, E., 1958. On the lithostratigraphy and tectonics of the Carmel. Bull. Res. Counc. Isr., 7G, 1-18.

Picard, L., 1943. Structure and evolution of Palestine with comparative notes on neighbouring countries. Geol. Dep. Hebrew Univ. Jerusalem.

Picard, L.Y., and E. Kashai, 1958. On the lithostratigraphy and tectonics of the Carmel. Bull. Res. Counc. Israel, 7G, 1-19.

Porat, N., Amit, R., Zilberman, E. and Enzel, Y., 1997. Luminescence dating of fault-related alluvial fan sediments in the southern Arava Valley, Israel. Quaternary Geochronology, 16, 397-402.

Porat, N., Wintle, A.G., Amit, R. and Enzel, Y., 1996. Late Quaternary earthquake chronology from luminescence dating of colluvial and alluvial deposits of the Arave Valley, Israel. Quaternary Research, 46, 107-117.

Quennel, A.M., 1959. Tectonics of the Dead Sea Rift. Int. Geol. Congr., 20th Mexico, 1956, Assoc. Serv. Geol. Afr., p. 385-405.

Rajendran, C.P. and Talwani, P., 1993. Paleoseismic indicator near Blufton, South Carolina: an appraisal of their tectonic implications. Geology, 21, 987-990.

Ron, H., Nur., A. and Hofstetter, A., 1990. Late Cenozoic and recent strike slip tectonics in Mount Carmel Northern Israel. Annales Tectonicae, 4, 70-80.

Ron, H., Freund, R., Garfunkel, Z. and Nur, A., 1984. Block rotation by strike slip faulting: structural and paleomagnetic evidence. J. Geophys. Res., 89, 6265-6270.

Rotstein, Y. and Arieh, E., 1986. Tectonic implications of recent microearthquake data from Israel and adjacent areas. Earth and Plan. Sci. Lett., 78, 237-244.

Rotstein, Y. and Arieh, E., 1986. Tectonic implication of recent microearthquake data from Israel and adjacent area. Earth and Plan. Sci. Lett., 78, 237-244.

Rotstein, Y., Bruner, I. and Kafri, U., 1993. High-resolution seismic imaging of the Carmel Fault and its implications for the structure of Mt. Carmel. Isr. Jour. of Earth Sci., 42, 55-69.

Sass, E., Bein, A., Arkin, Y. and Bartov, Y., 1977. Geological photomap (the Zikhron Ya'akov area). Israel sheet, 145-200, 1:10000, Geol. Surv. of Israel, Jerusalem.

Sass, E., 1957. Volcanic phenomenon in Mount Carmel. MS.c. thesis, Hebrew University, Jerusalem, (in Hebrew).

Sass, E. and A. Bein, 1978. Platform carbonates and reefs in the Judean hills, Carmel and Galilee. In: Guide book of the 10th international congress on sedimentology, 241-274, Jerusalem.

Sass, E., 1980. Late Cretaceous volcanism in Mount Carmel, Israel. Isr. Jour. of Earth Sci., 29, 8-24.

Saucier, R.T., 1991. Geoarchaeological evidence of strong prehistoric earthquakes in the New Madrid (Missouri) seismic zone. Geology, 19, 296-298.

Schulman, N. and Weiler, Y., 1972. The geometry of faulting in the Galilee (Freund, 1970): A discussion. Isr. Jour. of Earth Sci., 21, 50-58.

Scott, B. and Price, S., 1988. Earthquake-induced structures in young sediments. Tectonophysics, 147, 165-170.

Seeber, L. and Tuttle, M., 1991. Historic and prehistoric earthquake-induced liquefaction in Newbury, Massachusetts. Geology, 19, 594-597.

Seed, H.B. and Idriss, I.M., 1982. Ground motions and soil liquefaction during earthquakes. Berkeley, Earthquake engineering research institute, 134 p.

Seed, H.B. and Idriss, I.M., 1971. Simpilfied procedure for evaluating soil liquefaction potential. J. Soil Mech. & Foundations Division, 107(9), 1249-1274.

Seed, H.B., Mori, K. and Chan, C.K., 1975. Influence of seismic history on the liquefaction characteristics of sands. Report EERC 75-25, Earthquake Engineering Research Center, University of California, Berkeley.

Seed, H.B., Tokimatsu, K. and Harder, L.F., 1984. The influence of SPT procedures in evaluating soil liquefaction resistance. Report UCB/EERC-84-15, Earthquake Engineering Research Center, University of California, Berkeley.

Seed, H.B., Tokimatsu, K., Harder, L.F and Chung, R.M., 1985. Influence of SPT procedures in soil liquefaction resistance evaluations. J. Geotech. Engg., ASCE, 111(12), 1425-1445.

Shamir, G. and Shapira, A., 1994. Spatial and temporal distribution of earthquakes sequences in the Gulf of Elat. Abst. of the Isr. Geol. Soc., Annu. Meet., p. 98.

Shapira, A. and Feldman, L., 1987. Microseismicity of three locations along the Jordan Rift. Tectonophysics, 141, 89-94.

Sims, J.D., 1975. Determining earthquake recurrence intervals from deformational structures in young lacustrine sediments. Tectonophysics, 29, 141-152.

Sims, J.D. and Garvin, C.D., 1995. Recurrent liquefaction induced by the 1989 Loma Prieta earthquake and 1990 and 1991 aftershocks: implications for paleosesimicity studies. Bull. of Seis. Soc. of Ame., 85, 51-65.

Smith, D.G., and Jol, H.M., 1992. Ground-penetrating radar investigation of a Lake Bonneville delta, Provo level, Brigham City, Utah. Geology, 20, 1083-1086.

Stewart, J.P., Thomas, P., Seed, R.B., and Bray, J.D., 1994. Soil liquefaction and dynamic ground compaction. Geotechnical News, 12, 53-56.

Talwani, P. and Cox, J., 1985. Paleoseismic evidence for recurrence of earthquakes near Charleston, South Carolina. Science, 229, 379-381.

Tinsley, J. C. et al., 1985. Evaluating liquefaction potential, in Ziony, J.I., ed., Evaluating earthquake hazards in the Los Angeles region - an earth-science perspective. U.S.G.S. Prof. Paper 1360, p. 262-315.

Tuttle, M.P. and Schweig, E. S., 1995. Archeological and pedological evidence for large prehistoric earthquake in the New Madrid seismic zone, central United States. Geology, 23, 253-256.

VanEck, T. and Hofstetter, A., 1990. Fault geometry and spatial clustering of microearthquakes along the Dead Sea - Jordan rift fault zone. Tectonophysics, 180, 15-27.

Vered, M., 1978. The probable Maximum earthquake magnitude associated with the Jordan Rift. Isr. Jour. of Earth Sci., 27, 82-84.

Vered, M. and Striem, H.L., 1977. A macroseismic study and implications of structural damage of two recent major earthquakes in the Jordan Rift. Seis. Soc. of Ame. Bull., 67, 1607-1613.

Wachs, D. and Siman-Tov, O., 1991. A preliminary evaluation of the seismic hazards in the city of Haifa and the Zevulun Valley. Isr. Geol. Surv., Rep. GSI/31/91, 84 p.

Wachs, D., and Zilberman, E., 1994. Preliminary evaluation of the seismic hazard in the Elat area. Isr. Geol. Surv., Rep., GSI/13/94, 53 p.

Wells, D.L. and K.J. Coppersmith, 1994. New empirical relationships among magnitude, rupture length, rupture width, rupture area, and surface displacement. Bull. of the Seism. Soc. of Amer., 84, 974-1002.

Wesnousky, S.G. and Leffler, L.M., 1992. The repeat time of the 1811 and 1812 New Madrid earthquakes: a geological perspective. Seis. Soc. of Amer. Bull., 82, 1756-1785.

Yegian, M.K., Ghahraman, V.G., Nogole-Sadat, M.A.A. and Daraie, H., 1995. Liquefaction during the 1990 Manjil, Iran, earthquake, I: case history data. Seis. Soc. of Ame. Bull., 85, 66-82.

Youd, T.L., Harp, E.L., Keefer, D.K. and Wilson, R.C., 1985. Liquefaction generated by the 1983 Borah Peak, Idaho, earthquake. Proceedings of workshop 28 on the Borah Peak, Idaho, earthquake, A:625-644.

Youd, T.L. and Idriss, I.M., 2001. Liquefaction resistance of soils. Summary from the 1996 NCEER and 1998 NCEER/NSF workshops on evaluation of liquefaction resistance of soils. J. Geotechnical & Geoenvironmental Engng, ASCE, 127(4), 297-313.